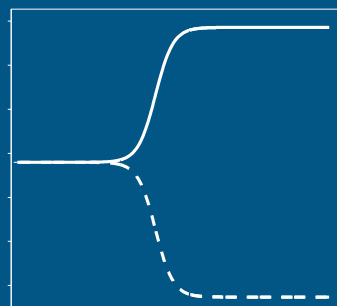
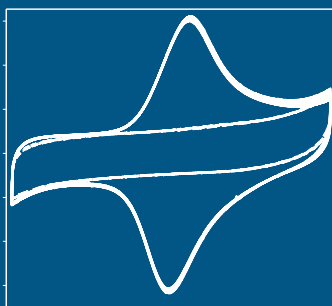
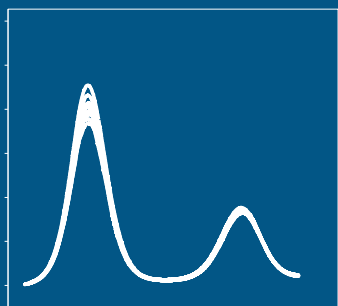
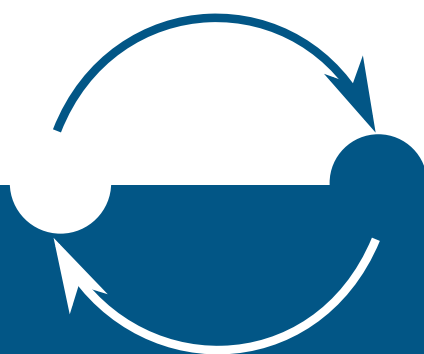


Redox cycling at nanospaced electrodes

Towards electrochemically amplified biomolecular sensing



Maarten van Megen

REDOX CYCLING AT NANOSPACED ELECTRODES
TOWARDS ELECTROCHEMICALLY AMPLIFIED BIOMOLECULAR SENSING

M.J.J. van Megen
July 12th 2013

Chair:

BIOS Lab on a Chip group

Faculty:

EEMCS, University of Twente

The research described in this thesis was carried out at the BIOS Lab on a Chip group of the MESA+ institute for Nanotechnology of the University of Twente, Enschede, The Netherlands. It was carried out in close cooperation with the Molecular Nanofabrication (MNF) group. The research was financially supported by European Research Council (ERC) through the ERC advanced grant titled 'Elab4life'.



Members of the committee:

Chairman	Prof.dr.ir. A.J. Moutaan	University of Twente
Promotor	Prof.dr.ir. A. van den Berg	University of Twente
Assistant promotor	Dr.ir. W. Olthuis	University of Twente
Members	Prof.dr. J.G.E. Gardeniers	University of Twente
	Prof.dr.ing. A.J.H.M. Rijnders	University of Twente
	Dr. P.M. Schön	University of Twente
	Prof.dr.rer.nat.habil. F. Lisdat	Wildau University
	Prof.dr E.M.J. Verpoorte	University of Groningen

Author:	Maarten van Megen
Title:	Redox cycling at nanospaced electrodes Towards electrochemically amplified biomolecular sensing PhD thesis, University of Twente, The Netherlands
ISBN:	978-90-365-3550-2
DOI:	10.3990/1.9789036535502
Publisher:	Wöhrmann Print Service, Zutphen, The Netherlands
Cover design:	Maarten van Megen

Copyright © 2013 by Maarten van Megen, Enschede, The Netherlands

REDOX CYCLING AT NANOSPACED ELECTRODES
TOWARDS ELECTROCHEMICALLY AMPLIFIED BIOMOLECULAR SENSING

PROEFSCHRIFT

ter verkrijging van
de graad van doctor aan de Universiteit Twente,
op gezag van de rector magnificus,
prof.dr. H. Brinksma,
volgens het besluit van het College voor Promoties
in het openbaar te verdedigen
op vrijdag 12 juli 2013 om 16:45

door

Maarten Jacobus Johannes van Megen
geboren op 29 juni 1984
te Arnhem

Dit proefschrift is goedgekeurd door:

Promotor

Prof.dr.ir. A. van den Berg

Assistent promotor

Dr.ir. W. Olthuis

Contents

	Page
1 Background and outline	1
1.1 Electrochemistry	2
1.2 Background	2
1.3 Outline	3
2 Theory of electrochemistry and redox cycling	7
2.1 Electrochemistry fundamentals	8
2.1.1 Electrode potential	8
2.1.2 Electrode reactions	9
2.1.3 Electrochemical cell	12
2.1.4 Non-faradaic processes	13
2.2 Amperometry	14
2.2.1 Chronoamperometry	14
2.2.2 Cyclic voltammetry	15
2.2.3 Amperometry and non-faradaic processes	18
2.3 Redox cycling	19
2.3.1 Steady state redox cycling	20
2.3.2 Amplified cyclic voltammetry	22
2.3.3 Differential cyclic voltammetry	23
2.3.4 Approach curves	24
2.4 Application of theory	26
3 Redox cycling applications	29
3.1 Introduction	30
3.2 Applications	31
3.2.1 Biosensing	31
3.2.2 Imaging	34
3.2.3 Physical properties	35
3.2.4 Miscellaneous applications	37
3.3 Concluding remarks	39

4	Differential cyclic voltammetry for selective and amplified detection	45
4.1	Introduction	46
4.2	Theory	49
4.2.1	Analytical expression	49
4.2.2	Optimal voltage	51
4.3	Materials and methods	53
4.4	Results and discussion	53
4.4.1	Voltammogram	53
4.4.2	Curve fitting	55
4.5	Concluding remarks	56
5	Surface attached redox labeled polyethylene glycol	59
5.1	Introduction	60
5.2	Theory	61
5.2.1	Calculating surface coverage	62
5.3	Materials and methods	63
5.4	Results and discussion	64
5.4.1	Surface coverage	64
5.4.2	Decay over time	64
5.4.3	Effect of NaClO ₄ concentration	66
5.5	Concluding remarks	70
6	Titaniumoxide as protection layer for on-chip gold electrodes	73
6.1	Introduction	74
6.2	Materials and methods	75
6.3	Results and discussion	75
6.4	Conclusion	76
7	Solid state nanogaps for electrochemical detection fabricated using edge lithography	79
7.1	Introduction	80
7.2	Fabrication process	82
7.2.1	Edge creation	82
7.2.2	Electrodes	83
7.2.3	Packaging	84
7.3	Materials and methods	84
7.4	Results and discussion	85

7.4.1	Fabrication	85
7.4.2	Electrochemistry	86
7.5	Concluding remarks	89
8	On chip redox cycling of surface attached molecules	93
8.1	Introduction	94
8.2	Planar electrodes	95
8.2.1	Materials and methods	95
8.2.2	Discrete DCV	95
8.2.3	Amplified CV	98
8.3	Thin layer cell	99
8.3.1	Materials and methods	99
8.3.2	Attached molecules	100
8.3.3	Control 1: blocked linker	102
8.3.4	Control 2: short molecule	102
8.3.5	Discussion	103
8.4	Conclusions	105
9	Summary and outlook	109
9.1	Summary	110
9.2	Outlook	112
9.2.1	E-beam fabricated interdigitated electrodes	112
9.2.2	Reducing gap spacing by electrodeposition	112
9.2.3	Influence of PEG chain length on mass transport	112
9.2.4	The future of dual-electrode surface-attached-molecule systems	113
A	Electrode cleaning protocol	115
A.1	Polishing	115
A.2	Electrochemical cleaning	116
B	Protocol for PEG-Fc synthesis	117
B.1	2-Ferroceneethylamine	117
B.2	PEG ₂₅₀ -(NHS) ₂	117
B.3	NHS-PEG ₂₅₀ -Fc	118
B.4	NHS-PEG _{10k} -Fc	118
	Frequently used abbreviations	119

Curriculum vitae	121
Samenvatting	123
Output	125
Acknowledgements	127

1

Background and outline

A brief introduction into the history of electrochemistry is given, followed by a description of the project's background. The chapter is concluded with an outline of this thesis.

1.1 Electrochemistry

The field of electrochemistry was started by the pioneering work of such men as Luigi Galvani and Alessandro Volta, who were already conducting electrochemical experiments as far back as the late 18th century [1–3]. Galvani discovered that the muscles of a dead frog would contract upon contact with an electrical spark, and he claimed the electrical source for this effect was stored within the frog, which is why he called it *animal electricity*. These results had a strong impact on the scientific community as scientists tried to confirm or disprove this newly discovered animal electricity. While some scientists choose other animals for their experiments, Galvani's nephew Giovanni Aldani performed his experiments on the corpse of an executed criminal [4]. It has been suggested that this research was the inspiration of Mary Shelley's novel *Frankenstein* [5]. Alessandro Volta did not believe in animal electricity and instead claimed the source of electricity originated from the metals used to connect to the frog tissues. His experiment eventually led to the development of the Voltaic pile, which became the first battery in history. An example of such a battery is shown in figure 1.1. Shortly afterwards, William Nicholson and Anthony Carlisle used the Voltaic pile for the electrolysis of water [6], and in 1834 Michael Faraday published one of his accounts of experimental research in electricity [7], in which he suggested the terms electrode, anode, cathode, electrolyte, electrolyze, ion, cation, and anion. Besides being responsible for these basic terms used even today, charge-transfer reactions occurring at the surface of an electrode now bear his name: faradaic reactions. With these results, the field of electrochemistry was born and it has developed into a field that is now over 200 years old and still actively researched in areas ranging from energy conversion and storage to biosensors and fundamental electrochemistry.

1.2 Background

This Phd project is funded through the European Research Council's Seventh Framework Programme as part of the Elab4life grant. Elab4life stands for electr(ochem)ical labs-on-a-chip for life sciences and the grant involves a budget of 2.4 M€ for a total of 5 Phd projects with the aim to develop new electrochemical techniques for health and life science applications in Lab-on-a-Chip devices. Within the grant this project is entitled *Redox cycling characterization of surface linked E-DNA using SECM* and it is strongly linked to a second project entitled *Surface modification for electrochemically amplified biosensing*. The combined aim of these projects is

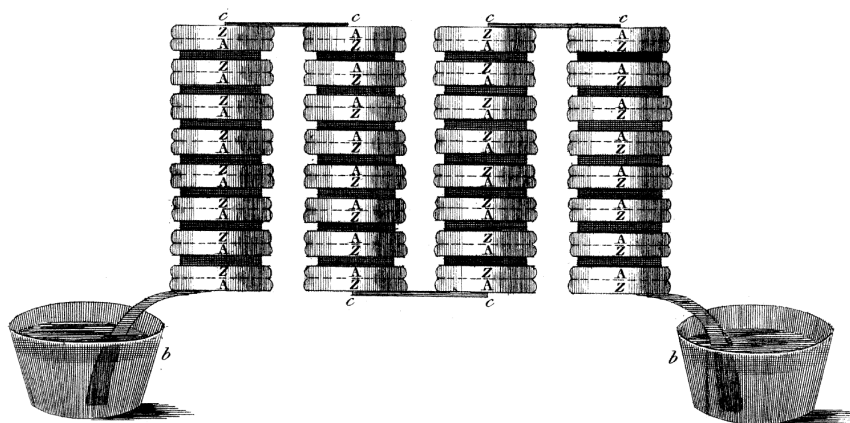


Figure 1.1: The first battery in history: the voltaic pile by Alessandro Volta. Stacks of silver and zinc disks are alternated with wet cloth soaked in salt water. When the ends of the pile are connected through a wire, an electric current is obtained. Image adopted from [2]

the detection of biomolecules such a DNA, using redox cycling and surface linked electroactive molecules such as electrochemically labeled DNA (E-DNA). While molecule synthesis is convenient on the small scale, electrode fabrication on the other hand, is more convenient on the large scale. In this project they had to meet each other halfway for the development of a twin electrode design featuring surface attached molecules undergoing redox cycling.

1.3 Outline

To establish a theoretical background for the following chapters, electrochemical basics such as (non)faradaic processes, kinetics and mass transport are described in chapter 2. These electrochemical basics are followed by the theory of surface attached electrochemistry and redox cycling. The effects of surface attachment on single electrode chronoamperometric measurements such as cyclic voltammetry (CV) are discussed, as well as various dual electrode measurement techniques employing the concept of redox cycling.

The application of redox cycling in fields ranging from fundamental electrochemistry to imaging and biosensing is discussed in chapter 3. The chapter starts with a brief historical overview of the development of redox cycling based devices, followed by a review of recent applications that make use of redox cycling, such as DNA sensing and the study of flow in nanochannels.

During this Phd project a new electrochemical mode of operation was investigated, which we labeled Differential Cyclic Voltammetry (DCV). Analytical expressions were derived for a thin layer cell geometry and these expressions matched experimental results obtained using a scanning electrochemical microscope (SECM). This is reported in Chapter 4.

In chapter 5 the results are shown for experiments where ferrocene labeled polyethylene glycol molecules (PEG-fc) were attached to gold electrodes. The obtained surface density and stability is evaluated, followed by an investigation of the voltammogram shape obtained for CVs at varying concentrations of the background electrolyte NaClO_4 . A correlation is observed between the background electrolyte concentration and the measured formal potential of the PEG-fc molecules. This shift is attributed to ion pairing.

During the fabrication of electrodes designed for redox cycling of surface attached molecules, an oxidized layer of titanium was found to block the electrochemical response of freely diffusing ferrocenedimethanol molecules. This was further investigated as a possible protection layer for gold electrodes being able to provide an alternative to gold cleaning which typically needs to be performed prior to electrochemical experiments. The result are briefly reported in chapter 6.

In chapter 7 the fabrication of nanospaced electrodes is reported. Using edge lithography a 50 nm gap was defined between two gold electrodes. To confirm their use for electrochemistry, measurements were performed in a ferrocenedimethanol solution. Both single electrode CVs and amplified CVs were recorded and compared to finite element simulations. The electrodes showed reversible kinetics and are therefore suited for electrochemistry.

These electrodes were subsequently modified with PEG-fc molecules and this is reported in chapter 8. Two electrode configurations were used. One, the planar nanogap device reported in chapter 7 and two, a nanofluidic thin layer cell fabricated in the group of Lemay. Redox cycling currents were observed for both devices. However, at this time it is not possible to determine which part of the current is contributed by the surface attached molecules and which part is due to freely diffusing molecules.

Finally in chapter 9 conclusions are drawn and recommendations are given for future research into redox cycling of surface attached molecules.

Bibliography

- [1] L. Galvani. *De viribus electricitatis in motu musculari commentarius*. 1792. 2
- [2] A. Volta. *Philosophical Transactions of the Royal Society of London*, **90**:403–431, 1800. 3
- [3] A. Volta. *Philosophical magazine*, **7**(28):289–311, 1800. 2
- [4] G. Aldini. *Essai theorique et experimentale sur le galvanisme (2 vol.)*. Fournier et Fils, Paris, 1804. 2
- [5] M. Piccolino. *Brain Research Bulletin*, **46**(5):381–407, 1998. 2
- [6] W. Nicholson and C. Carlisle. *Journal of Natural Philosophy, Chemistry and the arts*, **4**:179–187, 1801. 2
- [7] M. Faraday. *Philosophical Transactions of the Royal Society of London*, **124**:77–122, 1834. 2

2

Theory of electrochemistry and redox cycling

The fundamentals of electrochemistry form the basis of all measurements reported in this thesis. To establish a background for further chapters, electrochemical basics such as (non)faradaic processes, kinetics and mass transport are described. This is followed by a discussion on the use of single electrode measurement techniques at macro and micro electrodes for the measurement of freely diffusing or surface attached redox mediators. The chapter is finished with an overview of the various dual electrode measurement techniques employing the concept of redox cycling.

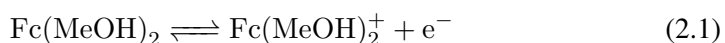
2.1 Electrochemistry fundamentals

This section is based on theory from Electrochemical Methods: Fundamentals and Applications by Bard and Faulkner, and Understanding Voltammetry by Compton and Banks [1, 2].

The measurements reported in this thesis are made using outer sphere redox mediators such as ferrocene and ruthenium hexamine. During the reported experiments, these redox mediators exchange electrons with electrodes instead of exchanging electrons with other chemicals. Reactions that are taking place at the interface between the electrolyte and the electrode are also known as heterogeneous reactions. These reactions are influenced, not only by the kinetics of the molecule itself, but also by other parameters such as mass transport.

2.1.1 Electrode potential

Consider the redox couple ferrocenedimethanol and ferroceniumdimethanol of which the half reaction is



with a concentration of C_{red} [M] and C_{ox} [M] respectively. For this situation the equilibrium voltage, E [V] at an electrode can be calculated through the change in free energy

$$E = -\frac{\Delta G}{nF} \quad (2.2)$$

with ΔG the change in free energy [J], F the faraday constant [C/mol], and n the number of electrons involved in the half reaction. The change in free energy can be found by summing over all the potential energy of the species involved.

$$\Delta G = \sum_{i=1}^{\infty} \mu_i s_i \quad (2.3)$$

where s_i is the stoichiometric coefficient and μ_i the chemical potential of species i [J/mol] which can be described by

$$\mu_i = \mu_i^0 + RT \ln \frac{m_i}{m_0} \gamma_i \quad (2.4)$$

with μ_i^0 an intrinsic species property [J/mol], R the gas constant [J/(mol K)], T the temperature [K], m_i the molality [mol/kg], m_0 the standard molality [mol/kg], and γ_i

the activity coefficient. For dilute aqueous solutions the molality is equal to molarity so we can substitute C_i and C_0 for m_i and m_0 respectively.

$$\mu_i = \mu_i^0 + RT \ln \frac{C_i}{C_0} \gamma_i \quad (2.5)$$

If only the ferrocenedimethanol couple is present, putting together equations 2.2, 2.3, and 2.5 gives

$$E = \frac{\mu_{ox} - \mu_{red}}{nF} + \frac{RT}{nF} \ln \frac{C_{ox} \gamma_{ox}}{C_0} - \frac{RT}{nF} \ln \frac{C_{red} \gamma_{red}}{C_0} \quad (2.6)$$

which can be simplified to

$$E = E^0 + \frac{RT}{nF} \ln \frac{C_{ox}}{C_{red}} + \ln \frac{\gamma_{ox}}{\gamma_{red}} \quad (2.7)$$

where E^0 is the standard potential of the redox couple [V]. Generally the activity coefficients of a species are unknown and influenced by factors such as the ionic strength of the electrolyte and ion pairing. As a result equation 2.7 is often rewritten in the form

$$E = E^{0'} + \frac{RT}{nF} \ln \frac{C_{ox}}{C_{red}} \quad (2.8)$$

with $E^{0'}$ the formal potential [V], a parameter which is experimentally determined¹. This equation is also known as the Nernst equation and it relates the observed electrode potential to the concentration of the redox species that are present.

2.1.2 Electrode reactions

Rewriting the Nernst equation it becomes clear that it is possible to change the concentration ratio at the electrode surface by applying the appropriate potential.

$$C_{ox}^{el}/C_{re}^{el} = e^{(E^{applied} - E^{0'})/(RT/nF)} \quad (2.9)$$

If the applied potential results in a change in concentration ratio at the surface compared to the bulk, conversion of ions from oxidized to reduced state or vice versa must take place at the electrode. The speed at which this process takes place is given by the flux at the electrode surface which is related to the current by

$$I = nFAN \quad (2.10)$$

¹formal potential and standard potential are easily mixed up. The formal potential is measured and depends strongly on experimental parameters, whereas the standard potential is an intrinsic property of a redox couple that should always have the same value.

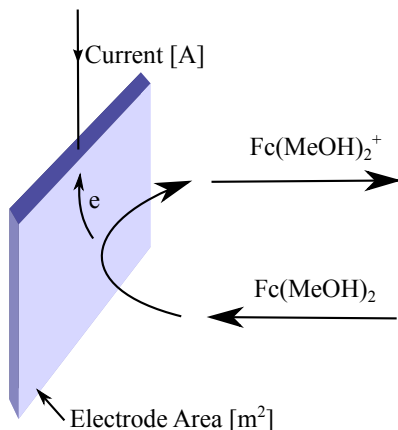


Figure 2.1: Illustrating the concept of a half reaction at an electrode. $Fc(MeOH)_2$ is converted to $Fc(MeOH)_2^+$ and the obtained flux is governed by mass transfer towards the electrode and electron transfer at the electrode.

with I the current [A], n the number of electrons involved in the reaction, A the electrode area [m^2], F the Faraday constant, and N the flux [$mol/(m^2s)$]. The flux at the electrode is determined by a number of processes such as mass transfer, electron transfer at the electrode, adsorption, crystallization, and catalysis. The slowest process determines the obtained flux and is called the rate determining step. For the redox mediators used in this thesis the flux is determined only by the first two processes: mass transfer towards the electrode and electron transfer at the electrode surface. This is shown schematically in figure 2.1.

2.1.2.1 Mass transport

The flux of ions in an electrolyte is the sum of three individual mass transfer processes. A flux of ions as a result of a concentration gradient is called diffusion. Charged ions can be moved if an electric field is applied, in which case it is called migration. If the electrolyte itself is moving and dragging the ions along, the process is called convection. These three mass transfer processes are combined into what is known as the Nernst-Planck equation.

$$\vec{N}_i = \underbrace{-D_i \nabla C_i}_{diffusion} - \underbrace{\frac{n_i F}{RT} D_i C_i \nabla \Phi}_{migration} + \underbrace{C_i \vec{u}}_{convection} \quad (2.11)$$

Where D_i is the diffusion coefficient [m^2/s], n_i the number of electrons involved in the reaction, $\nabla \Phi$ the electric field, and \vec{u} the liquid flow [m/s]. For experiments reported

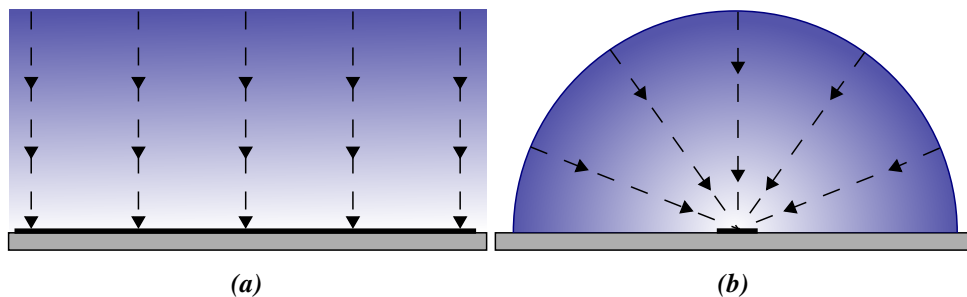
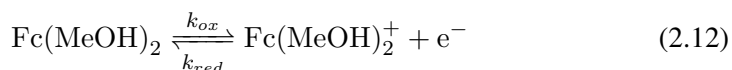


Figure 2.2: Difference between (a) linear and (b) hemispherical diffusion

in this thesis, a background electrolyte was added in order to eliminate migration and experiments were conducted under stagnant conditions. As a result, diffusion is the only form of mass transport present. Depending on the size of the electrode the nature of the diffusive layer changes from linear to hemispherical as is shown in figure 2.2. The effect of these diffusive regimes on the observed current is investigated in more detail in section 2.2.

2.1.2.2 Electron transfer

Besides mass transport, the flux is also determined by the speed of electron transfer at the electrode. This speed is described by the Butler-Volmer model for electrode kinetics. Consider the redox couple from section 2.1.1



with rate constants k_{ox} and k_{red} . These rate constants are given by

$$k_{red} = k_s e^{-\alpha(E_{applied} - E^{0'}) \frac{F}{RT}} \quad (2.13)$$

$$k_{ox} = k_s e^{(1-\alpha)(E_{applied} - E^{0'}) \frac{F}{RT}} \quad (2.14)$$

which is essentially a rewrite of the Arrhenius equation replacing the free energy by a voltage difference, with k_s the standard rate constant [m/s] which is a measure for the reactivity of a redox couple, and α the transfer coefficient which typically has a value of 0.5. Using these rate constants, the flux resulting from oxidation or reduction (N_{ox} and N_{red}) can be calculated by multiplying with the concentration of the reactant at

the surface of the electrode.²

$$N_{ox} = k_{ox} \cdot C_{red}^{el} \quad (2.15)$$

$$N_{red} = k_{red} \cdot C_{ox}^{el} \quad (2.16)$$

These two fluxes can be combined in order to calculate the net flux at the electrode resulting from electron transfer N_{et}

$$N_{et} = k_{ox} \cdot C_{red}^{el} - k_{red} \cdot C_{ox}^{el} \quad (2.17)$$

From equation 2.13, 2.14, and 2.17 follows that the direction of the flux can be influenced by the application of an electrode potential. If the applied potential is higher than the formal potential, the rate constant for oxidation is higher than the rate constant for reduction and the net result will be a conversion of ions from reduced to oxidized state. If the applied potential is lowered to values below the formal potential, the reverse happens and reduction becomes favorable. This process is strongly influenced by the value of the standard rate constant. For the redox couples used in this thesis, ruthenium hexamine, ferrocenedimethanol, and ferrocene, the rate constants are > 1 cm/s with values depending on the electrolyte that is used [3–5]. This is considered to be fast and it is typical of outer sphere one electron transfer processes [1]. As a result, the system quickly reaches its steady state concentration ratio as defined by the Nernst equation with mass transfer determining the flux at the electrode.

2.1.3 Electrochemical cell

In practice electrochemical reactions cannot be studied using a single electrode because the electrical circuit must be closed to allow the flow of electrons. As such, an electrochemical cell requires at least two electrodes connected through an electrolyte. The chemical reactions taking place in this cell are two independent half reactions, each describing the chemical changes at one of the electrodes. Generally only one of the two half reactions is investigated and the electrode at which this reaction occurs is called the working electrode. The other electrode is constructed such that the potential remains stable during experiments, and this electrode is called the reference electrode. Given that the reference electrode is stable, any changes in the electrochemical cell

²For outer sphere redox couples adsorption is not needed for electron transfer to take place, which means the definition of surface concentration is the concentration of redox species within tunneling distance of the electrode.

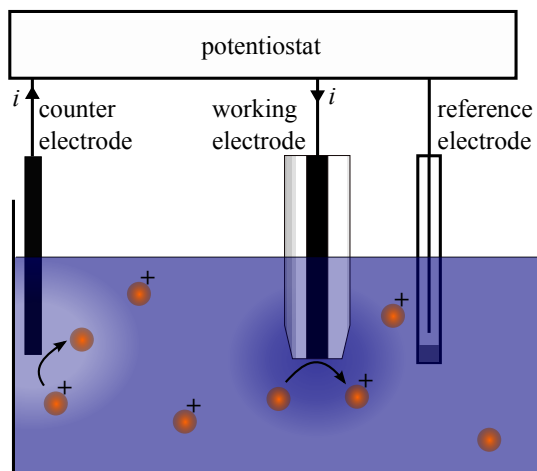


Figure 2.3: Example of a three electrode chemical cell consisting of a working, counter and reference electrode connected to a potentiostat.

can be attributed to the working electrode. Examples of reference electrodes used in measurements reported in this thesis are the silver-silver chloride electrode and the mercurous-mercurous sulphate electrode.

However, while these electrodes offer a stable potential in equilibrium, if enough current flows through the reference electrode, the concentration of its ions can be changed such that a potential shift occurs.³ This shift in the electrode potential is of course undesired. To eliminate this effect a third electrode is introduced which is called the counter electrode. An example of a three electrode chemical cell is shown in figure 2.3. The counter electrode acts as a sink for the working electrode current, eliminating the need for current to flow through the reference electrode and thereby increasing its lifetime. The hardware that controls the electrode potentials and monitors the currents is called a potentiostat. For redox cycling measurements an additional working electrode is needed and this requires a potentiostat capable of controlling the potential of two working electrodes. Potentiostats with this ability are known as bipotentiostats.

2.1.4 Non-faradaic processes

To eliminate migration, a background electrolyte is typically added to the solution, resulting in a high concentration of charged ions. If a potential is applied to the electrode,

³Microelectrodes often draw currents in the < 1 nA range. For these situations it is acceptable to use a two electrode setup [2]. This can be convenient if space for the electrodes is limited.

the electric field will either attract or repel these charged ions. As the background is meant to be inert, this charge cannot be transferred through the electrode-electrolyte interface resulting in an accumulation of charge at the interface. This is analogous to the behavior of a capacitor, with charged electrons on one side and charged ions on the other. It is due to these two charged layers that the capacitance is named double layer capacitance. If the potential is changed by E , this double layer capacitance results in a charging current

$$i_c = \frac{E}{R_s} e^{-t/R_s C_d} \quad (2.18)$$

with R_s the solution resistance [Ω], t the time [s], and C_d the double layer capacitance [F]. If the voltage is not stepped but ramped, as occurs in techniques like cyclic voltammetry, the charging current becomes

$$|i_c| = C_d \nu \quad (2.19)$$

where ν is the scanrate [V/s]. These charging currents are added to the current obtained through electrochemistry. Since the chemical reactions are of interest, the additional offset due to charging of the double layer can be regarded as unwanted. How this effects the various electrochemical measurement techniques is amongst others investigated in the following section.

2.2 Amperometry

In the following section various modes of amperometry are described. The response of each of these modes of operation is described assuming that diffusion is the only means of mass transport, and that the kinetics of the redox couple involved are fast enough for the charge transfer at the electrode to be diffusion limited, unless mentioned otherwise.

2.2.1 Chronoamperometry

In chronoamperometry a potential is applied to an electrode and the resulting current is measured. Rapidly a concentration profile is set up between the electrode surface and the bulk. This concentration profile depends strongly on the size of the electrode, as was already mentioned during the section regarding mass transport. For large electrodes, the diffusion profile is effectively one dimensional and perpendicular to the electrode surface. For this situation the response is given analytically by the Cottrell equation

$$i_{macro}(t) = nFAC_i^* \sqrt{\frac{D_i}{\pi t}} \quad (2.20)$$

with C_i^* the bulk concentration of the reactant i and D_i its diffusion coefficient. For smaller disk shaped electrodes, the current consist of two components: the time dependent Cottrell current, and a steady state current⁴

$$i_{micro}(t) = nFA C_i^* \sqrt{\frac{D_i}{\pi t}} + 4nFrD_i C_i^* \quad (2.21)$$

with r the radius of the electrode. At short timescales, the Cottrell current dominates and at large timescales only the steady state current remains. The time to reach steady state t_{ss} depends on the radius of the electrode and the diffusion coefficient of the reactant.

$$t_{ss} \sim \frac{r^2}{D_i} \quad (2.22)$$

These parameters of course vary from experiment to experiment. However as a rule of thumb, an electrode with a radius in the micrometer range will show a steady state current whereas larger electrodes show a Cottrell current. The smaller electrodes are called microelectrodes or ultramicroelectrodes while the larger electrodes are referred to as macroelectrodes.

2.2.1.1 Chronoamperometry on attached redox species

A special situation arises when chronoamperometry is performed on redox species that are not present in solution but attached to the electrode surface. In this situation mass transport to the electrode does not play a role and the reaction is solely based on electron transfer kinetics. Because diffusion does not play a role, the shape of the chronoamperometric response does not differ between micro and macro electrodes.

As this system is not limited by mass transfer, it can be used to determine the standard rate constant k_s and the transfer coefficient α of a redox couple. This is achieved by plotting the logarithm of the current versus the applied overpotential. This type of plot is known as a Tafel plot. For more information on using Tafel plots for the extraction of the kinetic parameters of surface attached species, see [6–8].

2.2.2 Cyclic voltammetry

Cyclic voltammetry (CV) is a technique where a current is measured while the voltage is swept over a predefined range at a certain scanrate ν [V/s], resulting in a

⁴There are also other electrode shapes, each with their own steady state current and time to steady state. For more information see section 5.3.1 of [1]

voltammogram where the electrochemical reactions of the redox species present can be observed. The voltammogram strongly depends on the electrode size and whether the investigated redox species is attached or not.

2.2.2.1 Macroelectrode

An example of a macroelectrode voltammogram for a freely diffusing redox species is shown in figure 2.4. In this example the voltage is scanned between -0.7 and 0.3 V and the redox species has a formal potential at approximately -0.19 V. The arrows indicate the scan direction. As the applied potential passes the formal potential, the rate constant of electron transfer at the electrode increases exponentially resulting in oxidation of the species in solution. Shortly after this moment, mass transfer becomes the rate limiting process and a decay in the current can be observed similar to Cottrell decay observed for chronoamperometry. After having reached the maximum potential the scan direction is reversed and the same process happens, this time for reduction.

An ideal macroelectrode voltammogram has a few identifying features. The height of the peaks is given by the Randles-Sevcik equation

$$i_p = 0.4463nFAC\sqrt{nF\nu D/RT} \quad (2.23)$$

From this equation follows that a peak height versus the square root of the scan rate plot should be linear and that parameters like the diffusion coefficient can be extracted from the slope. The distance between the peaks is $2.3RT/nF$ or 59 mV for a redox couple with $n = 1$ at 25 °C [1]. The formal potential is located in the middle between the two peak voltages

$$E^{0'} = \frac{E_{p_{ox}} + E_{p_{red}}}{2} \quad (2.24)$$

2.2.2.2 Microelectrode

An example of a microelectrode voltammogram is shown in figure 2.5. Similar to the chronoamperometry result, a microelectrode voltammogram approaches a steady state. In the example shown the formal potential is 0 V, and the applied potential is scanned from -0.2 to 0.2 V. As the applied potential passes the formal potential the current increases due to an increase in rate constant. This increase is limited by the steady state current resulting from hemispherical diffusion. This current is given by

$$i_{lim} = 4nFrD_iC_i^* \quad (2.25)$$

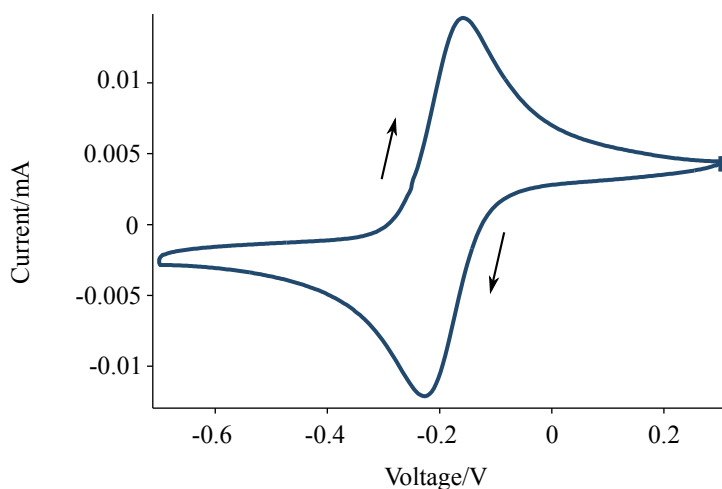


Figure 2.4: Theoretical macroelectrode voltammogram for freely diffusing redox species. Arrows indicate the scan direction.

Besides the limiting current, the microelectrode CV can also be assessed by looking at the potential difference between the potential values at which 1/4th and 3/4th of the limiting current is obtained. Ideally this difference between $E_{3/4}$ and $E_{1/4}$ should be 56.4 mV for $n = 1$ at 25 °C [1]. Deviation from this value is an indication of poor electron transfer kinetics. If the diffusion coefficients of the oxidized and reduced species are equal, the half-wave potential $E_{1/2}$ corresponds to $E^{0'}$. For unequal diffusion coefficients this becomes

$$E_{1/2} = E^{0'} + \frac{RT}{nF} \ln \sqrt{\frac{D_{ox}}{D_{red}}} \quad (2.26)$$

2.2.2.3 Cyclic voltammetry on attached redox species

An example of a voltammogram for a redox species attached to an electrode is shown in figure 2.6. As mass transport does not play a role, the size of the electrode does not matter for the shape of the voltammogram. The shape can be explained using the Nernst equation.

$$\frac{\Gamma_{ox}}{\Gamma_{re}} = e^{(E^{applied} - E^{0'}) / (RT/nF)} \quad (2.27)$$

Where Γ_{ox} and Γ_{red} are the surface concentrations of oxidized and reduced molecules [mol/m²]. A limited amount of molecules is available for oxidation and reduction.

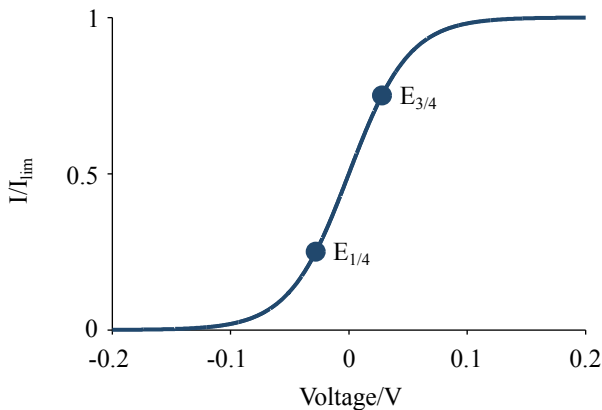


Figure 2.5: Theoretical microelectrode voltammogram for freely diffusing redox species.

Initially at potentials below the formal potential all of the surface attached molecules are in the reduced state. As the potential is increased the surface concentration ratio is changed, resulting in a current. This change in concentration ratio is highest at the formal potential and decreases again for higher values. If the applied potential is sufficiently above the formal potential, all surface attached species have become oxidized and there is nothing left to oxidize, resulting in an approach to zero current for higher potentials. As the potential is reversed, the same process occurs again, this time for reduction.

Key parameters in the shape of the voltammogram are the peak height i_p , the peak width at half maximum $\Delta E_{p1/2}$ and the separation between the peaks. Because mass transport is not present, the maximum change in surface concentration occurs at the formal potential for both the forward and backward scan and as a result, the separation between the oxidation and reduction peak should be zero. The width of the peak at half of the maximum value should be 90.6 mV for $n = 1$ at 25 °C [1]. The height of the peak is given by

$$i_p = \frac{n^2 F^2}{4RT} \nu A \Gamma_{tot} \quad (2.28)$$

where Γ_{tot} is the sum of the surface concentrations of the reduced and oxidized species.

2.2.3 Amperometry and non-faradaic processes

The previously described voltammogram shapes are those for ideal circumstances such as the absence of double layer charging currents. Double layer charging currents

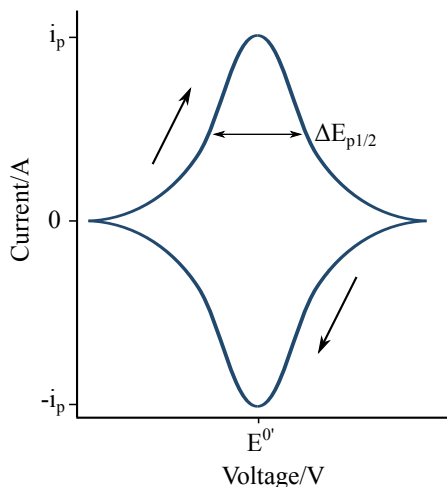


Figure 2.6: Theoretical voltammogram for an electrode with attached redox species. Arrows indicate scan direction. Adapted from [1].

appear as a positive offset in the forward scan and a negative offset in the backward scan. The higher this offset, the more challenging it becomes to measure the faradaic part of the current, especially at low concentrations. This is why for freely diffusing redox species a microelectrode is favorable. This can be explained by looking at the scaling of the current with respect to the electrode area. From equation 2.25 follows that the faradaic current for a microelectrode scales with r . The capacitive current however, scales with the area (πr^2). This means that for decreasing electrode sizes the capacitive current decreases faster than the faradaic current. As a result, a better faradaic current to capacitive current ratio is obtained for small electrodes.

However, as can be seen in equation 2.28, for surface attached species the faradaic current scales with the area. As such, there is no benefit in scaling down the electrode size when measuring surface attached species. This means that for surface attached experiments, macroelectrodes are more favorable as these provide a higher absolute current, resulting in a better signal to noise ratio.

2.3 Redox cycling

In essence redox cycling (RC) is the repeated oxidation and reduction of a reversible redox couple. For this process to occur the redox couple must be able to exchange electrons, either with another compound in solution, or at an electrode. This concept is known in areas such as biology [9–11], electrode enzyme interactions [12, 13],

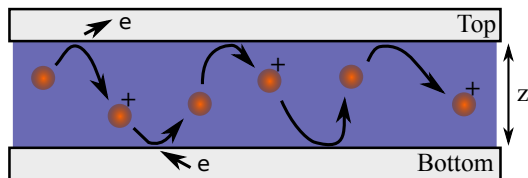


Figure 2.7: Example of a redox cycling configuration. Two parallel plate electrodes with one electrode oxidizing and the other reducing, separated by a distance z .

and photochemistry [14, 15]. In these areas, redox cycling involves either a single electrode or none at all.

In this thesis however, the focus is on systems where RC is performed using two electrodes, where one electrode is held at an oxidizing potential and another at a reducing potential. When RC is referred to in this thesis it refers to this dual electrode technique. The advantage of RC is that each molecule can contribute to the measured current multiple times, thus effectively creating (electro)chemical signal amplification. While in the next chapter the focus is on the history and application of this technique, in this section the various modes of operation are highlighted. As a frame of reference, consider a geometry consisting of two parallel plates as is shown in figure 2.7. The two plates are separated a certain distance z apart and between the plates a redox couple is present in solution at concentrations C_{ox} and C_{red} . While this is not the only geometry suitable for RC it is the most intuitive one when it comes to explaining the response of the system to the various applied potentials. As such, it will be used in the next sections to explain the different modes of operation for RC.

2.3.1 Steady state redox cycling

The basic mode of operation for redox cycling is to apply two steady state potentials, one oxidizing and one reducing and this gives rise to a steady state current as is shown in figure 2.8. This can be explained by seeing what happens when these potentials are applied to the electrodes. Suppose the top electrode is oxidizing and the bottom reducing. At each electrode one of the species is fully converted to the other, resulting in surface concentrations

$$C_{ox}^{top} = C_{ox}^* + C_{red}^* \quad (2.29)$$

$$C_{red}^{bot} = C_{ox}^* + C_{red}^* \quad (2.30)$$

$$C_{red}^{top} = 0 \quad (2.31)$$

$$C_{ox}^{bot} = 0 \quad (2.32)$$

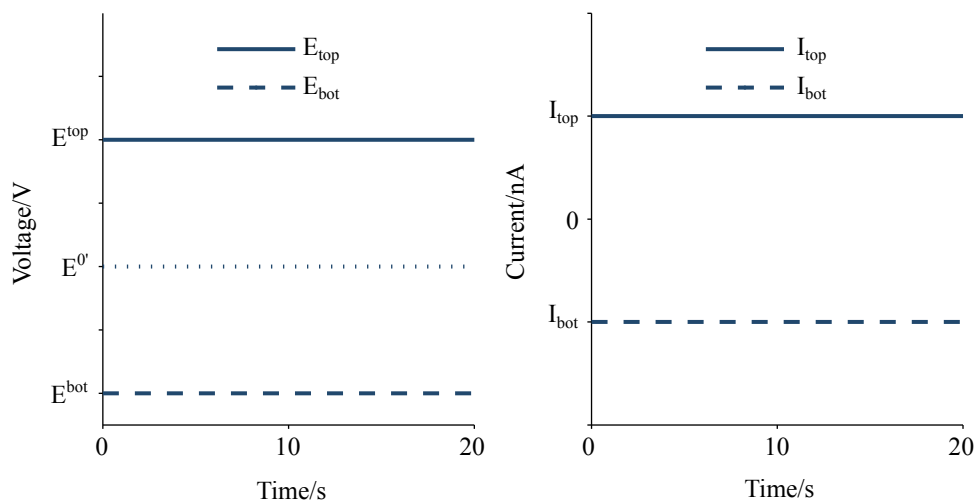


Figure 2.8: Steady state RC experiment, both electrode potentials remain constant over time. One electrode is set to an oxidizing potential and the other to a reducing potential. The result is a constant current.

where C_{ox}^* and C_{red}^* are the bulk concentrations. These concentrations result in a flux which is given by the one dimensional solution for diffusive mass transport, also known as Fick's first law of diffusion

$$N_i = -D_i \frac{dC_i}{dx} \quad (2.33)$$

As both concentration gradients are equal but with a reversed sign, the flux only needs to be calculated for a single species. Combining equation 2.10 with 2.33 the resulting current for the top electrode is found

$$I_{top} = \frac{nFAD_{ox}C_{ox}^{top}}{z} \quad (2.34)$$

This current is independent of time which means a steady state current is obtained. The only time the current is not at steady state is in the initial moments that the concentration gradient is set up. For a typical redox cycling system spaced micrometers or less apart, this is achieved in milliseconds. Additional molecules can also diffuse towards the electrode from the side, resulting in an additional current component. The relative contribution of flux from the sides is determined by the size of the electrodes and the spacing z . For the sake of convenience the flux from the sides is assumed negligible for this system.

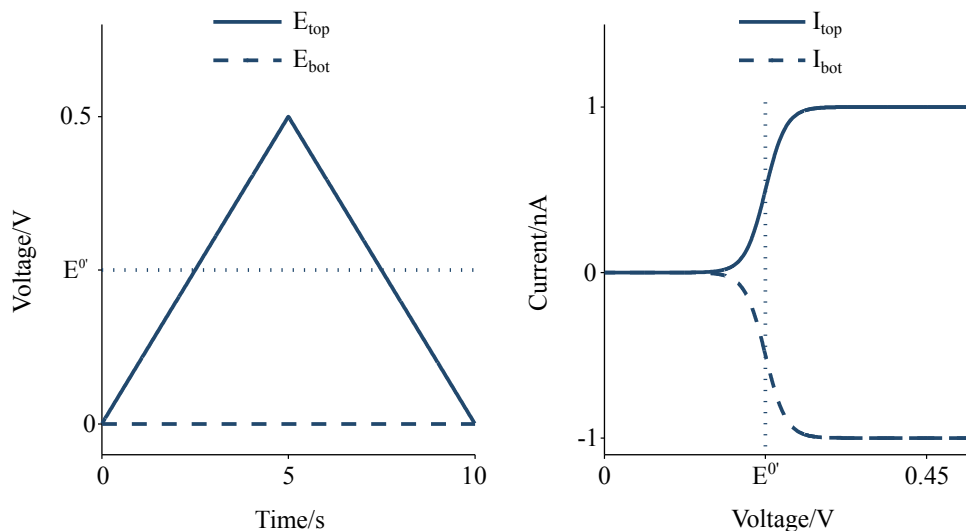


Figure 2.9: Amplified CV experiment. One electrode is at a stationary potential while the other is scanned similar to a cyclic voltammetry experiment. The result is a voltammogram similar to that obtained at a microelectrode CV. However, in this scenario the signal is amplified by redox cycling.

If the redox species that is present in solution is already known and the system is used for an application such as concentration detection, this system is already suitable as appropriate potentials can be applied based on the known formal potential of the redox species. If however, more information is required during the measurement, such as the determination of the formal potential, a slightly more complex strategy can be desired where at least one of the two electrode potentials is not stationary.

2.3.2 Amplified cyclic voltammetry

A technique which offers these capabilities is one where one of the electrodes is kept at a stationary potential while the other electrode potential is swept from reducing to oxidizing state. We label this technique amplified cyclic voltammetry⁵ because one of the applied potentials is similar to a CV experiment and the shape of the voltammogram is that of a microelectrode CV with the added benefit of redox cycling based amplification. An example of the applied potentials and resulting voltammogram is shown in figure 2.9.

⁵This technique should not be confused with ACV, which stands for alternating current voltammetry. This technique is not discussed in this thesis.

Suppose the bottom electrode is kept at a reducing potential while the top electrode is swept from reducing to an oxidizing state and back again. Initially as both are reducing, all of the molecules confined between the two plates will be reduced. If there are any oxidized molecules in the bulk solution these can diffuse towards the electrodes from the side resulting in a negative offset to the obtained current. As the potential of the top electrode is increased and it passes the formal potential, its surface concentration is changed from fully reduced to fully oxidized as given by equation 2.9, resulting in a change in concentration gradient between the two electrodes. Once the top electrode potential is high enough to have oxidized all molecules near the surface a similar concentration gradient (and resulting current) is obtained as was determined for the steady state scenario.

Using this method not only an absolute current is obtained but also the formal potential can be determined. In the voltammogram the formal potential is the voltage at which the concentration gradient is changed and the system 'turns on'. More specifically, the voltage at which the current is half the steady state value. This method has an additional benefit. If the current at the stationary electrode is measured it does not suffer from capacitive charging currents, unlike single electrode scanning techniques. Additional information can be found in papers by Zoski et al. and Nioradze et al. [16, 17]

2.3.3 Differential cyclic voltammetry

The third redox cycling technique is differential cyclic voltammetry (DCV). In this technique a CV waveform is applied on one electrode while the same waveform with a potential offset is applied to the other electrode. Due to this offset we have named this technique differential cyclic voltammetry. Initially this technique was shown as a proof of concept [18], followed by the development of analytical expression for the thin layer cell geometry [19]. A brief explanation of the technique and the derivation of the analytical expressions is given here, for more detail, see chapter 4.

An example of a DCV voltammogram is shown in figure 2.10. If both electrodes are above or below the formal potential they compete for the same reaction and the result is a small current. As the voltage sweep passes the formal potential of a redox species, one of electrodes is oxidizing while the other is reducing, and the current is amplified. This results in a peak in the voltammogram where the peak height is related to the concentration of the species present and the location of the peak supplies information regarding the species' formal potential.

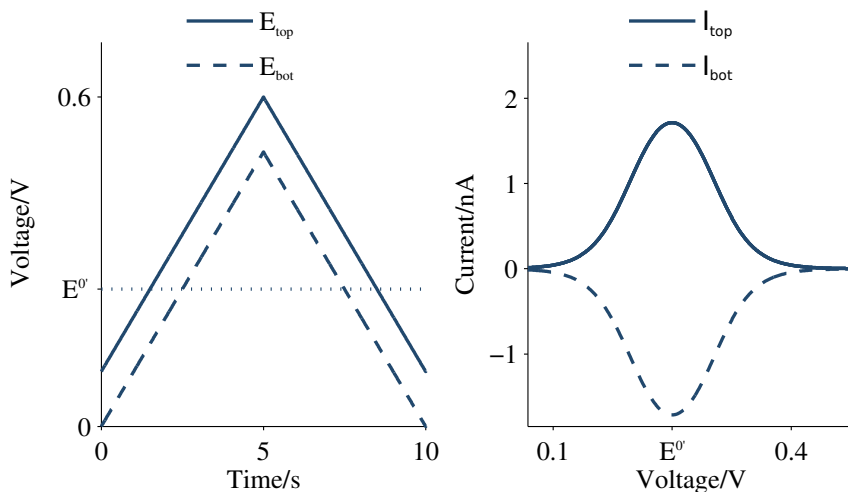


Figure 2.10: DCV experiment. Both potentials are scanned in a way similar to CV with one of the potentials at an offset compared to the other. If the formal potential of a species is passed, one of the electrodes is oxidizing and the other is reducing. This results in a peak in the voltammogram.

The shape of the voltammogram is given by the following equation

$$I = -nFAD \frac{C_{re}^{top} - C_{re}^{bot}}{z} \quad (2.35)$$

with C_{re}^{top} and C_{re}^{bot} given by

$$C_{re}^{top} = C^{bulk} / (e^{(E^{top} - E^0)/(RT/nF)} + 1) \quad (2.36)$$

$$C_{re}^{bot} = C^{bulk} / (e^{(E^{bot} - E^0)/(RT/nF)} + 1) \quad (2.37)$$

with C^{bulk} the sum of the concentrations of the oxidized and reduced state of a species and E^{bot} and E^{top} the applied potentials. The optimal separation between the top and bottom voltage is 0.1 V.

2.3.4 Approach curves

In this special case of redox cycling techniques, the applied potentials remain constant similar to section 2.3.1, but the distance between the electrodes is varied. This technique is used in scanning electrochemical microscopy to approach conductive surfaces, which is why the curve shown in figure 2.11 is called an approach curve.⁶

⁶If an isolating surface is approached, a negative feedback is observed. For a detailed mathematical investigation of both feedback types see [20–22].

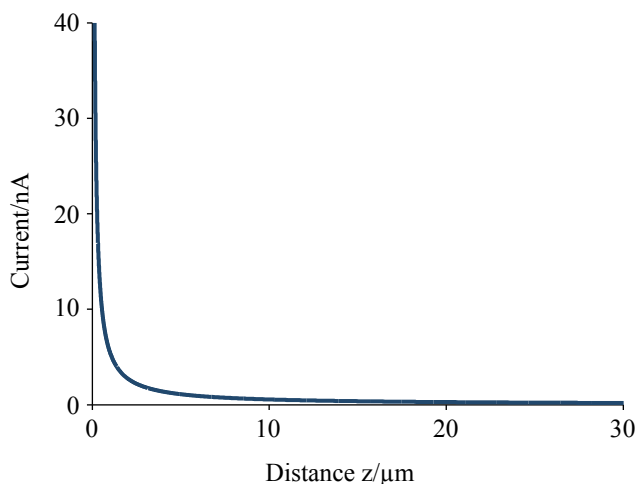


Figure 2.11: Positive approach curve based on the redox cycling effect. If the distance between the two electrodes is decreased, the cycling current increases.

In this figure the current of the top electrode is plotted versus the distance between the top and bottom electrode with the top electrode at an oxidizing potential. As already followed from equation 2.34, for a thin layer cell geometry the redox cycling amplification is inversely proportional to the distance z .

An interesting effect that is not used in other applications but is typical of SECM approach curves is that of passive feedback. The bottom electrode does not necessarily need to be set at a reducing potential for feedback to occur, provided the bottom electrode is much larger than the top electrode. If for example, the solution contains only the reduced form of a redox couple, the bottom electrode will obtain a reducing potential as is determined by the Nernst equation. If the top electrode is set to an oxidizing potential and approached to the surface it will locally change the concentration ratio of the redox couple. For the bottom electrode this local change in concentration ratio means a local potential change. However, this now means we have a substrate electrode which is subject to two concentration ratio's, one for the bulk and one below the top electrode. According to the Nernst equation this should result in a potential difference between parts of the bottom electrode. This potential difference results in a flow of electrons within the metal which in turn drives a counter reaction to eliminate the potential difference. The substrate electrode starts to reduce molecules below the top electrode and oxidizes molecules in areas away from the top electrode.

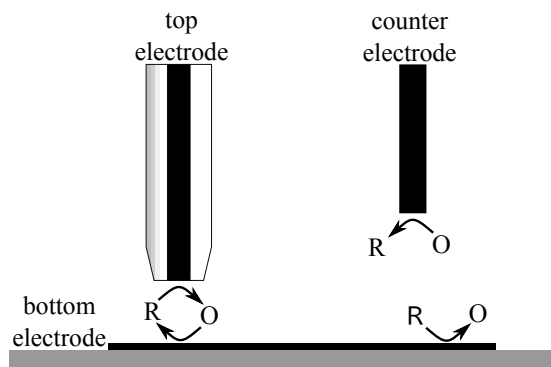


Figure 2.12: The concept of passive positive feedback in scanning electrochemical microscopy. The bottom electrode is left floating but it still contributes to a redox cycling current because of its larger size and connection to the bulk.

In the conventional redox cycling configurations the current for the bottom electrode is supplied directly to the electrode itself. In this configuration however, the additional current is supplied by the counter electrode and there is no net current flow into or out of the bottom electrode. This concept is shown in figure 2.12.

This technique could have its benefits for on-chip redox cycling as well. The thin layer cell configuration is easily evaluated analytically and by using a floating electrode the other electrically addressable electrodes can be fabricated in the same plane. This will allow easier chip to potentiostat connections.

2.4 Application of theory

The theory described in this chapter can be used for a number of applications, which for redox cycling are described in chapter 3. The difference between CVs of freely diffusing and surface attached molecules is used to determine the presence of surface attached molecules in chapter 5. In chapter 8 the theory of amperometry and redox cycling is combined for the detection of surface attached molecules by using redox cycling.

Bibliography

- [1] A. J. Bard and L. R. Faulkner. *Electrochemical Methods: Fundamentals and Applications*. Wiley, 2nd edition, 2001. ISBN 978-0-471-04372-0. 8, 12, 15, 16, 17, 18, 19
- [2] R. G. Compton and C. E. Banks. *Understanding Voltammetry*. Imperial College Press, 2nd edition, 2011. ISBN 978-84816-586-1. 8, 13
- [3] P. Sun and M. V. Mirkin. *Analytical Chemistry*, **78**(18):6526–6534, 2006. 12
- [4] M. A. G. Zevenbergen, B. L. Wolfrum, E. D. Goluch, P. S. Singh, and S. G. Lemay. *Journal of the American Chemical Society*, **131**(32):11471–11477, 2009.
- [5] M. V. Mirkin, T. C. Richards, and A. J. Bard. *The Journal of Physical Chemistry*, **97**(29):7672–7677, 1993. 12
- [6] M. Ravenscroft and H. Finklea. *The Journal of Physical Chemistry*, **98**:3843–3850, 1994. 15
- [7] A. Eckermann, D. Feld, J. Shaw, and T. Meade. *Coordination Chemistry Reviews*, **254**:1769–1802, 2010.
- [8] H. Finklea and L. Liu. *The Journal of Physical Chemistry*, **3654**(96):18852–18858, 1996. 15
- [9] G. M. Cohen and M. d’Arcy Doherty. *The British journal of cancer Supplement*, **8**:46–52, 1987. 19
- [10] S. Yang, Y.-H. Jan, J. P. Gray, V. Mishin, D. E. Heck, D. L. Laskin, and J. D. Laskin. *The Journal of biological chemistry*, 2013.
- [11] P. Gutierrez. *Front Biosci*, pages 629–638, 2000. 19
- [12] F. Hollmann, I. Arends, and K. Buehler. *ChemCatChem*, **2**(7):762–782, 2010. 19
- [13] W. S. Roberts, D. J. Lonsdale, J. Griffiths, and S. P. J. Higson. *Biosens Bioelectron*, **23**(3):301–318, 2007. 19
- [14] W. L. Miller, D. King, J. Lin, and D. R. Kester. *Marine Chemistry*, **50**(1-4):63–77, 1995. 20
- [15] Z. Wang, C. Chen, W. Ma, and J. Zhao. *The Journal of Physical Chemistry Letters*, **3**(15):2044–2051, 2012. 20
- [16] C. Zoski and C. Luman. *Analytical Chemistry*, **79**(13):4957–4966, 2007. 23
- [17] N. Nioradze, J. Kim, and S. Amemiya. *Analytical Chemistry*, **83**(3):828–35, 2011. 23
- [18] M. Odijk, J. Wiedemair, M. J. J. van Megen, W. Olthuis, and A. van den Berg.

- In *IEEE Sensors Conference 2010*, pages 918–922. IEEE, 2010. 23
- [19] M. van Megen, M. Odijk, J. Wiedemair, W. Olthuis, and A. van den Berg. *Journal of Electroanalytical Chemistry*, **681**:6–10, 2012. 23
- [20] R. Cornut and C. Lefrou. *Journal of Electroanalytical Chemistry*, **604**(2):91–100, 2007. 24
- [21] C. Lefrou and R. Cornut. *ChemPhysChem*, **11**(3):547–556, 2010.
- [22] C. Lefrou. *Journal of Electroanalytical Chemistry*, **592**(1):103–112, 2006. 24

3

Redox cycling applications

In this chapter an overview of the technique of redox cycling and its applications is given. Redox cycling is a technique where molecules are repeatedly oxidized and reduced between two electrodes, one electrode oxidizing and the other reducing, thus creating electrochemical signal amplification. A brief historical overview is given, starting with the initial development in the sixties and ending in the last decade with its integration into other experimental setups. This historical overview is followed by a review of the various applications that make use of redox cycling, ranging from DNA sensing to the study of flow in nanochannels. In this review the focus is on the applications of redox cycling, rather than the the development of new fabrication strategies.

3.1 Introduction

In conventional electrochemistry a single working electrode is biased versus a reference electrode in an electrochemical cell containing redox active molecules. Depending on the applied potential, the molecules in solution will be either reduced or oxidized at the electrode surface. The resulting current supplies information regarding the molecules' diffusion coefficient, concentration, and kinetics. However, in this setup each molecule only contributes once to the electrochemical reaction and new molecules need to be transported towards the electrode. As such, the current is quickly limited by mass transfer towards the electrode.

The obtained current can be amplified by using redox cycling. Redox cycling is based on cycling a reversible redox couple between two closely spaced electrodes, where one electrode is held at an oxidizing potential and another at a reducing potential. The advantage of this technique is that each molecule can contribute to the measured current multiple times, thus effectively creating (electro)chemical signal amplification.

Research using redox cycling was pioneered at the group of Reilly in the 1960s [1–4]. They used a twin working electrode setup where one electrode was connected to a fixed substrate and the other to a micrometer positioner. This way a thin-layer cell with parallel electrodes was obtained, which they used to study reactions of the Fe(II)/Fe(III) and quinone-hydroquinone redox couples.

This work was followed in the 1980s by the development of a probe that could move not just in the z direction, but also in x and y [5–7]. This led to the development of the field of “scanning electrochemical microscopy” (SECM) and the setup is called a scanning electrochemical microscope (SECM) conveniently abbreviated in the same way as its field of research. The experiments performed using a SECM are not limited to the redox cycling technique. The various modes of operation and its applications have been thoroughly reviewed over the years [8–12].

Around the same time as the development of SECM the first use of interdigitated electrodes (IDE's) for redox cycling was reported [13]. Using conventional lithography they fabricated planar electrodes spaced 20 μm apart which they used to cycle 1,1-Bis(hydroxymethyl)ferrocene. This first design only had a twin electrode setup, but this was followed by designs with multiple “fingers” [14, 15].

In the years following these developments research has focused on understanding and improving the experimental setups, with new analytical expressions being developed

for specific geometries and finite element modeling of complex systems. Improvements have largely focused on scaling down, as the redox cycling effect increases with decreasing electrode separation. SECM systems have been combined with atomic force microscopes (AFM) [16–19]. For on-chip based redox cycling devices the progress in performance has recently been reviewed by Katelhon et al. [20].

In this review we will focus instead on the applications of redox cycling. Looking across the different designs the aim is to give a general overview of the practical implementations of the redox cycling technique.

3.2 Applications

3.2.1 Biosensing

An area where electrochemical applications are often found is in biosensing. Biologically relevant substances can be measured either directly or by measuring the influence of a measurand on the cycling of a transducing compound. In redox cycling experiments the recorded current is a measure for the concentration of the relevant substance. Below a series of common electrochemical assays is described where redox cycling is applied.

3.2.1.1 Catecholamines

The catecholamines are a family of neurotransmitters such as dopamine, serotonin, adrenaline, and nor-adrenaline. They are all able to undergo redox cycling and they are also medically relevant. Dopamine for example, has been linked to Parkinson's disease [21]. Moreover, dopamine and others are able to provide diagnostic information directly from blood plasma [22]. Most of the work on catecholamine sensing has been performed using microscale IDE's [23–30]. Other types of devices have been thin layer cells [31, 32], micro and nano cavities [33–36], and a single nanogap [37]. An example of sensing in a nanogap is shown in figure 3.1.

Because electrochemistry allows the on-line measurement of catecholamines, it is a very suitable technique for continuous monitoring in clinical environments. In the related field of fast scan cyclic voltammetry this has already lead to in vivo experiments in rat brains for the detection of dopamine and norepinephrine on the subsecond timescale [38, 39]. To our knowledge there have been no reports of in vivo redox cycling experiments or experiments on biological samples.

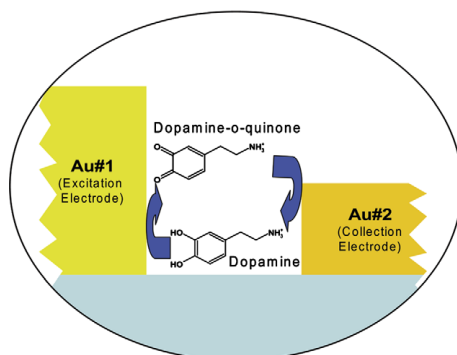


Figure 3.1: Example of dopamine sensing using redox cycling. Dopamine is oxidized to dopamine-*o*-quinone at one electrode, and back to dopamine at the other. Reprinted from McCarty et al. 2010 [37]. Copyright 2010, with permission from Elsevier.

The main challenge of measuring in biological samples like blood is the relatively high background concentration of other redox active species with similar standard potentials. Dopamine for example has blood levels in the sub nM range, while interfering compounds like ascorbic acid and uric acid have a typical concentration of 50 and 400 μM respectively [24, 27]. Luckily, ascorbic acid and uric acid are electrochemically irreversible redox species due to the instability of the oxidized product. This means that using redox cycling it is possible to selectively detect only dopamine, provided the amplification factor is high enough. The independence of clinically relevant interfering ascorbic acid concentrations has been shown [31, 34]. However, this has been shown with catechol concentrations in the μM range. In the group of Niwa there have been successful experiments with an enzyme modified pre-reactor to remove ascorbic acid concentrations up to 10 μM , while keeping detection limits of dopamine below 1 nM [27]. If all of the interferences are removed, lower levels of detection as low as 1 aM are possible [25].

3.2.1.2 Hybridisation detection

Hybridization is the coupling of DNA or RNA strands that have a matching sequence. This process can be used to bind a target sequence by choosing the appropriate probe sequence, and it has its applications in fields such as DNA diagnostics, forensics, and the detection of pathogens.

Two types of hybridization detection strategies employing redox cycling using IDE's have been reported so far. In the detection strategy reported by Zhu et al. the ferro/ferri

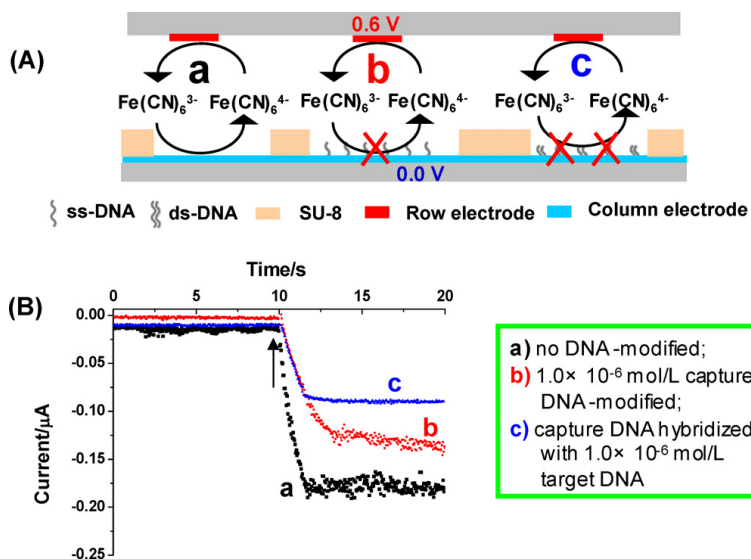


Figure 3.2: (a) Hybridization is detected by influenced mass transport in the channel between the row and column electrode. (b) This results in a decrease in observed current if hybridization occurs. Reprinted from Zhu et al. 2011 [40]. Copyright 2011, with permission from Elsevier.

cyanide couple provides a cycling current between two planar electrodes [40]. The electron transfer at one of the electrodes is influenced by the adsorption of probe DNA and subsequent hybridization with target DNA, as shown in figure 3.2. The introduction of DNA onto the device results in a decrease of the measured current, which allows detection of target concentration down to 30 nM.

Alternatively more sensitive devices have been developed where the redox species is not present initially [41–44]. By means of the enzymatic conversion of p-aminophenyl phosphate (p-APP) to p-aminophenol (p-AP) by Alkaline Phosphatase (ALP), the non cycling p-APP is converted to electrochemically active and reversible p-AP. The ALP is introduced either through labeling of the target strand or through labeling of an additional detection strand. Because initially there is no redox mediator present, this is a “signal on” type of sensor where the current increases with increasing target DNA or RNA concentration. This way a lower limit of detection of 16 fmol was obtained by Elsholz et al. for *E. coli* [43]. Their system was also able to analyze several other pathogens, such as *Pseudomonas aeruginosa*, *Enterococcus faecalis*, *Staphylococcus aureus*, and *Staphylococcus epidermidis*, which are involved in urinary tract infections. The same group has also used their device for the detection of cytomegalovirus,

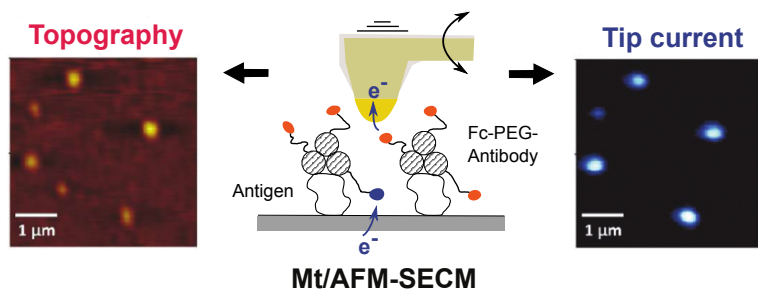


Figure 3.3: Surface attached protein imaging by means of redox immunomarked proteins. Reprinted with permission from Anne et al. 2011 [45]. Copyright 2011, American Chemical Society.

Epstein-barr virus, Hepes simplex virus in multiplex PCR processed clinical blood samples with detection limits of 2 nM [44].

3.2.1.3 Proteins

In advanced biosensors, surface attached proteins such as redox active enzymes play an important role as a transducing element [45]. An example of this is the DNA hybridization sensor using ALP, described in the previous section. A key parameter in the functioning of biosensors is the distribution of these proteins [46]. This distribution of proteins can be imaged using scanning probe techniques such as AFM and SECM. Anne et al. combined these two techniques in order to get both a topographical and electrochemical image of the protein distribution of mouse Immunoglobulin-G (Ig-G) on a gold surface [45]. This was achieved by coupling the Ig-G to its antibody labeled with ferrocene terminated polyethylene glycol (PEG) chains. An image of this sensing scheme is depicted in figure 3.3. Ig-G island were printed onto the gold substrate and subsequently labeled with the antibody. If the AFM probe is in close proximity to the proteins, the ferrocene labels are able to oxidize at the tip and reduce at the substrate. This way an image of the attached proteins is obtained with a resolution in the 100 nm range.

3.2.2 Imaging

As already shown in the previous section, localized redox cycling can provide the means to create an electrochemical image of a substrate. While the field of SECM is quite wide and allows for much more modes of imaging, only applications based on redox cycling will be mentioned.

3.2.2.1 Cells

Electrochemical imaging of cells is an interesting alternative to conventional imaging techniques such as fluorescent labeling because it can provide information on single cells without the requirement of labeling. In the SECM field a lot of work has been done in this area, mostly focused on other modes of operating that do not require a double electrode scheme [10]. This can be attributed due to the fact that a substrate electrode is difficult to combine with traditional petri dish culturing of cells, especially if the intention is to keep the cells alive. However, imaging of cells has been performed on arrays of redox cycling sensors by Ino et al. [47]. They fabricated a 16 by 16 array of interdigitated (IDA) electrodes which they used to analyze ALP activity from mouse embryonic bodies. Their aim is to monitor the differentiation of the embryonic bodies into dopaminergic neurons by first measuring the presence of ALP, and upon differentiation they expect to measure dopamine. The resolution is quite poor with every embryonic body taking up a single pixel. But they expect this can be improved by scaling down the size of the IDE's.

3.2.2.2 Fingerprints

A technique with direct applications in the field of forensics is that of fingerprint imaging [48]. In this example, a fingerprint is applied to a glass or PET substrate which is subsequently put into a magnetron sputtering system to apply a Al-doped ZnO thin film (ZAO). The film is only deposited onto areas that are free from the fingerprint ridges due to preferential condensation of the ZAO on the bare glass or PET substrate, as such a surface with alternating electro active and electro inactive structures is formed. By scanning over the fingerprint, an increase of the current can be observed when the electrode is above the thin film and a decrease can be observed when the electrode is above one of the fingerprint ridges. The concept is illustrated in figure 3.4.

3.2.3 Physical properties

Redox cycling has also been used in the field of analytical chemistry for the determination of molecular properties such as diffusion coefficients and reaction rates. While these parameters have been determined for over a hundred years, starting with the pioneering work from Graham, Fick, and Arrhenius [49–51], for certain species these properties are still unknown due to experimental limitations. For example, in the case of reactions rates, often the limitation is mass transport towards the electrode and not the reaction at the electrode itself.

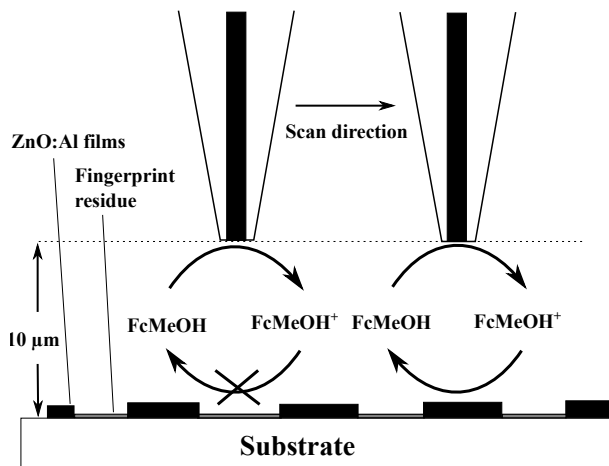


Figure 3.4: Concept of the fingerprint imaging system. Scanning a SECM over an electroactive Al-doped ZnO film. The fingerprint ridges cause a decrease in current and the thin film causes an increase. Reprinted from Zhang et al. 2012 [48], copyright 2012, with permission from Elsevier.

3.2.3.1 Reaction rates

This limitation can be overcome by increasing mass transport towards the electrode by decreasing the spacing between two electrodes. It is for this application that the first redox cycling devices were used by Anderson and Reilley to investigate Fe(II)-Fe(III) and the quinone-hydroquinone system [2, 3]. After the development of the SECM, this new setup was also used to investigate Fe(II) [52] and ferrocene [53]. More recent developments have focused on scaling down to the nanoscale [54, 55], or novel setups [11, 56]. Sun et al. scaled down the SECM system by using disk electrodes with a 70 nm radius, which they could approach to a distance of 5 nm from an electrochemically active substrate. They used this setup to investigate tetracyanoquinodimethane, rutheniumhexamine, ferrocene, and ferrocenemethanol. Zevenbergen et al. scaled down a thin layer cell geometry to a spacing of approximately 50 nm and used this system to investigate the effects of the background electrolytes KCl and NaClO₄ on the rate constant of ferrocenedimethanol. Dimutrescu et al. looked at the reactivity of a single wall carbon nanotube layer with less than 1% surface coverage using (ferrocenylmethyl)trimethylammonium. The rate constants they obtained suggest their sidewalls have considerable activity. This is interesting because for single walled nanotubes it is not yet known exactly at which sites the electron transfer occurs.

3.2.3.2 Diffusion coefficients

When measuring diffusion coefficients using redox cycling, the coefficients of the oxidized and reduced species are combined. Usually it is assumed that the values for the oxidized and reduced species are similar but this is not always so [57–59]. Martin and Unwin have shown this using a SECM by looking at the time it takes to reach steady state in a chronoamperometric response for an electrode positioned close to an electroactive surface. They were also able to extract similar parameters from the difference between approach curves in feedback and substrate generation/tip collection mode. Using this system they found that for the ferro/ferricyanide couple the ratio of diffusion coefficients is approximately 1.17. For p-benzoquinone and its radical, a ratio of 0.7 was found.

3.2.3.3 Single molecule

The first single molecule redox cycling experiments have been performed in the group of Bard [60]. They moved a recessed SECM tip close to a conductive substrate in order to confine a small volume between the tip electrode and the substrate. By analysis of the obtained tip current they claimed the detection of a single diffusing CpFeCpTMA^+ molecule. After this initial result nothing was published on this subject for over 15 years. Recently a new attempt has been made by Zevenbergen et al. [61]. In their thin layer cell with electrodes spaced 70 nm apart they recorded current traces that showed the presence of individual ferrocene molecules. Potentially this could lead to a new detection strategy for enzyme products or neurotransmitter release.

A more fundamental approach with limited applications is that of single molecule analysis using a scanning tunneling microscope (STM) [62]. In this work an STM tip is positioned close to a surface with an electroactive self assembled monolayer (SAM), and a connection is formed between tip and substrate through the SAM. By choosing the appropriate bias potentials they can obtain either a tunneling current or redox cycling enhanced tunneling current. Through analysis of the obtained tunneling current histograms they were able to conclude that they could measure the current transported through a single N,N'-bis(n-thioalkyl)-4,4'-bipyridinium bromide molecule.

3.2.4 Miscellaneous applications

In this section a few examples are highlighted that do not fall into the previous categories, but that are interesting examples nonetheless.

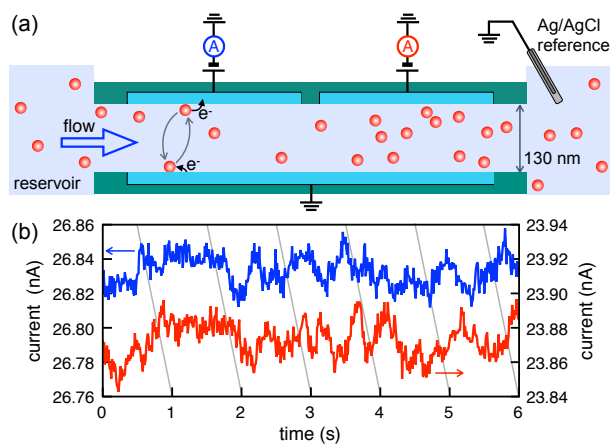


Figure 3.5: (a) Schematic of the flow measuring setup. (b) Time delay between upstream and downstream electrodes allows the calculation of the liquid flow rate. Reprinted with permission from Mathwig et al. 2012 [64]. Copyright 2012 by the American Physical Society.

3.2.4.1 Flow sensing

Typically in fluidic devices for redox cycling, flow is assumed absent and the data is analyzed based upon the assumption of a stationary concentration gradient between the two electrodes. Turning this around, the effect of flow on the obtained current can be used to create a flow sensor. In the work by Li et al. this is achieved by measuring the redox cycling current at two planar electrodes at various vibration speeds [63]. The enhanced mass transport due to displacement of the sensor gives rise to an increase in current, as such a seismic sensor is obtained.

In a more elaborate setup by Mathwig et al., flow was detected by measuring local changes in concentration at two sets of redox cycling electrodes within a nanochannel [64]. In their nanochannel (130 nm high, 5 μm wide) local changes in concentration can be observed which appear as noise on top of the DC redox cycling current. Both electrodes show a similar time trace with a slight shift in time. This can be seen in figure 3.5. The time delay is calculated through cross correlation and is then converted to a flow speed. Using this setup they obtained a lower limit of detection of 10 pL/min, which is the lowest value reported in literature.

3.2.4.2 Contamination sensing

Redox cycling has also been used to determine trace amounts of iron in ultrapure carbon [65]. Using an IDA electrode they were able to determine these trace amounts

at levels lower than the required 5×10^{-5} wt%. The conventional approach to detecting these trace elements is using Graphite-furnace atomic absorption spectrometry (AAS), and they claim their method offers a much cheaper detection method.

3.3 Concluding remarks

The concept of redox cycling in twin electrode systems is almost 50 years old and it has developed into a technique with applications in various fields of research. However, its developments are far from finished. In the area of biosensing, clinically relevant concentrations can already be measured. However, the stability over time of these devices still prevents them from being applied in a clinical setting. If these devices are to transition from proof of concepts to real world applications, additional optimization is needed. The developments in nanofabrication will likely lead to even smaller devices, which should give an impulse to the area of single molecule detection and the study of reaction rates. An example of this is the fabrication of nanospaced electrodes as is discussed in chapter 7 of this thesis.

Bibliography

- [1] D. M. Oglesby, S. H. Omang, and C. N. Reilley. *Analytical Chemistry*, **37**(11):1312–1316, 1965. 30
- [2] L. B. Anderson and C. N. Reilley. *Journal of Electroanalytical Chemistry*, **10**(4):295–305, 1965. 36
- [3] L. B. Anderson and C. N. Reilley. *Journal of Electroanalytical Chemistry*, **10**(5-6):538–552, 1965. 36
- [4] B. McDuffie and C. N. Reilley. *Analytical Chemistry*, **38**(13):1881–1887, 1966. 30
- [5] R. C. Engstrom, M. Weber, D. J. Wunder, R. Burgess, and S. Winqvist. *Analytical Chemistry*, **58**(4):844–848, 1986. 30
- [6] A. J. Bard, F. R. F. Fan, J. Kwak, and O. Lev. *Analytical Chemistry*, **61**:132–138, 1989.
- [7] J. Kwak and A. J. Bard. *Analytical Chemistry*, **61**(17):1794–1799, 1989. 30
- [8] S. Amemiya, A. J. Bard, F. R. F. Fan, M. V. Mirkin, and P. R. Unwin. *Annual Review of Analytical Chemistry*, **1**:95–131, 2008. 30
- [9] T. Yasukawa, T. Kaya, and T. Matsue. *Electroanalysis*, **12**:653–659, 2000.
- [10] M. A. Edwards, S. Martin, A. L. Whitworth, J. V. Macpherson, and P. R. Unwin. *Physiological Measurement*, **27**(12):R63–108, 2006. 35
- [11] G. Wittstock, M. Burchardt, S. E. Pust, Y. Shen, and C. Zhao. *Angewandte Chemie International Edition*, **46**(10):1584–1617, 2007. 36
- [12] M. V. Mirkin, W. Nogala, J. Velmurugan, and Y. Wang. *Physical Chemistry Chemical Physics*, pages 21196–21212, 2011. 30
- [13] D. G. Sanderson and L. B. Anderson. *Analytical Chemistry*, **57**(12):2388–2393, 1985. 30
- [14] O. Niwa, M. Morita, and H. Tabei. *Analytical Chemistry*, **62**(5):447–452, 1990. 30
- [15] A. J. Bard, J. A. Crayston, G. P. Kittlesen, T. Varco Shea, and M. S. Wrighton. *Analytical Chemistry*, **58**(11):2321–2331, 1986. 30
- [16] J. V. Macpherson and P. R. Unwin. *Analytical chemistry*, **73**(3):550–7, 2001. 31
- [17] C. Kranz, G. Friedbacher, B. Mizaikoff, A. Lugstein, J. Smoliner, and E. Bertagnolli. *Analytical Chemistry*, **73**(11):2491–500, 2001.
- [18] C. J. Slevin, N. J. Gray, J. V. Macpherson, M. a. Webb, and P. R. Unwin. *Electrochemistry Communications*, **1**(7):282–288, 1999.
- [19] J. Abbou, C. Demaille, M. Druet, and J. Moiroux. *Analytical Chemistry*,

- 74(24):6355–63, 2002. 31
- [20] E. Kätelhön and B. Wolfrum. *Reviews in Analytical Chemistry*, **31**(1), 2012. 31
- [21] M. C. J. Dekker, V. Bonifati, and C. M. van Duijn. *Brain : a journal of neurology*, **126**(Pt 8):1722–33, 2003. 31
- [22] D. Goldstein, G. Eisenhofer, and I. Kopin. *Journal of Pharmacology and Experimental Therapeutics*, **305**(3):800–811, 2003. 31
- [23] V. A. T. Dam, W. Olthuis, and A. van den Berg. *The Analyst*, **132**(4):365–370, 2007. 31
- [24] K. Hayashi, Y. Iwasaki, R. Kurita, K. Sunagawa, and O. Niwa. *Electrochemistry Communications*, **5**:1037–1042, 2003. 32
- [25] M. Morita, O. Niwa, and T. Horiuchi. *Electrochimica Acta*, **42**(20-22):3177–3183, 1997. 32
- [26] O. Niwa, H. Tabei, B. P. Solomon, F. Xie, and P. T. Kissinger. *Journal of Chromatography B*, **1**:21–28, 1995.
- [27] K. Hayashi, Y. Iwasaki, R. Kurita, K. Sunagawa, O. Niwa, and A. Tate. *Journal of Electroanalytical Chemistry*, **579**:215–222, 2005. 32
- [28] R. Kurita, H. Tabei, Z. Liu, T. Horiuchi, and O. Niwa. *Sensors and Actuators B: Chemical*, **71**:82–89, 2000.
- [29] H. Tabei, M. Takahashi, S. Hoshino, O. Niwa, and T. Horiuchi. *Analytical Chemistry*, **66**(20):3500–3502, 1994.
- [30] M. Odijk, J. Wiedemair, M. J. J. van Megen, W. Olthuis, and A. van den Berg. In *IEEE Sensors Conference 2010*, pages 918–922. IEEE, 2010. 31
- [31] B. Wolfrum, M. Zevenbergen, and S. Lemay. *Analytical Chemistry*, **80**(4):972–977, 2008. 31, 32
- [32] J. K. Cullison, J. Waraska, D. J. Buttaro, I. N. Acworth, and M. L. Bowers. *Journal of Pharmaceutical and Biomedical Analysis*, **19**(1-2):253–9, 1999. 31
- [33] W. R. Vandaveer, D. J. Woodward, and I. Fritsch. *Electrochimica Acta*, **48**(20-22):3341–3348, 2003. 31
- [34] F. Zhu, J. Yan, M. Lu, Y. Zhou, Y. Yang, and B. Mao. *Electrochimica Acta*, **56**(24):8101–8107, 2011. 32
- [35] E. Kätelhön, B. Hofmann, S. G. Lemay, M. A. G. Zevenbergen, A. Offenhäusser, and B. Wolfrum. *Analytical Chemistry*, **82**(20):8502–9, 2010.
- [36] E. Kätelhön, B. Hofmann, M. Banzet, a. Offenhäusser, and B. Wolfrum. *Procedia Engineering*, **5**:956–958, 2010. 31
- [37] G. S. McCarty, B. Moody, and M. K. Zachek. *Journal of Electroanalytical Chemistry*, **643**(1-2):9–14, 2010. 31, 32

- [38] D. L. Robinson, B. J. Venton, M. L. a. V. Heien, and R. M. Wightman. *Clinical Chemistry*, **49**(10):1763–73, 2003. 31
- [39] J. Park, P. Takmakov, and R. M. Wightman. *Journal of Neurochemistry*, **119**(5):932–44, 2011. 31
- [40] X. Zhu, K. Ino, Z. Lin, H. Shiku, G. Chen, and T. Matsue. *Sensors and Actuators B: Chemical*, **160**(1):923–928, 2011. 33
- [41] R. Thewes, F. Hofmann, A. Frey, B. Holzapfl, M. Schienle, C. Paulus, P. Schindler, G. Eckstein, C. Kassel, M. Stanzel, R. Hintsche, E. Nebling, J. Albers, J. Hassman, J. Schulein, W. Goemann, and W. Gumbrecht. In *2002 IEEE International Solid-State Circuits Conference. Digest of Technical Papers*, volume 1, pages 350–473. IEEE, 2002. 33
- [42] M. Schienle, C. Paulus, A. Frey, F. Hofmann, B. Holzapfl, P. Schindler-Bauer, and R. Thewes. *IEEE Journal of Solid-State Circuits*, **39**(12):2438–2445, 2004.
- [43] B. Elsholz, R. Wörl, L. Blohm, J. Albers, H. Feucht, T. Grunwald, B. Jürgen, T. Schweder, and R. Hintsche. *Analytical Chemistry*, **78**(14):4794–802, 2006. 33
- [44] E. Nebling, T. Grunwald, J. Albers, P. Schafer, and R. Hintsche. *Analytical Chemistry*, **76**:689–696, 2004. 33, 34
- [45] A. Anne, A. Chovin, C. Demaille, and M. Lafouresse. *Analytical Chemistry*, **83**(20):7924–32, 2011. 34
- [46] E. Casero, L. Vázquez, A. M. Parra-Alfambra, and E. Lorenzo. *The Analyst*, **135**(8):1878–903, 2010. 34
- [47] K. Ino, Y. Kanno, T. Nishijo, T. Goto, T. Arai, Y. Takahashi, H. Shiku, and T. Matsue. *Chemical Communications*, **48**(68):8505–7, 2012. 35
- [48] M. Zhang, G. Qin, Y. Zuo, T. Zhang, Y. Zhang, L. Su, H. Qiu, and X. Zhang. *Electrochimica Acta*, **78**:412–416, 2012. 35, 36
- [49] H. J. V. Tyrrell. *Journal of Chemical Education*, **41**(7):397, 1964. 35
- [50] J. Philibert. *Diffusion Fundamentals*, **4**:1–19, 2005.
- [51] A. J. Bard and L. R. Faulkner. *Electrochemical Methods: Fundamentals and Applications*. Wiley, 2nd edition, 2001. ISBN 978-0-471-04372-0. 35
- [52] D. O. Wipf. *Journal of The Electrochemical Society*, **138**(2):469, 1991. 36
- [53] M. V. Mirkin, T. C. Richards, and A. J. Bard. *The Journal of Physical Chemistry*, **97**(29):7672–7677, 1993. 36
- [54] P. Sun and M. V. Mirkin. *Analytical Chemistry*, **78**(18):6526–6534, 2006. 36
- [55] M. A. G. Zevenbergen, B. L. Wolfrum, E. D. Goluch, P. S. Singh, and S. G. Lemay. *Journal of the American Chemical Society*, **131**(32):11471–11477, 2009.

36

- [56] I. Dumitrescu, P. V. Dudin, J. P. Edgeworth, J. V. Macpherson, and P. R. Unwin. *The Journal of Physical Chemistry C*, **114**(6):2633–2639, 2010. 36
- [57] R. D. Martin and P. R. Unwin. *Analytical Chemistry*, **70**(2):276–284, 1998. 37
- [58] R. D. Martin and P. R. Unwin. *Journal of Electroanalytical Chemistry*, **439**(1):123–136, 1997.
- [59] R. G. Compton, B. a. Coles, J. J. Gooding, A. C. Fisher, and T. I. Cox. *The Journal of Physical Chemistry*, **98**(9):2446–2451, 1994. 37
- [60] A. J. Bard and F. R. F. Fan. *Accounts Of Chemical Research*, **29**:572–578, 1996. 37
- [61] M. A. G. Zevenbergen, P. S. Singh, E. D. Goluch, B. L. Wolfrum, and S. G. Lemay. *Nano Letters*, pages 2881–2886, 2011. 37
- [62] Z. Li, I. Pobelov, B. Han, T. Wandlowski, A. Blaszczyk, and M. Mayor. *Nanotechnology*, **18**(4):044018, 2007. 37
- [63] G. Li, D. Chen, J. Wang, C. Jian, W. He, Y. Fan, and T. Deng. *Procedia Engineering*, **00**:6–9, 2012. 38
- [64] K. Mathwig, D. Mampallil, S. Kang, and S. G. Lemay. *Physical Review Letters*, **109**(11):1–5, 2012. 38
- [65] D. Bustin, v. Mesároš, P. Tomčík, M. Rievaj, and V. Tvarožek. *Analytica Chimica Acta*, **305**(1-3):121–125, 1995. 38

Differential cyclic voltammetry for selective and amplified detection

We propose to combine two existing electrochemical techniques, CV and RC, in order to obtain *amplified* and *selective* detection of redox active species. This combination is achieved by applying CV waveforms to two electrodes spaced 1.20 μm apart, with one of the electrodes at a constant potential offset compared to the other. Due to this potential offset we have named this technique *differential cyclic voltammetry* (DCV). Analytical expressions for the DCV voltammogram are derived and an optimal potential offset is calculated. The optimal voltage difference for the trade-off between peak height and width is 0.1 V for redox couples with $n=1$. Experimental voltammograms show good agreement with the analytical expressions. The voltammogram for ferrocenedimethanol has been fitted ($R^2 = 0.9985$) using only the distance between the electrodes as fitting parameter. Therefore, this technique shows promise as a tool for amplified and selective detection of redox active species.¹

¹This chapter has been published as M.J.J. van Megen, M. Odijk, J. Wiedemair, W. Olthuis and A. van den Berg, *Journal of Electroanalytical Chemistry*, 681:6-10, 2012.

4.1 Introduction

Over the past few years development of micro and nanofabricated structures has generated a renewed interest in existing electrochemical methods. The nanoscale study and understanding of electrochemical processes combined with these structures have led to improved electrochemical detection capabilities. Here we propose to combine two existing and widely used techniques to obtain improved functionality.

The first technique we employ is that of CV. CV has been around for a long time and is a well known classification technique for electrochemical systems described in numerous textbooks [1–3]. In CV, current is measured while sweeping the voltage over a predefined range, resulting in a voltammogram where the electrochemical reactions of the various compounds present can be observed. This ability to show in one measurement the contributions of various compounds is a clear benefit of CV. Another benefit is that the shape of a voltammogram is well described, therefore any deviation from this shape is a clear indication of an issue with the measurement, e.g. electrode fouling or a drift in the reference electrode. This makes CV a useful tool for assessing the functioning of the electrochemical setup. As such it is often used as a test preceding other electrochemical techniques.

An important downside to CV is its susceptibility to non-faradaic currents caused by charging of the double layer capacitance as a result of the continuously changing potential in a CV measurement [1]. This capacitive charging current i_c can be calculated as follows:

$$|i_c| = AC_d v \quad (4.1)$$

Where A is the area [m^2], C_d the double layer capacitance [F/m^2], and v the scanrate [V/s]. This capacitive current can be regarded as an offset added to the faradaic current. An initial boost to the faradaic to offset ratio can be obtained by scaling the electrode down to a dimension where the diffusion profile becomes hemispherical instead of linear. This happens for electrode dimensions in the micrometer or sub-micrometer range. For a disk electrode with micrometer dimensions the faradaic current is given by [4].

$$i_{farad} = \beta AnFDC^*r \quad (4.2)$$

Where β is a prefactor based on the ratio between radius of the insulating material and the radius of the electrode r [m], n is the number of electrons involved in the reaction, F the faraday constant [C/mol], D the diffusion coefficient [m^2/s], and C^*

the bulk concentration [mol/m³]. From these two equations one can derive a signal to offset ratio.

$$snr = \frac{i_{f_{farad}}}{|i_c|} = \frac{\beta 4nFDC^*r}{AC_dv} \quad (4.3)$$

From equation 4.3 follows that detecting lower concentrations requires lower scanrates in order to distinguish the faradaic current from the capacitive background. This signal to offset ratio can be enhanced by introducing electrochemical amplification in the form of RC. Conventional RC is based on cycling a reversible redox couple between two closely spaced electrodes, where one electrode is held at an oxidizing potential and another at a reducing potential. The advantage of this technique is that each molecule can contribute to the measured current multiple times, thus effectively creating (electro)chemical signal amplification. This amplification can be used to achieve single molecule detection limits [5].

Selective detection using RC is feasible because only the current of reversible redox couples is amplified. For example, small amounts of catechol can be detected in the presence of an interfering compound such as ascorbid acid [6]. Both catechol and ascorbid acid are easily oxidized at approximately the same potential, but only the oxidation product of catechol can be reduced. Therefore, only the catechol related current is amplified by RC. It is also possible to achieve selective detection in a mixture of multiple reversible couples, e.g ferrocyanide and dopamine [7, 8], by applying the potentials such that only dopamine is subject to RC.

The majority of RC based sensors utilize interdigitated array (IDA) electrodes [7, 9–23] and more recently thin layers cells [24–26], because of their favorable geometries for RC. For an IDA electrode in bulk solution an amplification of ~65 times is reported [7]. An amplification factor of 100 was reported for an IDA electrode in a nanochannel [23]. The highest amplification factor currently reported is on the order of 10⁴ for a thin layer cell design [25].

Aside from these solid state sensors, SECM also makes use of the RC effect by means of a microelectrode that is (x,y,z) positionable with respect to the surface. Thus, one can for example distinguish between conductive and non-conductive substrates. In this field RC is known as positive feedback SECM [27].

Our 'best of both worlds' approach combines the benefits of both techniques, namely being able to measure multiple species at the same time using electrochemical amplification. This is illustrated in figure 4.1. This combination is obtained by applying a CV

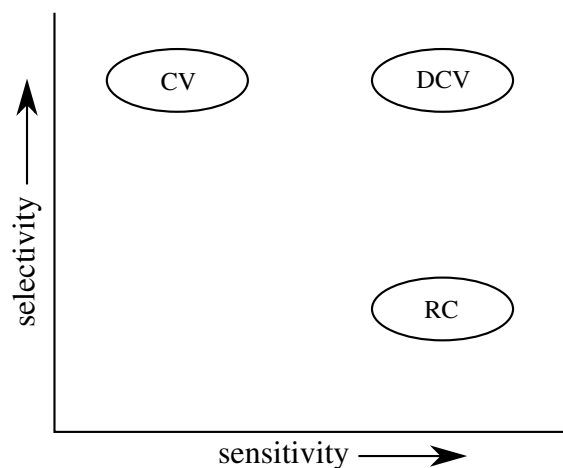


Figure 4.1: When scoring for selectivity and sensitivity, both CV and RC each perform well in one area, but poor in the other. DCV combines the performance of both techniques into a single technique that scores well on both categories, sensitivity and selectivity.

waveform on one electrode while applying the same waveform with a potential offset to the other electrode. Due to this offset we have named this technique differential cyclic voltammetry.

Another approach similar to DCV is performing CV on one electrode while keeping the other at a fixed potential. For example, by applying different substrate voltages for each CV at the tip electrode, one can vary the feedback mode from total feedback to total shielding or an inbetween state labeled partial feedback [28]. The total shielding mode is similar to substrate generation/tip collection (SG/TC) [29]. This SG/TC mode can be used with a fixed tip voltage and varying substrate potential. Because the tip current is measured while the voltage remains constant, this method elegantly removes the capacitive interference, leaving only the faradaic current. The numerical derivative of these voltammograms show a similar shape as is obtained through DCV, and the technique also combines the positive aspects of CV and RC, however DCV offers a few additional features. For example, the voltage difference between the electrodes is constant in DCV, whereas it is variable for the other technique. This prevents unwanted currents due to capacitive coupling of the electrodes. In DCV the height and width of the curve can be tuned through the voltage difference between tip and substrate, and finally, in DCV the compounds are addressed individually as the

sweep passes the formal potentials. In the previously mentioned SECM modes the currents resulting from multiple compounds would be summed.

Previous experiments in our group showed that the shape of the voltammogram obtained through DCV can be compared to those obtained for differential pulse voltammetry or square wave voltammetry. However, unlike these techniques the signal is amplified for DCV [30]. The peak voltage is related to $E_{0'}$ and the peak value to concentration. In this contribution analytical expressions are introduced for DCV between two parallel plates, a geometry found in thin layer cells and SECM tips close to a substrate. These expressions are compared to experimental results obtained from an SECM system in feedback mode.

4.2 Theory

4.2.1 Analytical expression

To achieve high redox amplification, devices need to have two electrodes with an inter-electrode spacing in the (sub)micrometer range. If the electrodes are facing each other, forming a parallel plate geometry, an analytical expression for the DCV peak shape can be obtained. A schematic of a DCV setup can be seen in figure 4.2.

Assuming that the kinetics (adsorption and electron transfer) at the electrode are fast enough for the Nernst equation to remain valid during the potential sweep, the Nernst equation can be rewritten to provide the ratio between the concentration of oxidized and reduced species at the electrode surface:

$$C_{ox}^{el}/C_{re}^{el} = e^{(E^{el}-E^{0'})/(RT/nF)} \quad (4.4)$$

Here E^{el} is the applied potential [V], $E^{0'}$ the formal potential of the redox species [V], R the universal gas constant [J/(mol K)], T the temperature [K], n the number of electrons involved in the reaction, and F the faraday constant [C/mol].

If migration is eliminated by adding a background electrolyte and there is no convection, the flux of particles can be attributed solely to diffusion. Fick's first law of diffusion in one dimension is described as:

$$N_i = -D_i \frac{dC_i}{dx} \quad (4.5)$$

Here D_i is the diffusion coefficient [m^2/s], $\frac{dC_i}{dx}$ the concentration gradient [mol/m] for species i . Assuming equal diffusion coefficients for the oxidized and the reduced

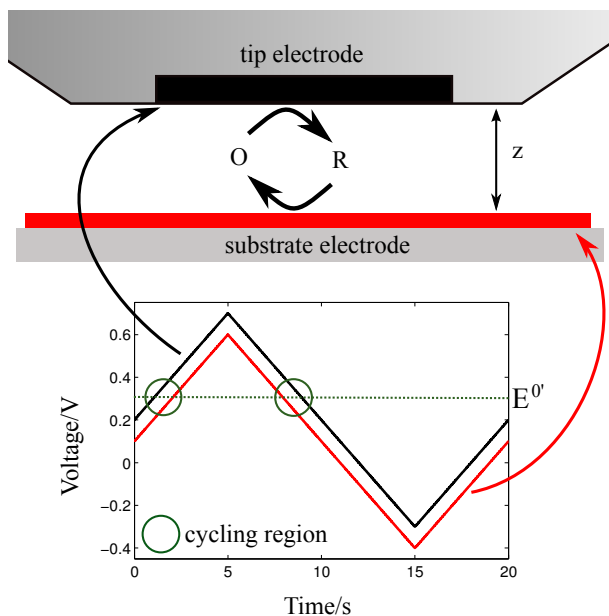


Figure 4.2: Schematic of a DCV measurement setup. Triangular waveforms are applied to the tip and substrate electrodes. Given a redox active species with $E^{0'}$ at 0.3V, cycling will occur as the electrodes pass this value. This happens once in the forward sweep and once in the backward sweep, resulting in two current peaks. Figure not to scale.

species ($D_{ox} = D_{re} = D$) the sum of the concentration of their ions at any point is equal to the sum of the bulk concentrations. For the tip and substrate electrode this means:

$$C_{re}^{tip} + C_{ox}^{tip} = C_{ox}^{bulk} + C_{re}^{bulk} = C^{bulk} \quad (4.6)$$

$$C_{re}^{sub} + C_{ox}^{sub} = C_{ox}^{bulk} + C_{re}^{bulk} = C^{bulk} \quad (4.7)$$

Equation 4.4 can be combined with 4.6 and 4.7 to yield expressions for the concentration of the reduced species at the electrodes:

$$C_{re}^{tip} = C^{bulk} / (e^{(E^{tip} - E^{0'}) / (RT/nF)} + 1) \quad (4.8)$$

$$C_{re}^{sub} = C^{bulk} / (e^{(E^{sub} - E^{0'}) / (RT/nF)} + 1) \quad (4.9)$$

The tip and substrate concentrations enforce a concentration gradient between the electrodes. To be able to calculate the flux from these surface concentrations, the concentration gradient between the electrodes needs to be linear. This can be validated by looking at the time it takes for this gradient to reach steady state, which is given

by:

$$t_{ss} = \frac{z^2}{D} \quad (4.10)$$

For a typical system ($z = 1 \mu\text{m}$, $D = 10^{-10} \text{ m}^2/\text{s}$) steady state is reached in approximately 10 ms. Assuming an SECM geometry with a large substrate electrode and a small insulated tip electrode, the math becomes more complicated. However, simulations using finite element modelling have shown that for equal diffusion coefficients the SECM geometry behaves similar to a thin layer cell (TLC) [31–33]. For a DCV experiment at a scanrate of $< 1 \text{ V/s}$ this timescale is fast enough to assume a linear concentration gradient between the electrodes. Therefore, the concentration gradient in equation 4.5 can be replaced with surface concentrations derived in equation 4.8 and 4.9 with z the distance between the electrodes.:

$$N_{re} = -D \frac{C_{re}^{tip} - C_{re}^{substrate}}{z} \quad (4.11)$$

Additional fluxes from the sides of the electrodes are neglected, which is reasonable provided the width of the electrodes is much larger than the height. Finally, the current can be related to the flux leading to:

$$I = -nFAD \frac{C_{re}^{tip} - C_{re}^{substrate}}{z} \quad (4.12)$$

Here A is the surface area of the tip electrode [m^2], other variables are as described before.

4.2.2 Optimal voltage

Equations 4.8, 4.9 and 4.12 can be used to calculate the shape of the voltammogram for different values of $E^{tip} - E^{sub} = \Delta E$. A small current peak width is desirable for two reasons: firstly to distinguish as many species as possible within the electrochemical potential window and secondly to detect species of which the $E^{0'}$ is close to the edge of the potential window. Larger current peak heights are desirable for better signal to noise ratios and require a large ΔE . An optimal value for ΔE can be found by dividing the current peak height by the full width at half maximum (FWHM). The ratio of these values for ΔE between 50 mV and 250 mV is shown in figure 4.3. The optimal ΔE is 0.104 V for a reversible redox couple with $n=1$.

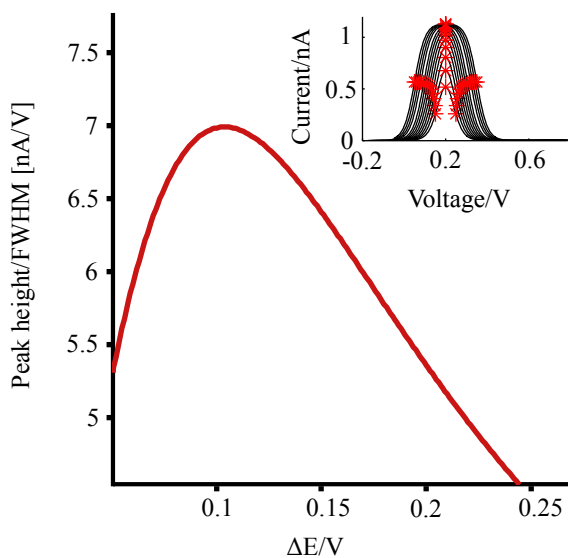


Figure 4.3: The maximum peak height divided by FWHM for ΔE ranging from 50 to 250 mV. An optimum is found for 0.104 V. Inset shows the shape of the DCV curves for the various ΔE values and the FWHM and peak max locations. Values are calculated for a species with an $E^{0'}$ at 0.2 V and $n=1$.

4.3 Materials and methods

Experiments are performed using ElProScan, a commercially available SECM system by HEKA. The substrate is a glass chip containing a gold working electrode (radius 1200 μm) and platinum counter electrode fabricated using conventional lithography and lift-off processes. Connections to this chip are made using a custom built electrochemical cell. Voltages are referenced to an Ag/AgCl electrode (BASi RE-6). The tip is a quartz-platinum microelectrode ($r = 3.23 \mu\text{m}$, $R_g = 12.5$, Thomas Recording). The following chemicals were used: Hexaamineruthenium(III) chloride ($[\text{Ru}(\text{NH}_3)_6]\text{Cl}_3$, 98%, Sigma-Aldrich), Potassium Chloride (KCl, >99% Sigma-Aldrich), and 1,1'-Ferrocenedimethanol ($\text{Fc}(\text{MeOH})_2$, 98%, Acros Organics). All solutions were prepared in 18.2 M Ω cm deionized water (Millipore).

4.4 Results and discussion

4.4.1 Voltammogram

In figure 4.4 the voltammogram is shown, recorded in a solution of 0.5 mM $\text{Fc}(\text{MeOH})_2$ and 1 mM $[\text{Ru}(\text{NH}_3)_6]\text{Cl}_3$ with 0.1 M KCl as supporting electrolyte. These redox active compounds have been chosen for their well-separated potentials to clearly illustrate the DCV model. Using the SECM system, the tip was approached to the surface and stopped when the current reached three times the bulk value. From the theoretical model follows that the closer the tip is positioned to the substrate, the higher the amplification factor and the shorter the time to reach steady state will be. However, to avoid a potential tip crash, an amplification factor of 3 was deemed high enough for these experiments. The potential of the tip electrode was swept between -0.3 V and 0.5 V and the substrate between -0.4 V and 0.4 V ($\Delta E = 0.1$ V) for 5 cycles at a 10 mV/s scanrate.

Three parameters determine the difference between the two peaks: formal potential, concentration, and diffusion coefficient. The formal potential determines the location of the peak on the horizontal axis, while concentration and diffusion coefficient are linearly related to peak height. The ratio between the peaks heights is approximately 2.5. The species concentrations have a ratio of 2:1 meaning that the diffusion coefficients should differ by a factor 1.25. In a separate experiment the diffusion coefficient for $\text{Fc}(\text{MeOH})_2$ and $[\text{Ru}(\text{NH}_3)_6]^{3+}$ in 0.1 M KCl were determined through the steady state current at a microelectrode with a 10 μm diameter. The diffusion coefficient

was $6.3 \times 10^{-10} \text{ m}^2/\text{s}$ for $\text{Fc}(\text{MeOH})_2$, and $7.8 \times 10^{-10} \text{ m}^2/\text{s}$ for $[\text{Ru}(\text{NH}_3)_6]^{3+}$. Both are in good agreement with literature values [10, 24, 34, 35], and with a ratio of 1.24 close to the expected ratio of 1.25. The correlation of the peak current ratio with the concentrations and diffusion coefficients of the involved species shows a good agreement between the theoretical model and the experimental results.

An unexpected result is the deviation between the forward and the reverse scan for the $[\text{Ru}(\text{NH}_3)_6]^{2+} / [\text{Ru}(\text{NH}_3)_6]^{3+}$ couple. From literature it is found that the diffusion coefficients for the $[\text{Ru}(\text{NH}_3)_6]^{2+} / [\text{Ru}(\text{NH}_3)_6]^{3+}$ couple are not equal [34]. This might cause local accumulation or depletion of ions within the channel, which has been shown previously for SECM in feedback and SG/TC modes [32, 33]. In the forward scan the formal potential is approached from a reduced state whereas the reverse scan approaches the formal potential from an oxidized state. This change in state and corresponding accumulation/depletion could explain the difference between the forward and reverse scans. This effect is not taken into account for the DCV model. Furthermore, a decrease over time can be observed for the peak related to the $[\text{Ru}(\text{NH}_3)_6]^{2+} / [\text{Ru}(\text{NH}_3)_6]^{3+}$ couple. Since the $\text{Fc}(\text{MeOH})_2$ related peak does

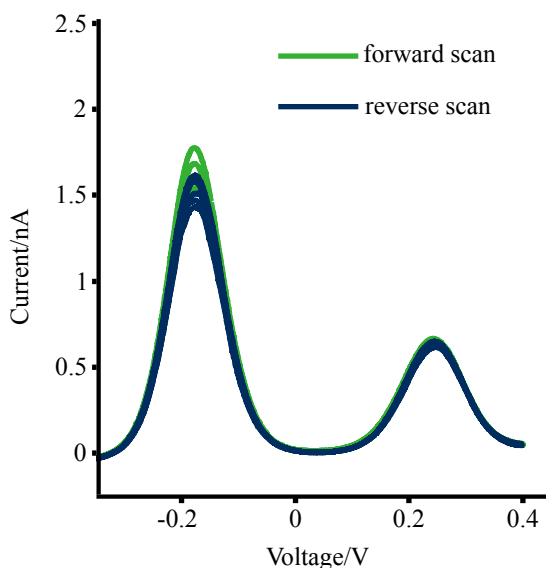


Figure 4.4: Measured data for 1 mM $[\text{Ru}(\text{NH}_3)_6]\text{Cl}_3$ and 0.5 mM $\text{Fc}(\text{MeOH})_2$ with 0.1M KCl as supporting electrolyte. Data from 5 consecutive sweeps with green the forward sweeps and blue the reverse sweeps. $\Delta V = 100 \text{ mV}$, scanrate 10 mV/s, $I/I_{\text{bulk}} = 3$, Ag/AgCl reference.

not show this effect it is likely a local change in concentration of the $[\text{Ru}(\text{NH}_3)_6]^{2+} / [\text{Ru}(\text{NH}_3)_6]^{3+}$ couple, either through the depletion mentioned earlier or through poor stability of the generated $[\text{Ru}(\text{NH}_3)_6]^{2+}$.

4.4.2 Curve fitting

To compare experimental results with theory, curve fitting was performed using OriginPro. The approach curve obtained shortly before the DCV experiment was used to determine r and Rg using an analytical expression for positive feedback approach curves [36]. An optimal fit was obtained for r and Rg values of $3.23 \mu\text{m}$ and 12.5 , respectively. For these values, a positive feedback amplification factor of 3 corresponds to a tip to substrate distance (z_{approach}) of $1.07 \mu\text{m}$. The obtained r value was used in the analytical expression for the DCV peak shape (equation 4.12) along with the other known parameters, leaving the tip to substrate distance (z_{dcv}) as the only fitting parameter. The result of this fitting is shown in figure 4.5. E^0 is 0.24 V versus the Ag/AgCl electrode, F is 96485 C/mol , T is 295 K , R is 8.31 J/K mole , r is $3.23 \mu\text{m}$, and n is 1. Since in figure 4.4, a slope in the measurement can be observed, a slope of 9.5 pAV^{-1} was added to the model in order to get a proper fit. Using these

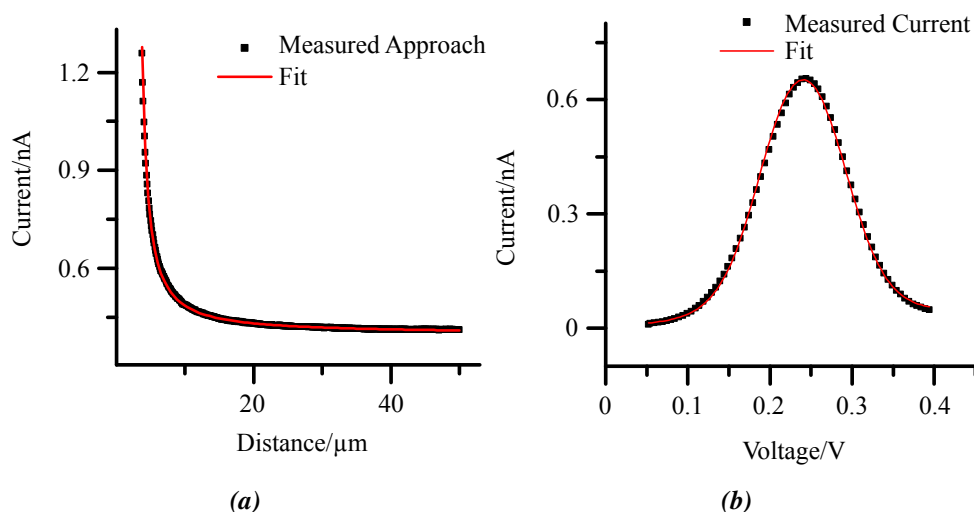


Figure 4.5: (a) Approach curve fit using r and Rg values of $3.23 \mu\text{m}$ and 12.5 respectively (b) Fitting the theoretical curve to measured data using tip substrate distance as the only fitting parameter an optimal fit is obtained for a distance z of $1.2 \mu\text{m}$ ($R^2 = 0.9985$). Potentials referenced versus Ag/AgCl electrode.

parameters a minimum least squares error was obtained for z is 1.20 μm . Thus there is only a 13% deviation between z_{approach} and z_{dcv} . The most plausible explanation for such discrepancy is the effect of fluxes from the sides being neglected only in the DCV model. However, these would have resulted in an underestimation of z_{dcv} . The fact that z_{dcv} is higher than z_{approach} indicates that side effects are not significant. An interesting case has been made recently for temperature control in SECM systems, as a temperature drift can give rise to a drift in tip-substrate separation of 5-150 nm/min [37]. Other reasons for the deviation could be sample tilt or electrode fouling, but the exact origin is unknown. However, the difference between z_{approach} and z_{dcv} of only 13% indicates that the DCV model is valid for positive feedback SECM experiments. Additionally we expect the model will also be valid for experiments with thin layer cells due to similarity in geometry. The benefit of those systems is that the separation between the electrodes is very well defined, as such it will be a useful tool for the investigation of reversible redox couples.

4.5 Concluding remarks

The novel technique of DCV, combining conventional CV with RC, shows potential as a tool for amplified and selective detection of multiple reversible redox couples. The analytical model derived for this technique is in good agreement with experimental results. The optimal voltage difference for the trade-off between peak height and width is 0.1 V for redox couples with $n=1$. Experiments using this voltage showed good correlation of the peak ratios with the concentrations and diffusion coefficients of the species involved.

Bibliography

- [1] A. J. Bard and L. R. Faulkner. *Electrochemical Methods: Fundamentals and Applications*. Wiley, 2nd edition, 2001. ISBN 978-0-471-04372-0. 46
- [2] J. Wang. *Analytical Electrochemistry*. WILEY-VCH, 2nd edition, 2000. ISBN 978-0471282723.
- [3] R. G. Compton and C. E. Banks. *Understanding Voltammetry*. Imperial College Press, 2nd edition, 2011. ISBN 978-84816-586-1. 46
- [4] C. Lefrou and R. Cornut. *ChemPhysChem*, **11**(3):547–556, 2010. 46
- [5] F. R. F. Fan and A. J. Bard. *Science*, **267**:871–874, 1995. 47
- [6] B. Wolfrum, M. A. G. Zevenbergen, and S. G. Lemay. *Analytical Chemistry*, **80**(4):972–977, 2008. 47
- [7] V. A. T. Dam, W. Olthuis, and A. van den Berg. *The Analyst*, **132**(4):365–370, 2007. 47
- [8] M. Odijk, W. Olthuis, V. A. T. Dam, and A. van den Berg. *Electroanalysis*, **20**:463–468, 2008. 47
- [9] D. G. Sanderson and L. B. Anderson. *Analytical Chemistry*, **57**:2388–2393, 1985. 47
- [10] A. J. Bard, J. A. Crayston, G. P. Kittlesen, T. Varco Shea, and M. S. Wrighton. *Analytical Chemistry*, **58**(11):2321–2331, 1986. 54
- [11] B. Seddon, H. Girault, and M. Eddowes. *Journal of Electroanalytical Chemistry*, **266**:227–238, 1989.
- [12] Y. Iwasaki and M. Morita. *Current Separations*, **14**:1–8, 1995.
- [13] P. Jin, A. Yamaguchi, F. A. Oi, shigeki Matsuo, J. Tan, and H. Misawa. *Analytical Science*, **17**:841–846, 2001.
- [14] J. Min and A. J. Baeumner. *Electroanalysis*, **16**(9):724–729, 2004.
- [15] O. Niwa, H. Tabei, B. P. Solomon, F. Xie, and P. T. Kissinger. *Journal of Chromatography B*, **1**:21–28, 1995.
- [16] M. Paeschke, U. Wollenberger, C. Kohler, T. Lisec, U. Schnakenberg, and R. Hintsche. *Analytica Chimica Acta*, **305**:126–136, 1995.
- [17] X. Yang and G. Zhang. *Comsol Proceedings and user presentations CD*, **1**:1–6, 2005.
- [18] F. Bjorefors, C. Strandman, and L. Nyholm. *Electroanalysis*, **12-4**:255–261, 2000.
- [19] K. Hayashi, Y. Iwasaki, R. Kurita, K. Sunagawa, O. Niwa, and A. Tate. *Journal of Electroanalytical Chemistry*, **579**:215–222, 2005.

- [20] R. Kurita, H. Tabei, Z. Liu, T. Horiuchi, and O. Niwa. *Sensors and Actuators B: Chemical*, **71**:82–89, 2000.
- [21] H. Tabei, M. Takahashi, S. Hoshino, O. Niwa, and T. Horiuchi. *Analytical Chemistry*, **66**(20):3500–3502, 1994.
- [22] K. Ueno, M. Hayashida, J. Y. Ye, and H. Misawa. *Electrochemistry Communications*, **7**:161–165, 2005.
- [23] E. D. Goluch, B. Wolfrum, P. S. Singh, M. A. G. Zevenbergen, and S. G. Lemay. *Analytical and Bioanalytical Chemistry*, **394**(2):447–456, 2009. 47
- [24] M. A. G. Zevenbergen, P. S. Singh, E. D. Goluch, B. L. Wolfrum, and S. G. Lemay. *Analytical Chemistry*, **81**(19):8203–8212, 2009. 47, 54
- [25] M. A. G. Zevenbergen, B. L. Wolfrum, E. D. Goluch, P. S. Singh, and S. G. Lemay. *Journal of the American Chemical Society*, **131**(32):11471–11477, 2009. 47
- [26] M. A. G. Zevenbergen, D. Krapf, M. R. Zuiddam, and S. G. Lemay. *Nano Letters*, **7**:384–388, 2007. 47
- [27] A. J. Bard, F. R. F. Fan, J. Kwak, and O. Lev. *Analytical Chemistry*, **61**:132–138, 1989. 47
- [28] C. G. Zoski, C. R. Luman, and J. L. *Analytical Chemistry*, **79**(13):4957–4966, 2007. 48
- [29] N. Nioradze and J. Kim. *Analytical Chemistry*, pages 828–835, 2011. 48
- [30] M. Odijk, J. Wiedemair, M. J. J. van Megen, W. Olthuis, and A. van den Berg. In *IEEE Sensors Conference 2010*, pages 918–922. IEEE, 2010. 49
- [31] A. J. Bard, G. Denuault, R. A. Friesner, B. C. Dornblaser, and L. S. Tuckerman. *Analytical Chemistry*, **63**(13):1282–8, 1991. 51
- [32] R. D. Martin and P. R. Unwin. *Journal of Electroanalytical Chemistry*, **439**(1):123–136, 1997. 54
- [33] R. D. Martin and P. R. Unwin. *Analytical Chemistry*, **70**(2):276–284, 1998. 51, 54
- [34] Y. Wang, J. G. Limon-Petersen, and R. G. Compton. *Journal of Electroanalytical Chemistry*, **652**(1-2):13–17, 2011. 54
- [35] H. Xiong, J. Guo, K. Kurihara, and S. Amemiya. *Electrochemistry Communications*, **6**(6):615–620, 2004. 54
- [36] C. Lefrou. *Journal of Electroanalytical Chemistry*, **592**(1):103–112, 2006. 55
- [37] J. Kim, M. Shen, N. Nioradze, and S. Amemiya. *Analytical Chemistry*, **84**(8):3489–3492, 2012. 56

Surface attached redox labeled polyethylene glycol

In this chapter an overview will be given regarding the properties of ferrocene (Fc) labeled polyethylene glycol (PEG) attached to a gold electrode using cystamine. The obtained surface density, stability over time, and the effect of the background electrolyte are investigated. An average surface density of $1.16 \times 10^{-6} \text{ mol/m}^2$ and $1.22 \times 10^{-6} \text{ mol/m}^2$ was obtained for two electrodes ($n=6$), indicating the molecules are in a dense brush configuration. A decay in time in the response of the electro active layer was observed. Finally a correlation is observed between the sodiumperchlorate concentration of the background electrolyte and the measured formal potential of the ferrocene. This effect is attributed to ion pairing of the perchlorate and the oxidized ferrocene. Combining this system with a second closely spaced electrode should allow redox cycling of PEG-Fc between the two electrodes.¹

¹This chapter was written in close collaboration with Tom Steentjes, MNF group, University of Twente

5.1 Introduction

The need for simple, rapid and portable detection schemes for biosensing has led to the development of micro and nanoscale biosensors. An example is the field of electrochemical DNA sensing which is used for applications such as pathogen detection, and the screening for genetic disorders [1–4]. The developments in this field have even led to a number of commercial applications [4]. Electrochemical DNA detection relies on the detection of an hybridization event between a surface attached probe and a target by measuring current changes through an electrode. So far, these experiments have typically focused one single electrode systems with the redox label attached to the probe [1, 2], or redox cycling systems with a freely diffusing redox mediator, as is described in chapter 3, section 3.2.1.2 of this thesis. [5–9]. To our knowledge no results have been reported on the cycling between two electrodes, of a surface attached redox labeled DNA probe.

Such a system requires a probe of sufficient length to cross the gap between two closely spaced electrodes. Assuming an electrode gap of approximately 50 nm, a spacer is needed to extend the length of a DNA probe. PEG is a good candidate as a spacer, it is commercially available and at molecular weights of 10000 g/mol or higher, its size is sufficient to cross the gap. The concept of a redox cycling system using a surface-attached redox-labeled molecule is illustrated in figure 5.1. The use of ferrocene labeled PEG has been reported previously by Anne and Demaille, both in single [10–12] and dual electrode systems [13–16]. For their experiments they synthesized PEG molecules bearing an N-hydroxysuccinimide (NHS) activated ester at one end, and a ferrocene molecule at the other end. They did this for molecular weights of 600, 3400, and 20000 g/mol. The NHS group can be used to attach the molecule to an electrode surface. For glassy carbon electrodes this was done by polishing the electrodes in the presence of ammonia, thereby generating amino groups on the surface. At gold electrodes, modification is performed by using cysteamine, which is a thiol with an amine group at the end.² Using this system, they investigated the flexibility of the PEG chains, by means of CV at fast scan rates. For their dual electrode experiments, the modified PEG molecules were attached either to an AFM tip or a gold substrate electrode, after which the tip was approached to the surface. As the tip approaches the surface, an increase in current is observed which can be

²Cysteamine and cystamine are two closely related molecules, cysteamine has a single thiol group while cystamine is a disulfide with two amine groups. In the experiments reported in this thesis, cystamine is used.

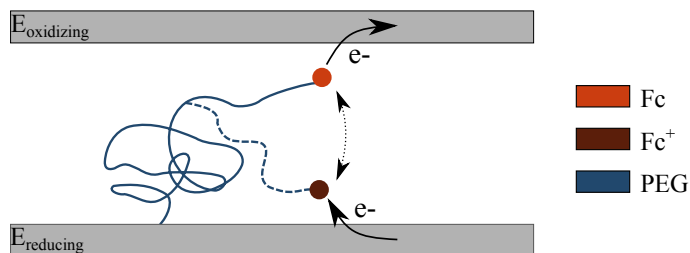


Figure 5.1: Illustration of the RC concept using surface attached redox labeled molecules. The PEG molecule is large enough to reach both of the electrodes with its ferrocene (Fc) redox label. As a result, the ferrocene can undergo repeated oxidation and reduction reactions, thereby shuttling electrons between the two electrodes.

attributed to the redox cycling of the molecule layer. This is the first system that applies redox cycling on surface attached layers without a freely diffusing redox mediator.

In this chapter the properties of surface linked PEG chains labeled with ferrocene will be explored for the single electrode case. The obtained surface density, stability, and dependence on the background electrolyte concentration will be explored.

5.2 Theory

Surface grafted polymer chains in a good solvent (e.g. water) and low surface density occupy a half sphere with a radius comparable to the Flory radius of a coil freely diffusing in a good solvent [17, 18]. This is also known as the mushroom regime. The Flory radius can be calculated by

$$R_f = aN^{3/5} \quad (5.1)$$

where a [m] is the size of the individual ethylene glycol monomer, which is 0.35 nm for PEG [19], and N the number of monomer units. This equation was used to determine the Flory radii for various molecular weights, as shown in table 5.1. If the surface density of the PEG molecules becomes too high, the individual molecules start to interact and the PEG will go from a mushroom configuration to a brush configuration where they extend a certain length $L_{max} > L > R_f$ from the surface. This concept is illustrated in figure 5.2 and the maximum density for keeping a mushroom configuration is listed in table 5.1.

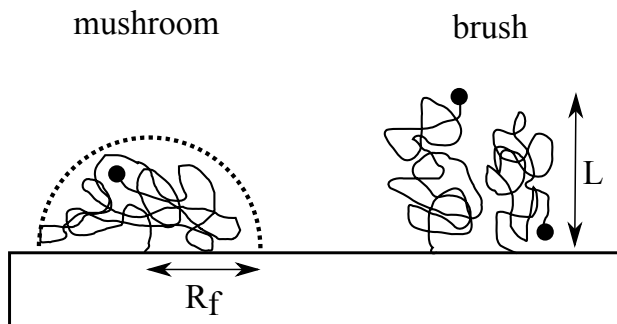


Figure 5.2: The two configurations for PEG based on their surface density. Low density PEG confines to a mushroom configuration while high density PEG takes on a brush configuration.

Table 5.1: Properties of PEG macromolecules for various molecular weights.

mol. weight [g/mol]	N	R_f [nm]	L_{max} [nm]	max. density [mol/m ²]
250	6	1.0	2.1	5.3e-7
3400	77	4.7	27	2.4e-8
5000	114	6.0	40	1.5e-8
10000	227	9.1	79	6.4e-9

5.2.1 Calculating surface coverage

Unlike conventional bulk electrochemistry where there is a continuous supply of new molecules diffusing from the bulk towards the electrode, in the surface attached situation only a limited amount of molecules is available. After these molecules have reacted, the current drops back down to a baseline value, as is illustrated in figure 5.3. By integrating the current resulting from the oxidation or reduction reaction over time, the total amount of charge transferred can be calculated. This resulting charge value can be used to calculate the surface coverage using equation 5.2

$$coverage = \frac{C_{peak}}{eA_V A} = \frac{C_{peak}}{FA} \quad (5.2)$$

where C_{peak} [C] is the charge transferred in either the oxidation or reduction peak, e the elementary charge $1.6e-19$ C, A_V Avogadro's constant $6.022e-23$ 1/mol, and A the area [m²]. This yields a value for the coverage in [mol/m²]. However, in literature the coverage is often expressed in terms of [mol/cm²].

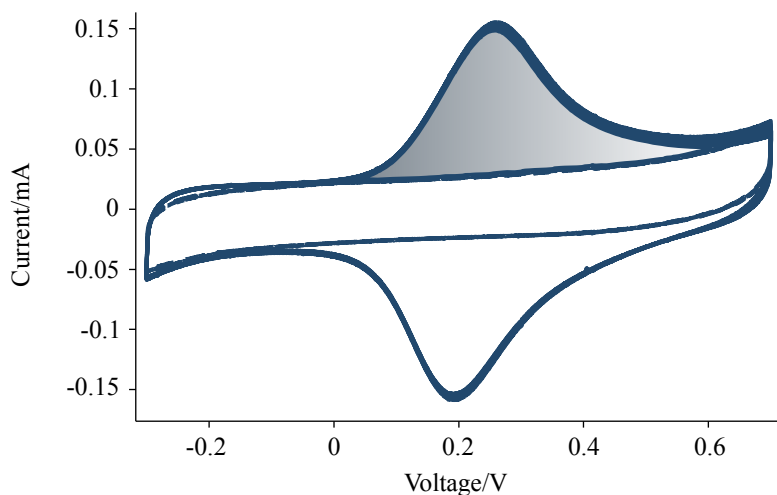


Figure 5.3: Two voltammograms are shown, one for a layer of NHS-PEG₂₅₀-Fc and the other for a layer of cystamine. By integrating the current in the CV resulting from oxidation of the Fc label (grey area), the surface coverage of the PEG layer can be calculated. The CV from the cystamine layer provides a baseline which is subtracted before the current is integrated. Measurement performed in 0.1 M KCl using an Ag/AgCl electrode, scanrate was 2 V/s.

5.3 Materials and methods

The experiments have been performed using either NHS-PEG₂₅₀-Fc or NHS-PEG_{10k}-Fc on gold disk electrodes with a diameter of 2 mm (CH instruments). For a detailed protocol on the synthesis of the PEG molecules see appendix B. Before modification the electrodes were polished using alumina particles (50 nm diameter, CH instruments), followed by extensive rinsing using ethanol and DI water (Millipore), and 5 minutes of ultrasonic treatment in ethanol and DI water respectively. After the ultrasonic treatment the electrodes were electrochemically cleaned in 0.5 M H₂SO₄. The electrode potential was scanned from -0.61 V to 1.1 V and back for a total of 35 cycles at a scanrate of 100 mV/s, using a mercurous sulphate reference electrode (BASI) and platinum counter electrode (CH instruments). The initial 30 cycles were used to let the voltammogram stabilize and the final 5 were used to check whether the gold oxidation showed the three independent peaks that are an indication of a clean gold surface [20]. An example of a cleaning curve is shown in appendix A. After cleaning, the electrodes were put into DI water containing 20 mM cystaminedihydrochloride (FLUKA) to allow the cystamine monolayer to form overnight. The

PEG chains were subsequently attached to the cystamine layer by putting the electrodes in dichloromethane (for PEG₂₅₀-Fc) or water (for PEG_{10k}-Fc) contain the PEG chains. Finally, the electrodes were extensively rinsed using DI water, after which they were ready for use. Electrochemical measurements were performed using a SP300 bi-potentiostat (Bio-Logic, France). The solutions used were, 1 M NaClO₄ in DI water, and 0.5 M Tetrabutylammonium hexafluorophosphate in dichloromethane.

5.4 Results and discussion

Below are the results of a series of experiments on the stability of PEG₂₅₀-Fc layers. For each experiment, 10 CV cycles between -0.7 V and 0.3 V vs a mercurous sulphate electrode are recorded at a 2 V/s scanrate, followed by 5 minutes of floating at open circuit potential. This protocol is looped 10 times.

5.4.1 Surface coverage

The surface coverage was calculated for each of the time decay experiments listed below using the theory explained in section 5.2.1. For each experiment, the 10th CV of the first loop was used to determine the charge transferred. The average charge transferred over all experiments was $0.35 \pm 0.04 \mu\text{C}$ and $0.37 \pm 0.13 \mu\text{C}$ for two electrodes. This yields a surface coverage of $1.16\text{e-}6 \text{ mol/m}^2$ and $1.22\text{e-}6 \text{ mol/m}^2$. The experiments were performed using PEG₂₅₀-fc of which the maximum density that allows a mushroom configuration is $5.3\text{e-}7 \text{ mol/m}^2$. This can either mean the PEG molecules are in brush configuration, or that the actual surface is larger than that of a perfectly flat disk electrode, due to surface roughness.

5.4.2 Decay over time

As initial experiments showed a decay over time of the oxidative and reductive peaks, an attempt was made to determine the cause for this degradation. Two of the most likely candidates for signal degradation were tested: non-specific desorption, and instability of the electro-generated Fc⁺ ion. To test the issue of non-specific desorption two parameters were varied, the solvent type and the use of an ultrasonic bath. As the PEG₂₅₀-fc molecules are solvable in dichloromethane but not in water the hypothesis is that the peaks decay faster in dichloromethane than in water. The ultrasonic bath could potentially remove the non-specifically attached molecules before the experiment, resulting in less decay over time. For each of these parameter combinations, the average oxidative peak height of each loop was determined as is

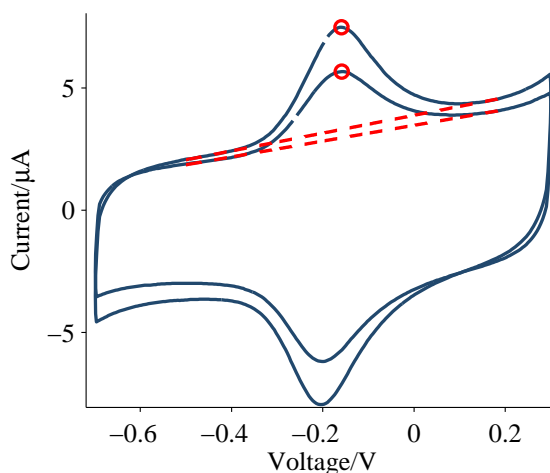


Figure 5.4: The peak height is determined as the difference between the peak current (circle) and the baseline current (dashed line). In order to be able to determine the baseline, a linear fit was made from the current values between -0.5 and -0.4 V and the current values between 0.15 and 0.2 V. The data shown is from the 1st and 10th loop of one of the electrodes from the H_2O with sonication experiment. Potentials referenced versus $Hg/HgSO_4$ electrode.

shown in shown in figure 5.4. The results from the experiments are shown in figure 5.5.

While some curves show a decrease in degradation over time, none of the curves reach steady state within the 45 minutes the experiment took place. The overall variation between electrodes is larger than the difference between experiments (data not shown). From this it can be concluded that none of the experiments yield a stable result and that the signal decay originates from another source, possibly the stability of the Fc^+ ion.

In literature there have been claims of its excellent stability [12] as well as recommendations to use other ions as ferrocene quickly degrades [21]. To investigate if the decay over time was influenced by the redox state, an experiment similar to the previous one was performed. Again sets of 10 CVs were performed every 5 minutes. However, in between these CVs the electrode was set to either a reducing voltage of -0.6 V or an oxidizing voltage of 0.1 V instead of keeping the circuit at open potential. The resulting decay over time is shown in figure 5.6. There is no significant difference in the decay over time for both potentials. This indicates that the decay cannot be attributed to instability of the Fc^+ ion.

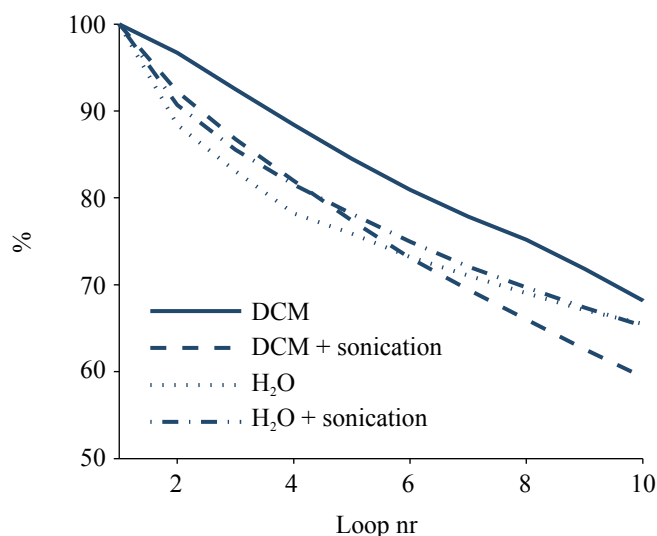


Figure 5.5: Peak height decay of PEG₂₅₀-fc molecules over time for different solvents and the application of an ultrasonic treatment for 5 minutes. Each curve represents the average value of three electrodes.

As the sets of CVs were performed relatively quickly no appreciable change in signal was observed for each set. However during the 5 minute delay between measurements, the signal decayed, indicating that cycling itself is not the reason for the decay. Just having the sensor in solution is already enough to see the decay happening. If the decay is not the result of the release of non specifically bound molecules, or the instability of the Fc⁺ ion, what then can it be attributed to? Given the fact that thiol chemistry is quite stable, the most likely candidate is the degradation of the PEG molecules themselves. This would mean the loss of signal over time is inherent to using PEG as a spacer. As a result, this system is not suitable for continuous measuring for an extended period of time. However, this system would work without issue for proofs of principle or one-time use sensors that only need a short operating time, and are disposed afterwards.

5.4.3 Effect of NaClO₄ concentration

NaClO₄ was used as the background electrolyte because it had been shown previously that this combination of background electrolyte and PEG₃₄₀₀-fc yields a clear voltammogram [13–16]. However, because the background electrolyte can have an influence on the performance (e.g. peak height or location) of an electro active SAM

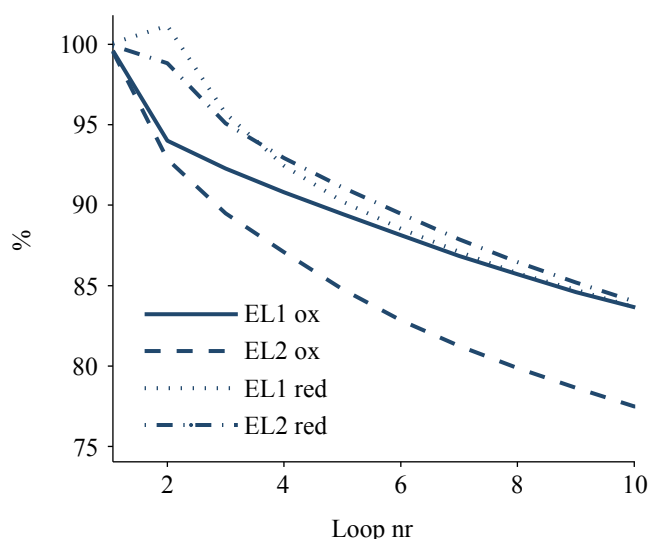


Figure 5.6: Peak height decay of PEG₂₅₀-fc molecules over time for two electrodes each at two different redox states.

[22], the effect of the NaClO₄ concentration was investigated. Since the oxidized Fc ion has a positive charge, it was hypothesized that the different concentrations would have an effect on the screening of the charged Fc ion due to an increase in the Debye length. For two electrodes, CVs were recorded from PEG₂₅₀-fc and PEG_{10k}-fc in concentrations between 1 mM and 5 M at a scanrate of 2 V/s. Each CV was scanned from -0.7 to 0.3 V versus a Hg/HgSO₄ electrode. As an example, the CVs from electrode two are presented in figure 5.7. From each CV the location of the oxidative and reductive peaks were determined in order to calculate the formal potential $E^{0'}$ using:

$$E^{0'} = \frac{E_{red} + E_{ox}}{2} \quad (5.3)$$

The shift in $E^{0'}$ is shown in figure 5.8 for PEG₂₅₀-fc, and in figure 5.9 for PEG_{10k}-fc. A logarithmic relation is found between the NaClO₄ concentration and the observed $E^{0'}$. Fitting the obtained result, yields a slope of -58 and -56 mV per decade for PEG₂₅₀-fc and -53 mV and -54 mV for PEG_{10k}-fc.

This result can be explained if there is an interaction between the NaClO₄ and the Fc. For other monolayers a similar dependence has been observed [23–27], which was

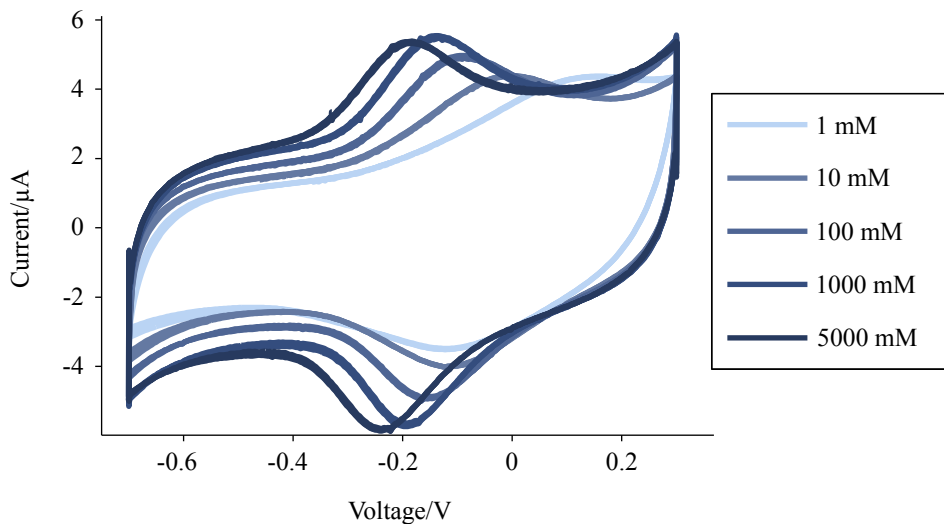
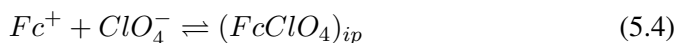


Figure 5.7: The effect of the background electrolyte on the CV of PEG₂₅₀-fc at different concentrations. (1 mM, 10 mM, 100 mM, 1 M, 5M NaClO₄). Upon decreasing concentration, the formal potential shifts towards a higher value. Scanrate 2 V/s. Potentials referenced versus Hg/HgSO₄ electrode.

attributed to ion pairing. As the ferrocenes in the PEG layer are oxidized, the poorly solvated perchlorate ion prefers to bind to the ferrocenium ion. The ferrocenium ion pairs with the dissolved perchlorate ion according to the following stoichiometry:



As a result, according to the Nernst equation this means a dependence of $E^{0'}$ on the NaClO₄ concentration of -59 mV per decade should be expected [26]. With an average response of -55 mV per decade the PEG chain response is close to this theoretical value.

Besides this shift in $E^{0'}$, two additional effects can be observed if the background electrolyte concentration is decreased. The peak height decreases and the peak separation increases. This type of behavior is typically attributed to either ohmic drop in the solution or a decrease in electrode kinetics. Experiments using ohmic drop compensation showed a similar behavior which indicates the kinetics are influenced by the change in background electrolyte concentration. The change in kinetics is either

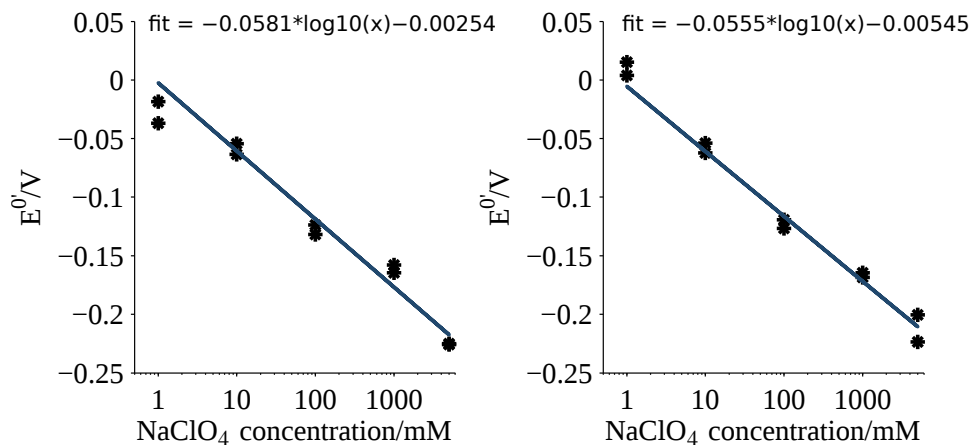


Figure 5.8: Effect of NaClO_4 concentration on the observed formal potential of $\text{PEG}_{250}\text{-fc}$. Left and right figure contain data from experiments at two electrodes with concentrations measured from low to high. Potentials referenced versus Hg/HgSO_4 electrode.

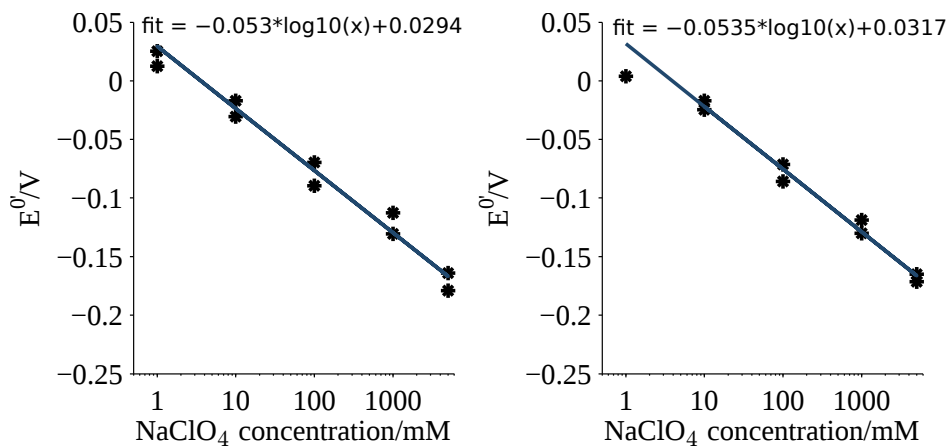


Figure 5.9: Effect of NaClO_4 concentration on the observed formal potential of $\text{PEG}_{10k}\text{-fc}$. Left and right figure contain data from experiments at two electrodes with concentrations measured from low to high. Potentials referenced versus Hg/HgSO_4 electrode.

the result of the ion pairing effect or it is the result of a change in charge screening. Experiments are ongoing to determine the rate constants using CV at various scanrates, in order to define the change in kinetics more quantitatively. Moreover, it would be interesting to perform a similar experiment using a different background electrolyte in order to separate the ion pairing effect from screening effect.

5.5 Concluding remarks

Although the NHS-PEG_x-fc system shows a decay over time, initially a strong signal can be observed of which the decay is less than 40% over a period of 50 minutes. Provided the measurement is performed shortly after introduction to an electrochemical cell, combining this system with a second closely spaced electrode, redox cycling of the attached ferrocene should be possible. The fabrication of such a closely spaced electrode is discussed in chapter 7.

Besides its use in sensor type applications this system is also useful for fundamental electrochemical studies of the PEG_x-fc molecule. The change in peak separation as a result of a decrease in background electrolyte concentration should be investigated further to check whether it results from ion pairing. Initially an experiment with a different background electrolyte should be conducted followed by experiments on other chain lengths.

Bibliography

- [1] E. G. Hvastkovs and D. A. Buttry. *The Analyst*, **135**(8):1817–1829, 2010. 60
- [2] F. Ricci and K. W. Plaxco. *Microchimica Acta*, **163**:149–155, 2008. 60
- [3] K. J. Odenthal and J. J. Gooding. *The Analyst*, **132**(7):603–10, 2007.
- [4] F. Lucarelli, S. Tombelli, M. Minunni, G. Marrazza, and M. Mascini. *Analytica Chimica Acta*, **609**(2):139–59, 2008. 60
- [5] R. Thewes, F. Hofmann, A. Frey, B. Holzapfl, M. Schienle, C. Paulus, P. Schindler, G. Eckstein, C. Kassel, M. Stanzel, R. Hintsche, E. Nebling, J. Albers, J. Hassman, J. Schulein, W. Goemann, and W. Gumbrecht. In *2002 IEEE International Solid-State Circuits Conference. Digest of Technical Papers*, volume 1, pages 350–473. IEEE, 2002. 60
- [6] M. Schienle, C. Paulus, A. Frey, F. Hofmann, B. Holzapfl, P. Schindler-Bauer, and R. Thewes. *IEEE Journal of Solid-State Circuits*, **39**(12):2438–2445, 2004.
- [7] B. Elsholz, R. Wörl, L. Blohm, J. Albers, H. Feucht, T. Grunwald, B. Jürgen, T. Schweder, and R. Hintsche. *Analytical Chemistry*, **78**(14):4794–802, 2006.
- [8] E. Nebling, T. Grunwald, J. Albers, P. Schafer, and R. Hintsche. *Analytical Chemistry*, **76**:689–696, 2004.
- [9] X. Zhu, K. Ino, Z. Lin, H. Shiku, G. Chen, and T. Matsue. *Sensors and Actuators B: Chemical*, **160**(1):923–928, 2011. 60
- [10] A. Anne and C. Demaille. *Journal of the American Chemical Society*, **130**(30):9812–23, 2008. 60
- [11] A. Anne and J. Moiroux. *Macromolecules*, **32**(18):5829–5835, 1999.
- [12] A. Anne, C. Demaille, and J. Moiroux. *Macromolecules*, **35**(14):5578–5586, 2002. 60, 65
- [13] A. Anne, E. Cambрил, A. Chovin, C. Demaille, and C. Goyer. *ACS Nano*, **3**(10):2927–40, 2009. 60, 66
- [14] A. Anne, A. Chovin, C. Demaille, and M. Lafouresse. *Analytical Chemistry*, **83**(20):7924–32, 2011.
- [15] A. Anne, E. Cambрил, A. Chovin, and C. Demaille. *Analytical Chemistry*, **82**(15):6353–6362, 2010.
- [16] J. Abbou, A. Anne, and C. Demaille. *Journal of the American Chemical Society*, **126**(32):10095–108, 2004. 60, 66
- [17] P. J. Flory. *Principles of polymer chemistry*. Cornell University Press, Ithaca, N.Y., 7th edition, 1969. ISBN 0-8014-0134-8. 61
- [18] P. de Gennes. *Macromolecules*, **1075**(19):1069–1075, 1980. 61

- [19] C. Allen, N. Dos Santos, R. Gallagher, G. N. C. Chiu, Y. Shu, W. M. Li, S. a. Johnstone, a. S. Janoff, L. D. Mayer, M. S. Webb, and M. B. Bally. *Bioscience Reports*, **22**(2):225–50, 2002. 61
- [20] J. Zhang, S. Song, L. Wang, D. Pan, and C. Fan. *Nature Protocols*, **2**(11):2888–95, 2007. 63
- [21] D. Kang. *Analytical Chemistry*, **81**(21):9109–9113, 2009. 65
- [22] G. Valincius, G. Niaura, B. Kazakeviciene, Z. Talaikyte, M. Kazemekaite, E. Butkus, and V. Razumas. *Langmuir*, **20**(16):6631–8, 2004. 67
- [23] G. K. Rowe and S. E. Creager. *The Journal of Physical Chemistry*, **98**(21):5500–5507, 1994. 67
- [24] S. E. Creager and G. K. Rowe. *Analytica Chimica Acta*, **246**(1):233–239, 1991.
- [25] X. Yao, J. Wang, F. Zhou, J. Wang, and N. Tao. *The Journal of Physical Chemistry B*, **108**(22):7206–7212, 2004.
- [26] J. Redepenning, E. Castro-Narro, G. Venkataraman, and E. Mechalke. *Journal of Electroanalytical Chemistry*, **498**(1-2):192–200, 2001. 68
- [27] K. Uosaki, Y. Sato, and H. Kita. *Langmuir*, **7**(7):1510–1514, 1991. 67

Titaniumoxide as protection layer for on-chip gold electrodes

In this chapter, we propose the use of a thin titanium dioxide film as protection layer for gold electrodes. Despite the large number of cleaning methods for gold surfaces, it remains a challenge to prevent contamination of or damage to the surface caused by cleaning. In this contribution we suggest an alternative to the cleaning of electrochemical sensors. A titanium dioxide sacrificial layer is applied which can be removed before use to expose the clean gold structure underneath. This method can be beneficial for sensors which rely on clean surfaces for their surface chemistry, for example, thiol chemistry at gold electrodes. Electrode performance is tested through CV in a ferrocenedimethanol solution. After removal of the titanium dioxide layer, a clear voltammogram is obtained with a peak separation of 67 mV, indicating a clean surface. This means that the removal of a sacrificial layer is a good alternative to conventional electrochemical cleaning methods, while also protecting the electrodes during wafer handling.

6.1 Introduction

For electrochemical reactions at gold electrodes, especially surface chemistry, a clean surface is of vital importance [1]. This is a challenge in everyday lab environments where (organic) contaminants will quickly deposit onto any surface [2, 3]. To overcome this problem, a wide variety of cleaning techniques have been developed such as: polishing, submersion in cleaning solution, uv-irradiation, or electrochemical cleaning [1, 2, 4–6].

Despite this wide variety of cleaning techniques it continues to remain a challenge to remove contaminants while at the same time keeping the gold surface intact [6] and/or free from the chemicals used during the cleaning process [5]. If the electrode is not directly accessible, for example in microfluidic devices, techniques such as polishing or irradiation cannot be used. However, as an alternative to cleaning, it is also possible to protect the sample by shielding it against contaminants by means of a protective layer. For example, the active area in template stripped surfaces is shielded by the wafer it is deposited onto [3]. This way it is only exposed to air the moment it is used, keeping it free from any contaminants provided the original substrate was clean. It is also possible to use a molecular monolayer as a protection layer that can be electrochemically desorped from a surface [7]. However, the best way to protect a surface is to add a protective layer to the gold in the same high vacuum environment that was used to deposit the gold.

This means that the protective layer should be a material that can be sputtered or evaporated together with gold, and an etchant must be available that selectively etches this material. In this contribution titanium was chosen because it readily oxidizes and forms a chemically stable titaniumdioxide layer which can be further enhanced through oxygen plasma, anodic oxidation, or annealing [8, 9]. The chemical resistance of TiO_2 thin films has been extensively reviewed in a thesis by B.S. Richards [10]. Typically the TiO_2 layer is resistant to any of the typical cleanroom solvents, acids or bases with the exception of concentrated H_2SO_4 or HF. The etch rates vary based on the crystal phase of the TiO_2 layer, which is related to the annealing temperature. Since gold does not etch in HF or H_2SO_4 it is possible to selectively etch the protecting layer. Besides offering protection against contamination during electrode fabrication or storage, the gold surface is also protected against scratching or roughening of the surface during wafer handling. It should be noted that this method can only be used once for each sensor. However, if not used as a disposable it is possible to use the previously mentioned procedures for electrode cleaning.

6.2 Materials and methods

Electrodes were fabricated by evaporating a sandwich of 15 nm Ti, 110 nm Au, and 15 nm Ti onto a silicon wafer with a 6 μm oxide layer on top. After evaporation a patterning step using Ion beam Etching (IBE) was performed, which was followed by an oxygen plasma to remove the patterning resist and to oxidize the titanium layer. The following chemicals were used: 1,1'-Ferrocenedimethanol ($\text{Fc}(\text{MeOH})_2$, 98%, Acros Organics), Sulfuric acid (H_2S_{04} , 95%-98%, Sigma Aldrich), Sodium Perchlorate (NaClO_4 , 98% extra pure, Acros Organics). All solutions were prepared in 18.2 M Ω cm deionized water (Millipore). Electrochemical measurements were carried out using a SP300 bi-potentiostat (Bio-Logic, France).

6.3 Results and discussion

X-ray photoelectron spectroscopy (XPS) measurements on the fabricated samples confirmed that the titanium surface had been fully oxidized, with a Ti2p3 peak at 458 eV corresponding to TiO_2 , as can be seen in figure 6.1. At least the first 5 nm of the 15nm Ti layer had been fully oxidized, providing a chemically resistant layer. Samples with this layer were put into a solution of concentrated sulfuric acid heated to 105 $^\circ\text{C}$ to etch away the Ti/ TiO_2 layer. Samples were removed once the brown color of the titaniumoxide turned to gold, indicating complete removal of the protective layer. Due to the gradual change in color it is difficult to define an exact etch time, which was generally between 4 to 5 minutes. This etch time corresponds to an etch rate of 3 to 3.75 nm/min, which is of the same order as a previously reported etch rate of 1.7 nm/min at 120 $^\circ\text{C}$ [11]. The temperature of the etching solution is a critical parameter. At room temperature no color changes were observed for a period of over 24 hours, corresponding to an etch rate of less than 0.01 nm/min.

Before and after the etching step, a CV was recorded in a 1 mM 1,1'-ferrocenedimethanol solution with a background electrolyte of 1 M Sodium Perchlorate, using a Mercury/Mercurous Sulphate reference electrode and a platinum counter electrode. The voltage was scanned between 0.3 V and -0.7 V at a scanrate of 2 V/s. Figure 6.2 shows the CVs before and after etching. Before etching the electrode is fully shielded from the ferrocenedimethanol and only a small current contribution can be observed at more reducing potentials. This is likely due to electrochemical reduction of the TiO_2 layer. The shielding against the ferrocenedimethanol reaction confirms that TiO_2 layer completely covers the electrode.

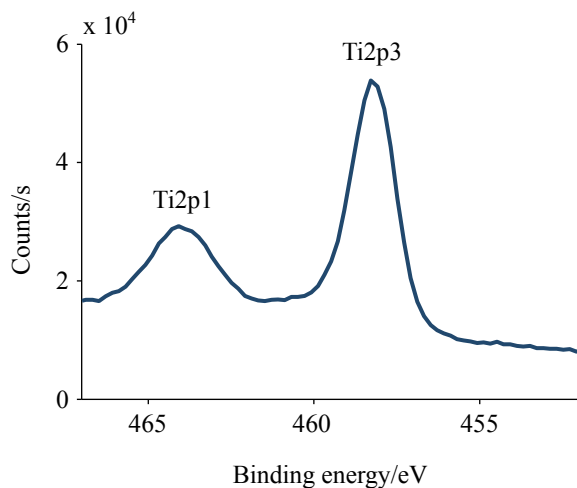


Figure 6.1: XPS element spectrum for titanium. The Ti2p3 peak at 458 eV indicates the Ti has been fully oxidized to TiO_2 .

After etching a typical ferrocenedimethanol CV is obtained with a formal potential at -0.19 V and a peak separation of 67 mV. The peak separation close to the theoretical 59 mV for reactions with one electron transfer, is an indication that a clean surface has been obtained.

6.4 Conclusion

Gold electrodes for electrochemical sensing can be shielded from contaminations through a sacrificial protection layer. With the ability to selectively remove this protection layer without damaging the gold it is possible to keep electrodes stored until needed without risk of contamination. The current application of a TiO_2 layer is resistant to most chemical etchants making the protection layer compatible with additional cleanroom processing for more advanced structures.

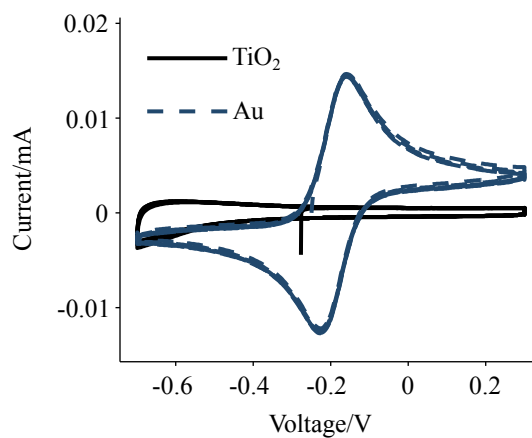


Figure 6.2: Cyclic voltammogram of 1 mM ferrocenedimethanol at a gold electrode with or without TiO₂ protection layer. 6 cycles recorded at a scanrate 2 V/s using a Hg/HgSO₄ reference electrode.

Bibliography

- [1] Z. Yang, A. Gonzalez-Cortes, G. Jourquin, J.-C. Viré, J.-M. Kauffmann, and J.-L. Delplancke. *Biosensors and Bioelectronics*, **10**(9-10):789–795, 1995. 74
- [2] T. Ishida, S. Tsuneda, N. Nishida, and M. Hara. *Langmuir*, **7463**(30):4638–4643, 1997. 74
- [3] J. J. Blackstock, Z. Li, M. R. Freeman, and D. R. Stewart. *Surface Science*, **546**(2-3):87–96, 2003. 74
- [4] L. M. Fischer, M. Tenje, A. R. Heiskanen, N. Masuda, J. Castillo, A. Bienten, J. Émneus, M. H. Jakobsen, and A. Boisen. *Microelectronic Engineering*, **86**(4-6):1282–1285, 2009. 74
- [5] M. White and J. Drobek. *Journal of Physical Chemistry*, **4238**(1):3432–3436, 1966. 74
- [6] J. Kang and P. A. Rowntree. *Langmuir*, **23**(2):509–16, 2007. 74
- [7] C. Wälti, R. Wirtz, and W. Germishuizen. *Langmuir*, (11):981–984, 2003. 74
- [8] D. Blackwood, R. Greef, and L. Peter. *Electrochimica Acta*, **34**(6):875–880, 1989. 74
- [9] F. Heakal and K. Awad. *International Journal of Electrochemical Science*, **6**:6483–6502, 2011. 74
- [10] B. Richards. Ph.D. thesis, 2002. 74
- [11] E. T. Fitzgibbons, K. J. Sladek, and W. H. Hartwig. *Journal of The Electrochemical Society*, **119**(6):735, 1972. 75

Solid state nanogaps for electrochemical detection fabricated using edge lithography

Nanogap electrodes have uses in fields such as chemical sensing, molecular transport, plasmonics, and DNA sequencing. In this chapter a new fabrication strategy for nanospaced electrodes is reported. Using this fabrication strategy, electrodes have been successfully created featuring gap sizes of 100, 50, and 30 nm. Using electrodes with 50 nm spacing, the electrochemical behavior is evaluated by means of CV in combination with RC. The obtained voltammogram corresponds to finite element simulations and the shape of the voltammogram indicates an almost nernstian quasi-reversible CV is obtained for a reversible redox couple, which means the devices are suited for electrochemical detection. Due to the high yield of fabrication, it should be possible to scale the gap size down to values below 30 nm.

7.1 Introduction

Nanogap electrodes have over the years attracted interest from fields such as chemical sensing [1, 2], single molecule electron transport, molecular electronics [3, 4], plasmonics [5–7], and DNA sequencing [8]. These nanogap electrodes are essentially two electrodes spaced < 100 nm apart. However, depending on the desired application the specific geometry varies widely. For example, in single molecule applications a very small electrode area is desired in order to make sure only a single molecule is able to bridge the gap between the two electrodes. This results in designs featuring a sharp tip or small band at the nanogap location. In contrast, for the other applications a larger facing surface area is favorable due to its increase in signal. This results in designs where at least one of the dimensions is in the micron or larger range, while keeping the spacing between the electrodes in the nanometer range.

For electrochemical applications small electrode spacings are desirable if RC is used. RC is based on cycling a reversible redox couple between two closely spaced electrodes, where one electrode is held at an oxidizing potential and another at a reducing potential. The advantage of this technique is that each molecule can contribute to the measured current multiple times, thus effectively creating (electro)chemical signal amplification. This amplification increases with decreasing electrode spacing. A commonly used design for RC applications is that of an interdigitated array electrode. The first use of interdigitated electrodes (IDE's) for redox cycling was reported in 1985 [9]. This first design only had a twin electrode setup, but this was followed by designs with multiple “fingers” [10, 11]. In recent years these devices have gone from micro down to nanoscale spacings [12–16]. Other nanoscale geometries are nanofluidic thin layer cells [17–22], nanocavities [23, 24], or a single nanogap [25].

Typically these nanoscale devices are fabricated using either focused ion beam (FIB) [24, 26–30], or e-beam lithography (EBL) [15–17, 31]. These fabrication methods allow gaps as small as 3 nm [27]. Even though the obtained spacing results are very impressive, the fabrication of these devices is expensive and of low throughput as each device needs to be written individually.

As a result, alternatives have been developed to achieve similar spacings using conventional UV lithography. The basic concepts of these alternatives are shown in figure 7.1. An example of such alternative is that of shadow evaporation [8, 32]. By evaporating the metal layer for the second electrode at an angle, a part of the surface is shadowed by the first electrode, thereby creating a gap between the electrodes. This technique

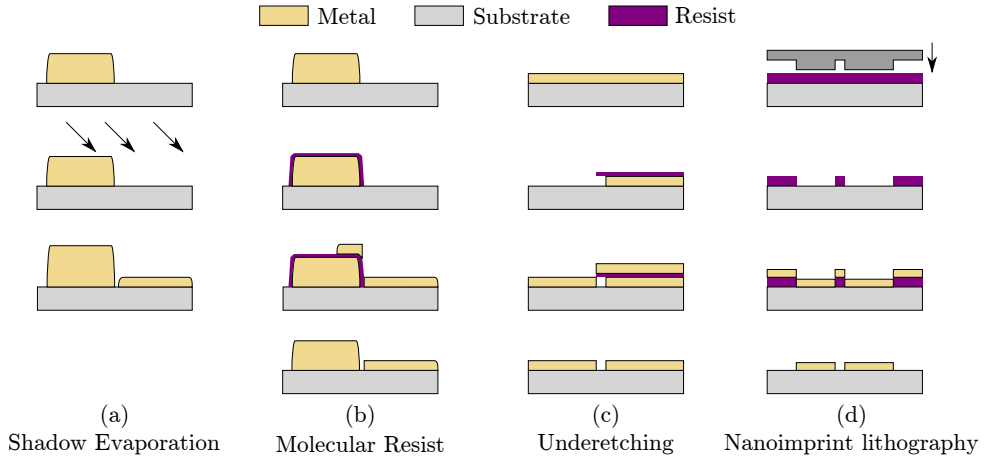


Figure 7.1: Four different fabrications strategies for nanogaps that do not directly rely on FIB or e-beam techniques.

has been used to create gap spacings as small as 9 nm [8]. Another technique featuring even smaller electrode spacings uses molecular resists to achieve spacings below 4 nm [25, 33]. After the first electrode pattern is defined, thiol chemistry is used to create a dense molecular resist on the surface. The second electrode pattern is then applied with a small overlap onto the first electrode. The molecule layer prevents contact between the two electrodes. In a final step the molecule layer is stripped electrochemically in order to expose the gap. It is also possible to fabricate gaps by making use of underetching [34]. Initially the first metal layer is etched using a patterned resist and this results in a slight underetch. A second metal layer is applied and the resist shadows the underetched area. The resist is then lift-off, exposing the gap underneath. Using this technique a spacing of 100 nm has been obtained. Finally, it is also possible to define nanospaced gaps using nanoimprint lithography [13]. This technique is not completely free from EBL as it is required for the fabrication of the stamp. However, once the stamp is fabricated, it can be re-used on multiple wafers. Using this technique a spacing of 100 nm was obtained.

In this contribution a technique similar to that of shadow evaporation and underetching is presented. However, unlike the previously mentioned methods, our method requires only a single metal deposition step to define both of the electrodes. Moreover, by tuning parts of the fabrication process, the inter electrode spacing can be precisely defined.

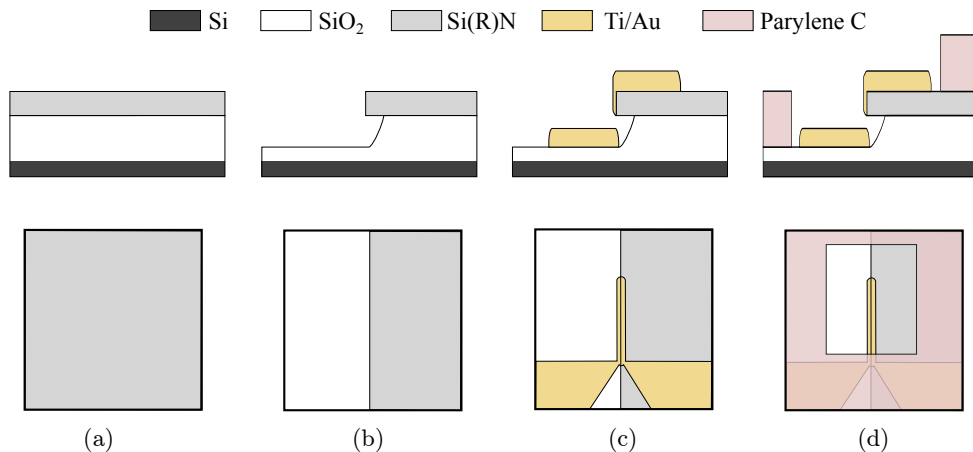


Figure 7.2: Summary of the fabrication process in side and top view. (a) Fabrication is started on a sandwich of silicon (Si), silicon dioxide (SiO_2) and silicon rich nitride (SiRN). (b) By subsequent reactive ion etching (RIE) and buffered hydrogen fluoride (BHF) etching, an overhanging ridge is created (c) Metal is deposited and patterned on the wafer and at the ridge, there is no connection between the two gold structures. (d) to passivate gold lead wiring, a Parylene layer is applied and selectively opened to expose the gap electrodes.

7.2 Fabrication process

The fabrication process is illustrated in figure 7.2. By creating an overhanging ridge in the insulating substrate, the subsequently deposited metal layer is broken on the edge of the ridge. Using this technique a 50 nm spacing between the two electrodes is obtained.

7.2.1 Edge creation

Fabrication is started using a silicon $\langle 100 \rangle$ wafer onto which a $8 \mu\text{m}$ SiO_2 layer is grown using thermal oxidation. This oxide layer is covered by a 100 nm layer of silicon rich nitride (SiRN) using low pressure chemical vapour deposition (LPCVD). SiRN is chosen for its low stress properties, reducing the chance of bending of the overhanging ridge. Ellipsometry is used to confirm the thickness of the SiRN layer by means of a dummy wafer without the SiO_2 layer. Subsequently a $1.7 \mu\text{m}$ thick photoresist is applied and patterned to expose the area where the SiRN layer will be removed. The SiRN is removed using reactive ion etching (RIE). As this process is not selective for SiRN with respect to SiO_2 , the etch process is monitored using an interferometer and stopped at the moment the SiRN layer is removed. To validate that

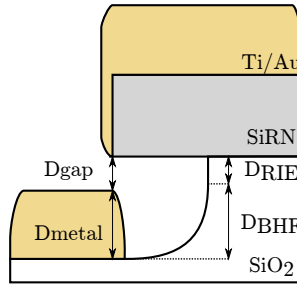


Figure 7.3: By choosing the appropriate RIE and BHF etch depths and metal deposition height, the gap depth can be precisely controlled. The gap depth is the smallest distance between the two gold electrodes and it is defined as the total etch depth minus the height of the metal deposition.

the SiRN layer has been removed at the exposed areas, the conductance of the dummy wafer is measured using a probe station. If the SiRN layer is removed, bare silicon is exposed and the surface should conduct. Once the silicon is exposed, the etch depth is measured using a surface profiler to determine the amount of over etching into the SiO₂ layer. Following the RIE etch, the wafers are put into buffered hydrogen fluoride (BHF) in order to etch the exposed SiO₂ layer. Due to the isotropic nature of the etching process, underetching occurs below the nitride layer. The total etch depth of both the RIE overetch and the BHF etch is a critical parameter in defining the spacing between the two electrodes. Because the metal evaporation process also covers the side of the overhanging ridge, the obtained minimal spacing is the total etch depth minus the height of the metal deposition as is illustrated in figure 7.3. Therefore, if the desired metal height and RIE overetch are known, the required BHF etch depth can be calculated. From this required depth an etch time can be calculated. For example, given a desired gap of 50 nm, a 15/110 nm layer of Ti/Au, and an RIE overetch of 5 nm, a BHF etch depth of 170 nm is desired. As BHF etches at approximately 75 nm/min at 19°C, the wafers are etched for 2 minutes and 15 seconds to obtain the desired depth. The photoresist is then removed using an oxygen plasma and the surface profiler is used to confirm if the desired etch depth has been reached. In the next step the electrodes are defined.

7.2.2 Electrodes

A sandwich layer of 15/110/15 nm of Ti/Au/Ti respectively is evaporated onto the wafers. If the etch depth as determined from the surface profiler measurement deviates

slightly from the desired value, this can be corrected for by changing the amount of deposited gold. Due to the underetch into the SiO_2 , the gold contact is broken at the edge. To define the electrode pattern in the metal layers, a $1.7\ \mu\text{m}$ thick photoresist is applied. Excess metal is then removed from the wafer using subsequent etching in 1% HF, gold etchant, and 1% HF in order to remove the Ti/Au/Ti layers respectively. This results in two closely spaced electrodes of $47\ \mu\text{m}$ length and $2.5\ \mu\text{m}$ width. However, care must be taken not to overetch each layer as this will decrease the width of the electrodes. A critical step is the alignment of the electrode pattern onto the edge of the ridge, as each electrode pattern is only $2.5\ \mu\text{m}$ wide and some losses result from overetching. If the alignment is off by more than $2 - 2.5\ \mu\text{m}$, the edge is not patterned and only a single electrode remains. After the electrodes are fabricated, the resist is removed in 99% HNO_3 and the wafers are ready for packaging. As an alternative to wet etching the metal, it is also possible to define the electrode pattern using reactive ion beam etching (RIBE), this eliminates the underetching of gold at the cost of re-deposition of metals at the sides of the electrodes. This re-deposition can cause the two electrodes to become shorted.

7.2.3 Packaging

To shield the leads running to the electrode pair from solution during electrochemical measurements, a $1\ \mu\text{m}$ layer Parylene C is applied using a Parylene coater. This coating is removed locally at the nanogap and at the electrode contact pads by application of a photoresist layer and RIE etching. After etching the resist is removed and the wafers are diced into individual 1 by 2 cm chips. Shortly before use the top Ti layer can be removed using 1% HF to expose the clean gold underneath.

7.3 Materials and methods

To test the electrochemical functioning of the fabricated electrodes, CV and RC measurements are performed. For each electrode a CV is recorded between 0 V and 0.5 V vs an Ag/AgCl electrode at 50 mV/s with the other electrode either floating, at 0 V, or at 0.5 V vs Ag/AgCl. Electrochemical measurements were performed using a SP300 bi-potentiostat (Bio-Logic, France). Connections to the chips are made using a custom built electrochemical cell. Reference: Ag/AgCl electrode (BASi RE-6), Counter: 2 mm Pt disk (CH Instruments). The following chemicals were used: Potassium Chloride (KCl, >99% Sigma-Aldrich), and 1,1'-Ferrocenedimethanol ($\text{Fc}(\text{MeOH})_2$, 98%, Acros Organics). Solutions were prepared in $18.2\ \text{M}\Omega\text{cm}$ deionized water (Millipore).

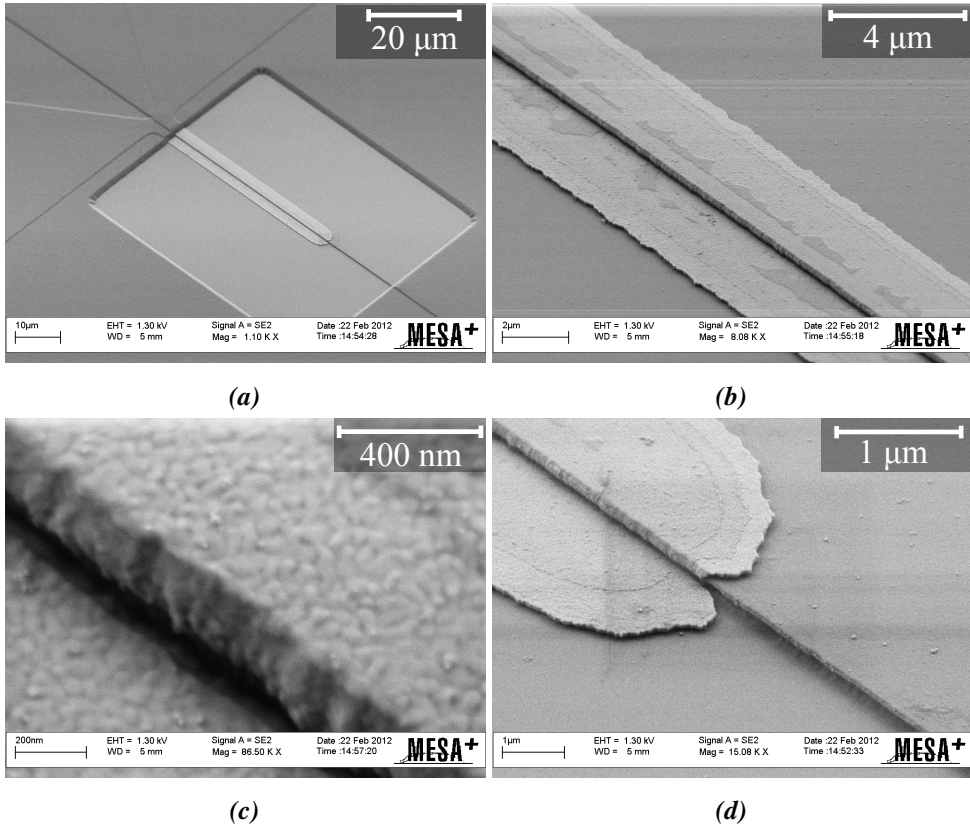


Figure 7.4: SEM images of the realized structure at various zoom levels. (a) Overview of the device showing the exposed area with the two electrodes in the center. Beneath the Parylene coating the electrode leads can be observed. (b/c) Two close-ups of the gap area indicating the uniformity of the gap over a large distance. (d) In this image the underetch into the SiO₂ can be observed. It also shows that the metals are deposited onto the side of the nitride ridge.

7.4 Results and discussion

7.4.1 Fabrication

Devices have been fabricated with 100 and 50 nm gap spacing. Each spacing had a 96% yield with more than 25 devices tested for each gap size. In figure 7.4, SEM images are shown from a device with a 50 nm gap. At lower zoom levels the devices seem smooth over the complete 47 μm electrode length. However, at higher zoom levels some roughness can be observed, both at the outer edge of the electrode and the gap itself. This is attributed to resist residues sticking to the edge of the mask features.

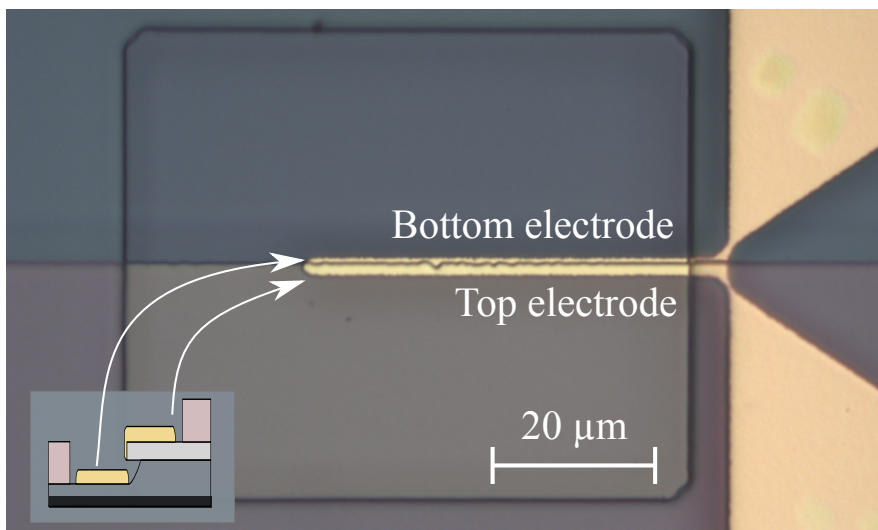


Figure 7.5: Microscope image of one of the realized devices. Electrode length is $47\ \mu\text{m}$. Top electrode $1.7\ \mu\text{m}$ wide and bottom electrode $0.6\ \mu\text{m}$ wide.

If a mask is re-used multiple times without cleaning in between uses, this effect is increased. This effect might increase the risk of electrically shorted electrodes, as the gap is less well defined. However this was not observed during fabrication.

Underetching into the metal layers beneath the photoresist had a clear impact on the yield of the fabricated devices. In figure 7.5 the device is shown that was used for electrochemical testing, of which the results are described in the following section. While the electrode width defined in the mask is $5\ \mu\text{m}$ wide, after etching only $2.3\ \mu\text{m}$ remains. The top electrode is $1.7\ \mu\text{m}$ wide and the bottom electrode is $0.6\ \mu\text{m}$ wide. This overetch also influences the connections towards the electrode. As can be seen in the figure the connections towards the electrodes are almost broken due to the overetch. Typically failed devices were either missing one of the electrodes or had the connections towards the electrode broken. However, for the nanogaps itself none of the devices showed a short circuit.

7.4.2 Electrochemistry

To test the electrochemical functioning, a batch of $50\ \text{nm}$ spaced electrodes was used in three different electrochemical modes. First a CV was performed at one electrode while the other was left floating, followed by a measurement with the other electrode at $0\ \text{V}$, and lastly a CV was recorded while the other electrode was set to $0.5\ \text{V}$. After

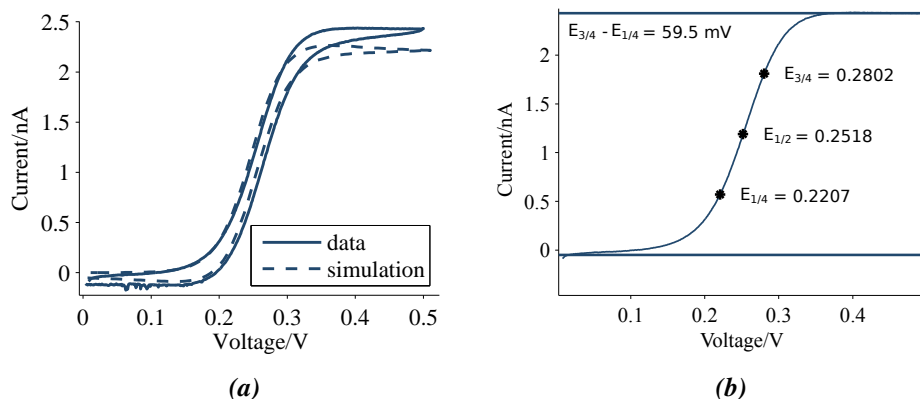


Figure 7.6: (a) Comparison between the experimental voltammogram obtained for the top electrode and a simulation using finite element modeling. (b) Evaluation of the shape of the top electrodes' forward CV. The different between $E_{3/4}$ and $E_{1/4}$ is 59 mV at a scanrate of 50 mV/s, only slightly higher than the 56.4 mV expected for an ideal system [35]. Measurement performed in 0.1M KCl and 1 mM Ferrocenedimethanol in DI water. Potentials referenced versus Ag/AgCl electrode.

the three CVs were performed the electrode connections were switched and the same set was repeated. The measurements were performed in 1 mM ferrocenedimethanol with 0.1 M KCl as background electrolyte using an Ag/AgCl reference electrode. First the shape of a single electrode CV is evaluated. The results are shown in figure 7.6.

The electrodes most closely resemble band microelectrodes. However, as there are no analytical expressions available for the current at a band microelectrode CV, the experimental results can only be compared with simulations. This is shown in figure 7.6.a. The current for the top electrode is plotted together with the current simulated using finite element modeling in Comsol Multiphysics. The shape of the curves matches closely with only a 10% difference in limiting currents. This difference is most likely the result of the model assuming a completely flat 1.7 by 47 μm electrode whereas in reality the electrode is 110 nm high. This means the electrode sidewalls account for an additional 13% in surface area which is neglected in the model. Besides the simulations, additional information can be retrieved from the shape of the experimental voltammogram. For a microelectrode CV the voltage difference between $E_{3/4}$ and $E_{1/4}$ should be 56.4 mV, where $E_{3/4}$ and $E_{1/4}$ are the voltages at which the current is 3/4 and 1/4 of the limiting current respectively [35].

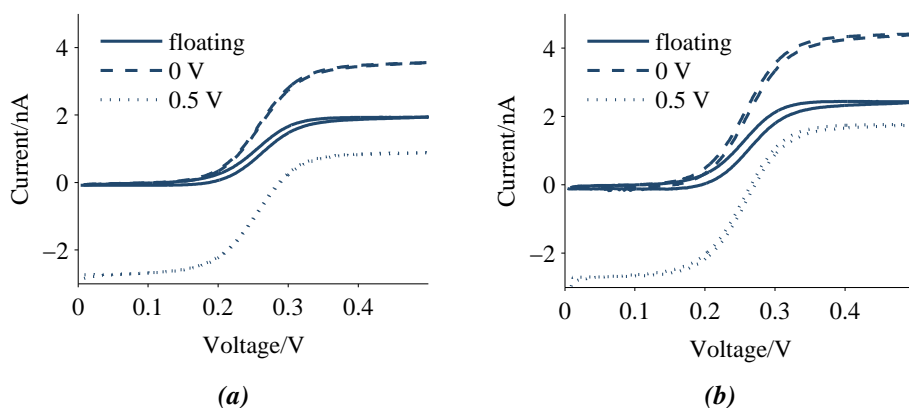


Figure 7.7: CV in combination with RC results. (a) CV results from the bottom electrode at three top electrode potentials. (b) CV results from the top electrode at three bottom electrode potentials. Measurement performed at a scanrate of 50 mV/s, using an Ag/AgCl reference electrode. Measurement performed in 0.1M KCl and 1 mM Ferrocenedimethanol in DI water.

In the voltammogram for the top electrode this difference is 59.5 mV as is shown in figure 7.6.b. This only slight deviation from theory indicates an almost nernstian quasi-reversible CV is obtained.

The results for the different electrode potentials are shown in figure 7.7. The bottom electrode which is shown in figure 7.7.a obtains lower currents than the top electrode shown in figure 7.7.b. For the single electrode measurement (where the other electrode is left floating) the bottom electrode reaches a steady state value of 1.9 nA whereas the top electrode reaches 2.4 nA. This can be explained by looking at the size of the electrodes. The top electrode is 1.7 μm wide while the bottom electrode is only 0.6 μm wide. The scaling of the current with respect to the electrode area is not linear due to the microband shape of the electrodes.

If the other electrode is set to 0 V the current is increased to a value of 3.55 nA and 4.4 nA for bottom and top electrode respectively, which is a factor 1.8 increase in current for both electrodes due to the effect of RC. If the other electrode is set to 0.5 V, the electrodes start to compete for the same reaction and the current drops to 0.88 nA and 1.77 nA for bottom and top electrode respectively. For the bottom electrode only 45% of the original current remains while for the top electrode 72% is left. This is the result of the larger size of the top electrode and because the top electrode is “shadowing” the bottom electrode. At 0 V an increase in reduction current can be observed. The

current from both electrodes increases by a factor 27 from -0.1 nA to -2.7 nA as a result of the local increase in the oxidized ferrocenedimethanol concentration due to the the other electrode.

7.5 Concluding remarks

Using edge lithography as described in this chapter, electrodes with spacings down to 50 nm can be successfully fabricated without EBL or FIB. The electrodes fabricated in this way show electrochemical behavior that matches with theory. The electrochemical experiments show that these devices can be used for RC of a freely diffusing redox mediator. The obtained amplification is maximally a factor 1.8 for freely diffusing species. However, it is our intention to use these devices for redox cycling of surface attached molecules, which should result in higher amplification values. The yield of the fabricated devices is high (96%), indicating the lower limit of the fabrication technique has not been reached. It should be possible to scale the gap size down to values below 30 nm. At these size ranges the fabricated devices are suitable for the investigation of electron transport in molecular systems.

Bibliography

- [1] J. Lee, W. Shim, J.-S. Noh, and W. Lee. *Chemphyschem : a European journal of chemical physics and physical chemistry*, **13**(6):1395–403, 2012. 80
- [2] L. Rassaei, K. Mathwig, E. D. Goluch, and S. G. Lemay. *The Journal of Physical Chemistry C*, **116**(20):10913–10916, 2012. 80
- [3] R. L. McCreery, H. Yan, and A. J. Bergren. *Physical Chemistry Chemical Physics*, pages 1065–1081, 2012. 80
- [4] T. Li, W. Hu, and D. Zhu. *Advanced Materials*, **22**(2):286–300, 2010. 80
- [5] M. Jin, H. van Wolferen, H. Wormeester, A. van den Berg, and E. T. Carlen. *Nanoscale*, **4**(15):4712–8, 2012. 80
- [6] B. Moody and G. S. Mccarty. *Applied Physics Letters*, **94**:122104, 2009.
- [7] K. Kim, J.-Y. Choi, and K. S. Shin. *Spectrochimica Acta Part A: Molecular and Biomolecular Spectroscopy*, **100**:3–9, 2013. 80
- [8] X. Liang and S. Y. Chou. *Nano Letters*, **8**(5):1472–6, 2008. 80, 81
- [9] D. G. Sanderson and L. B. Anderson. *Analytical Chemistry*, **57**(12):2388–2393, 1985. 80
- [10] O. Niwa, M. Morita, and H. Tabei. *Analytical Chemistry*, **62**(5):447–452, 1990. 80
- [11] A. J. Bard, J. A. Crayston, G. P. Kittlesen, T. Varco Shea, and M. S. Wrighton. *Analytical Chemistry*, **58**(11):2321–2331, 1986. 80
- [12] K. Ueno, M. Hayashida, J. Y. Ye, and H. Misawa. *Electrochemistry Communications*, **7**:161–165, 2005. 80
- [13] M. Beck, F. Persson, P. Carlberg, M. Graczyk, I. Maximov, T. Ling, and L. Montelius. *Microelectronic Engineering*, **73-74**:837–842, 2004. 81
- [14] L. H. D. Skjolding, C. Spegel, A. Ribayrol, J. Emnéus, and L. Montelius. *Journal of Physics: Conference Series*, **100**(5):52045, 2008.
- [15] E. D. Goluch, B. Wolfrum, P. S. Singh, M. A. G. Zevenbergen, and S. G. Lemay. *Analytical and Bioanalytical Chemistry*, **394**(2):447–456, 2009. 80
- [16] K. Hayashi, J. Takahashi, T. Horiuchi, Y. Iwasaki, and T. Haga. *Journal of the Electrochemical Society*, **155**:J240–J243, 2008. 80
- [17] B. Wolfrum, M. Zevenbergen, and S. Lemay. *Analytical Chemistry*, **80**(4):972–977, 2008. 80
- [18] M. A. G. Zevenbergen, B. L. Wolfrum, E. D. Goluch, P. S. Singh, and S. G. Lemay. *Journal of the American Chemical Society*, **131**(32):11471–11477, 2009.

- [19] M. A. G. Zevenbergen, D. Krapf, M. R. Zuiddam, and S. G. Lemay. *Nano Letters*, **7**:384–388, 2007.
- [20] M. A. G. Zevenbergen, P. S. Singh, E. D. Goluch, B. L. Wolfrum, and S. G. Lemay. *Analytical Chemistry*, **81**(19):8203–8212, 2009.
- [21] M. A. G. Zevenbergen, P. S. Singh, E. D. Goluch, B. L. Wolfrum, and S. G. Lemay. *Nano Letters*, pages 2881–2886, 2011.
- [22] K. Mathwig, D. Mampallil, S. Kang, and S. G. Lemay. *Physical Review Letters*, **109**(11):1–5, 2012. 80
- [23] E. Kätelhön, B. Hofmann, S. G. Lemay, M. A. G. Zevenbergen, A. Offenhäusser, and B. Wolfrum. *Analytical Chemistry*, **82**(20):8502–9, 2010. 80
- [24] S. Neugebauer, A. Zimdars, P. Liepold, M. Gebala, W. Schuhmann, and G. Hartwich. *ChemBioChem*, **10**(7):1193–1199, 2009. 80
- [25] G. S. McCarty, B. Moody, and M. K. Zachek. *Journal of Electroanalytical Chemistry*, **643**(1-2):9–14, 2010. 80, 81
- [26] T. Nagase, T. Kubota, and S. Mashiko. *Thin Solid Films*, **438**:374–377, 2003. 80
- [27] T. Nagase, K. Gamo, T. Kubota, and S. Mashiko. *Thin Solid Films*, **499**(1-2):279–284, 2006. 80
- [28] G. C. Gazzadi, E. Angeli, P. Facci, and S. Frabboni. *Applied Physics Letters*, **89**(17):173112, 2006.
- [29] T. Blom, K. Welch, M. Stromme, E. Coronel, and K. Leifer. *Nanotechnology*, **18**(28):285301, 2007.
- [30] A. K. Singh, N. S. Rajput, N. Shukla, S. K. Tripathi, J. Kumar, and V. N. Kulkarni. *Nuclear Instruments and Methods in Physics Research Section B: Beam Interactions with Materials and Atoms*, **268**(19):3282–3286, 2010. 80
- [31] Y. Wu, T. Akiyama, S. Gautsch, and N. de Rooij. *Procedia Engineering*, **25**:1661–1664, 2011. 80
- [32] C. Wälti, R. Wirtz, and W. Germishuizen. *Langmuir*, (11):981–984, 2003. 80
- [33] G. S. McCarty. *Nano Letters*, **4**(8):1391–1394, 2004. 81
- [34] K. Yu, X. Wang, X. Yu, and A. Zhao. In *Proceedings of the 2011 6th IEEE International Conference on Nano/Micro Engineered and Molecular Systems*, pages 1124–1127. 2011. 81
- [35] A. J. Bard and L. R. Faulkner. *Electrochemical Methods: Fundamentals and Applications*. Wiley, 2nd edition, 2001. ISBN 978-0-471-04372-0. 87

On chip redox cycling of surface attached molecules

This chapter contains the results obtained by combining surface attached molecules with solid state nanospaced electrodes. Two electrode configurations were used. One, the planar nanogap device reported in chapter 7 and two, a nanofluidic thin layer cell fabricated in the group of Lemay. The planar device only shows a hint of RC but is at least guaranteed to be free from freely diffusing molecules in the liquid. The thin layer cell on the other hand shows clear RC behavior, however a control experiment using PEG chains that are too short to cross the gap also shows a RC current. This indicates there are still freely diffusing molecules present in the device. At this time it is not possible to determine which part of the current is contributed by the surface attached molecules and which part is due to freely diffusing molecules. This indicates that the best approach is to optimize the planar electrode design in order to achieve a better signal to offset ratio.¹

¹Parallel plate results were obtained in close collaboration with the Nanoionics group. Thanks especially to Shuo Kang for her assistance in data collection and Serge Lemay for discussions.

8.1 Introduction

In chapter 5 and 7, surface modification and electrode fabrication were discussed. In this chapter this work is continued by combining the fabricated electrodes with the surface attached molecules in order to measure the RC based current resulting from these attached molecules.

The aim of this project is to use this redox cycling of surface attached molecules as a transducing element in an electrochemical sensor. For example, by adding a small fragment of single stranded DNA to the PEG chains, the measured current can be influenced by a hybridization event between the DNA that is connected to the PEG chain and a freely diffusing complementary DNA strand. This effectively creates a DNA sensor for the freely diffusing DNA and it has been shown to function at a single electrode for a configuration where the redox label is attached to the surface [1–4] as well as a dual electrode system with a freely diffusing redox mediator [5–9].

RC of surface attached molecules has previously been achieved by Demaille et al. using an AFM with an electroactive tip that was approached to a surface [10–13]. Their experiments typically involved either the tip or the substrate to be modified with PEG₃₄₀₀-fc. However, a more elaborate experiment also involved the addition of surface attached proteins between the electrode and the PEG₃₄₀₀-fc chains [11]. Their goal is that of single protein imaging using this system.

The important difference between our experimental setup and that of Demaille et al. is that they use a scanning probe system whereas for this project, the measurements are performed in a solid state device. The benefit of a scanning probe system is the ability to approach to the surface until a signal occurs, and there is no lower limit in the spacing that can be obtained. However, the downside of this approach is that the separation between tip and substrate is never exactly known because the force curves and the electrochemical current do not show any discrete steps upon contact with the surface because of the flexibility of the layer of attached molecules. This problem is solved by performing the measurements with a solid state sensor. For a solid state sensor, the geometry is defined through careful cleanroom processing and can be confirmed by techniques such as high resolution scanning electron microscopy (HR-SEM), as was shown in chapter 7.

For both scanning probe systems and solid state devices, the goal is to place two electrodes in close proximity to each other. In this chapter results will be shown for

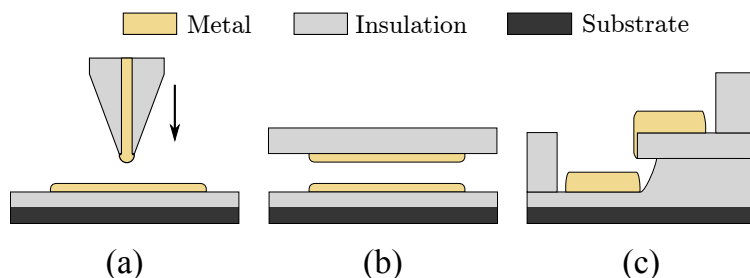


Figure 8.1: Three different geometries discussed in the introduction. (a) The probe based system. (b) The thin layer cell. (c) The planar device.

two solid state devices that accomplish this goal. The nanogap electrode, as described in chapter 7, and a nanofluidic thin layer cell device previously reported by the group of Lemay [14–19]. An overview of the different geometries is shown in figure 8.1.

8.2 Planar electrodes

8.2.1 Materials and methods

The experiments have been performed using NHS-PEG_{10k}-fc. For a detailed protocol on the synthesis of the PEG molecules see appendix B. Electrochemical measurements were performed using either a SP300 bi-potentiostat (Bio-Logic, France) or a model 700E bi-potentiostat (CH instruments, USA).

Electrodes fabricated as described in chapter 7 were cleaned for 30 seconds in piranha solution. Subsequently they were rinsed and put into DI water containing 20 mM cystaminedihydrochloride (FLUKA) to allow the cystamine monolayer to form overnight. The NHS-PEG_{10k}-fc chains are subsequently attached to the cystamine layer by putting the electrodes overnight in water containing the PEG chains. Finally, the electrodes were extensively rinsed using DI water to remove the unbound PEG chains, after which they were ready for use. Measurements were recorded in a solution of 1 M NaClO₄ (Sigma).

8.2.2 Discrete DCV

The first experimental results are from a protocol that is a mix of the DCV and conventional RC techniques. This protocol is most aptly described as the application of the DCV waveform at discrete voltage intervals. Therefore, this technique will be referred to as discrete DCV. An example of the applied potential steps is shown in

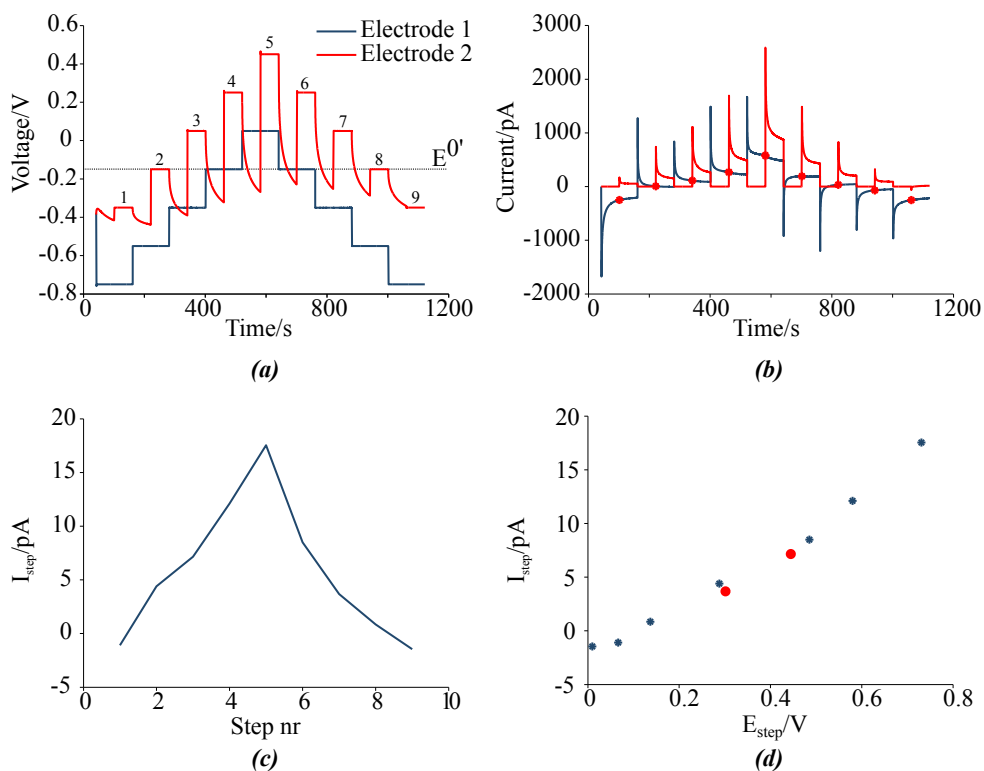


Figure 8.2: Discrete DCV experimental results at a 7 nm gap chip. (a) Applied voltages for both nanogap electrodes. (b) Recorded current for these electrodes. (c) Current step at electrode 1 resulting from the applied potential on electrode 2. (d) Current step at electrode 1 versus the voltage difference between the applied step and the open circuit potential at electrode 2. Red dots correspond to steps 3 and 7, for details see text. Potentials referenced versus Hg/HgSO₄ electrode.

figure 8.2.a and the resulting current is shown in figure 8.2.b. Measurements were performed on devices with a spacing of 7 nm.

Initially one of the two electrodes is set to a constant potential for one minute. After this minute the second electrode is stepped from open circuit potential to a potential biased 0.2 V above the other electrode's potential and both electrodes are kept at their potentials for another minute. After these two minutes, the first electrode is stepped to the next voltage while the second electrode is left floating again. This is repeated for a series of voltages ranging from below to above the formal potential of the ferrocene label. The idea behind the application of this technique is that for the first minute the faradaic current on the first electrode gets a chance to stabilize, as well as eliminating

the initial charging current. If after the first minute the second potential is applied to a value above the formal potential while the first electrode is still below the formal potential, RC will occur. This RC effect should result in a step in the current response the moment the second electrode is set to its potential. For potential values where both electrode are either above or below the formal potential, this current step should not occur. Given the voltages applied as shown in figure 8.2 this means that a maximum current step should be obtained for steps 3 and 7. As can be seen in figure 8.2.c this does not occur and a maximum current is found for step 5. This can be explained by plotting the voltage step from open circuit to applied potential for the second electrode versus the measured current step. This result is shown in figure 8.2.d. As can be seen in the figure an almost linear relation exists between the potential step on the second electrode and the observed current step on the first electrode. This is the result of a capacitive coupling between the two electrodes. This capacitive coupling does not necessarily have to be an issue as it should still be possible for the RC current to provide an offset to this capacitive current. In other words, as long as the current steps recorded at potential step 3 and 7 are above the linear trend, it would already prove the presence of the redox cycling effect. Currently this is not the case for the 7 nm spaced devices. Measurements at 50 nm spaced electrodes show a similar behavior (data not shown). To make sure that the lack of signal is not due to a failure in electrode modification, CVs are performed at an on-chip gold macroelectrode. Due to the strong capacitive currents, the CVs for the nanogap electrodes do not show the peaks related to the presence of PEG_{10k}-fc. However, the macroelectrode did show the CV that is typical for the presence of PEG_{10k}-fc, as is shown in figure 8.3. Given that the larger electrode is made up of the same material as the nanogap electrodes as well as having been subject to the same modification protocol, it is safe to assume the molecules are also present on the nanogap electrodes.

Given that the molecules are attached to the surface, the reason for not observing a RC based signal is that it is obscured by the capacitive offset. This can be solved by amplifying the RC current through a decrease in electrode spacing, or decreasing the capacitive offset. As these devices have a 7 nm spacing and a relatively low yield, achieving an even lower electrode spacing is not an option. Therefore, the solution must be found in reducing the capacitive offset, either through engineering even more insulated devices or through a different measurement protocol. For this reason a second set of experiments was performed using the technique of amplified CV.

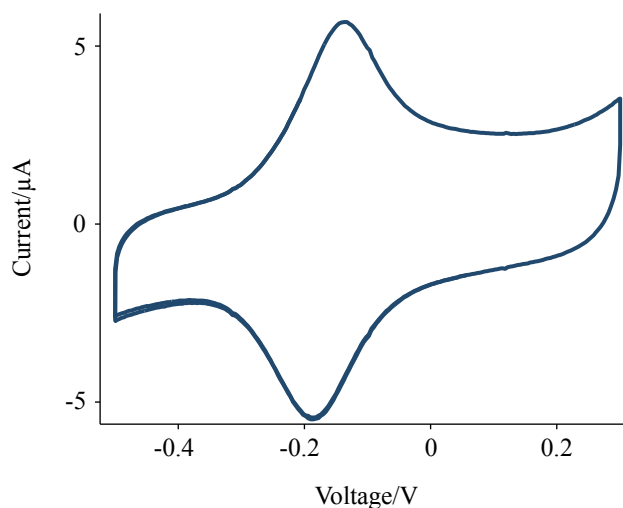


Figure 8.3: CV of a macroelectrode on the same sample showing the peaks that correspond to the presence of PEG_{10k}-fc, an indication that surface modification was successful. Potential referenced versus a Mercurous/Mercurousulphate reference electrode, potential was scanned at a scanrate of 2 V/s. Peak separation is 49 mV. Potentials referenced versus Hg/HgSO₄ electrode.

8.2.3 Amplified CV

Amplified CV as described in chapter 2 was performed at a device with a 50 nm electrode spacing. In this experiment the potential was scanned at one of the electrodes from 0 V to 0.5 V at a scanrate of 1 mV/s while the other electrode was kept at a potential of 0 V. The voltammogram of the first electrode was also recorded while the other electrode was left floating, resulting in a single electrode voltammogram. The results are shown in figure 8.4. In the voltammogram a small plateau can be observed around 0.4 V for both the positive and negative RC currents, in the single electrode voltammogram this plateau is absent.

The increase in current is the result from the second electrode being set to 0 V. A leakage current as a result of a short circuit can be eliminated as a cause for this effect because it would have resulted in a linear increase of the current as the potential difference between the two electrodes increases, and this cannot be observed in the voltammogram. This means that the most likely candidate for the current increase is RC. However, the potential at which this occurs is relatively high, as the formal potential for PEG_{10k}-fc is approximately 0.2 V versus Ag/AgCl, which should result

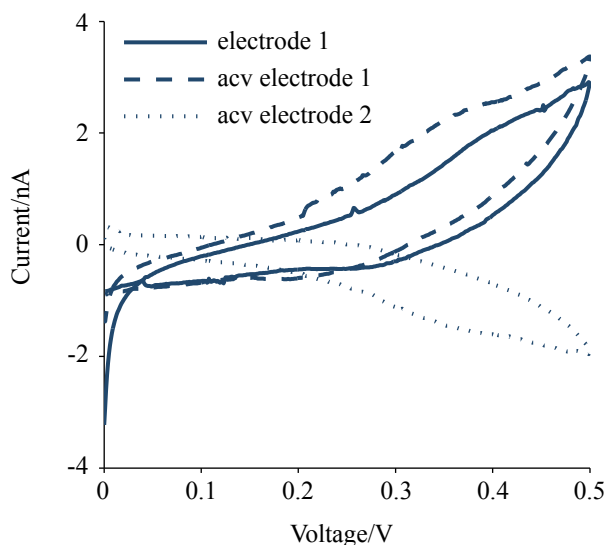


Figure 8.4: Amplified CV data for $PEG_{10k}\text{-fc}$ at an electrode pair with a 50nm spacing. In the amplified CV a plateau can be observed at 0.4 V that is not present for the single electrode voltammogram. Scanrate 1 mV/s, potentials referenced versus an Ag/AgCl electrode.

in a plateau value at 0.3 V. This 0.1 V shift in formal potential can be explained if there are poor electron transfer kinetics at the electrode surface. However, as the surface modification succeeded and the standard modification protocol was followed, there is no indication why for this experiment the electrode surface showed a decreased electron transfer.

The increase in current itself is relatively small compared to the single electrode case. This can be explained by the geometry of the electrode. As each electrode is $2.5\ \mu\text{m}$ wide, only a small fraction of the electrodes is contributing to RC. In order to see if the signal would improve by having a larger fraction of the surface contributing to RC, additional experiments were performed in a nanofluidic thin layer cell.

8.3 Thin layer cell

8.3.1 Materials and methods

The experiments have been performed using NHS- $PEG_{3400}\text{-fc}$, NHS- $PEG_{10k}\text{-fc}$, and NHS- $PEG_{10k}\text{-fc}$ where the NHS group has been blocked by ethanolamine. Electrochemical measurements were performed using either a model 700E bi-potentiostat

(CH instruments, USA) or a custom built setup based on two 6430 Sub-Femtoamp Remote SourceMeters (Keithley, USA).

Before use, the chromium sacrificial layer was removed using chromium etchant to expose a 70 nm high nanochannel. By recording the current flow between the top and bottom electrode, the removal of the chromium layer could be monitored. After the electrode was successfully opened, the chromium etchant was replaced by a 0.5 M H₂SO₄ solution. In this solution the devices were cleaned electrochemically by scanning the potential between 1.2 V and -0.15 V versus Ag/AgCl at a scanrate of 50 mV/s. After the electrochemical cleaning the devices were flushed with DI water followed by flushing with 20 mM cystaminedihydrochloride (FLUKA), to allow the cystamine monolayer to form overnight. In the morning the devices were flushed with DI water followed by the introduction of the NHS-PEG_{10k}-fc containing solution. This was left for 3 hours to let the molecules attach to the surface. After 3 hours the device was flushed several times with 1M NaClO₄ solution. In this same solution the measurements were performed.

8.3.2 Attached molecules

Results from the first experiment are shown in figure 8.5. In this experiment the standard modification protocol was followed, allowing the NHS-PEG_{10k}-fc chains to attach to the surface. To confirm that the solution of freely diffusing molecules had been flushed out of the channel, a single electrode CV was recorded at the top electrode. For freely diffusing molecules at this electrode a microelectrode type CV shape would be expected. However, for attached molecules we would expect to see two peaks. Given that two peaks can be observed in the experimental voltammogram of figure 2.6.b and there is no indication of a microelectrode type shape, it can be concluded that surface attached molecules were dominating the reaction and that the solution has been flushed enough. A peak separation of 0 V is obtained at a formal potential of 0.21 V versus Ag/AgCl.

To evaluate the RC behavior, amplified CVs were recorded at 1 mV/s. This relatively low value for the scanrate was chosen to eliminate capacitive currents as much as possible, as these obscured the cycling signal for higher scanrates. The result is shown in figure 2.6.a. A steady state current of approximately 80 pA was obtained with a halfwave potential of 0.19 V.

Combining the single electrode and cycling results, an apparent diffusion coefficient can be calculated. The peaks in the single electrode voltammogram show a charge

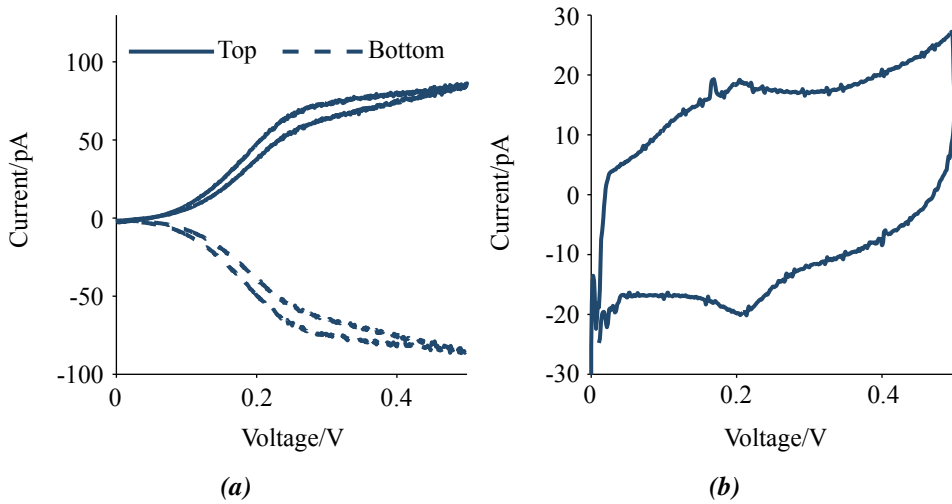


Figure 8.5: Results from the experiment where molecules were allowed to attach to the surface. (a) Amplified CV recorded at 1 mV/s, showing a steady state of approximately 80 pA. (b) Single electrode CV recorded at the top electrode at 50 mV/s showing the typical peaks resulting from surface attached molecules. Potentials referenced versus Ag/AgCl electrode.

transfer of $11e-12$ C. As described in chapter 5, given an elementary charge of $1.6e-19$ C the total number of molecules present is calculated to be $6.7e7$. The area of the top electrode is $60 \mu\text{m}^2$ of which $30 \mu\text{m}^2$ is overlapping with the bottom electrode. Assuming that the molecules are able to cross the gap between the electrodes, the molecules at the overlapping portion of the bottom electrode are able to react as well. This means that the total active surface area for the molecules is $60 \mu\text{m}^2$ for the top electrode and $30 \mu\text{m}^2$ for the bottom electrode. Dividing the number of molecules by the total surface area yields a density of $5.1e17$ molecules/ m^2 . However, only the molecules present in the overlapping area of the electrodes are able to contribute to the RC current. Given that the overlapping area is $30 \mu\text{m}^2$ and molecules from both the the top and bottom electrode can contribute a total of $4.6e7$ molecules is available for RC. The RC current is described by the following equation [17]

$$I = \frac{NeD}{z^2} \quad (8.1)$$

which can be re-written to obtain the diffusion coefficient

$$D = \frac{Iz^2}{Ne} \quad (8.2)$$

with I the steady state current (80 pA), e the elementary charge, N the number of

molecules, D the diffusion coefficient, and z the distance between the electrodes (70 nm). This yields a value for the diffusion coefficient of $5.3 \times 10^{-14} \text{ m}^2/\text{s}$. The diffusion coefficient of a single PEG unit is $7 \times 10^{-10} \text{ m}^2/\text{s}$ and according to the Rouse model this should be divided by the number of units in the chain to obtain the effective diffusion coefficient of a PEG chain [13, 20]. PEG_{10k} has 227 units so its expected diffusion coefficient is $3 \times 10^{-12} \text{ m}^2/\text{s}$. This is two orders of magnitude higher than what was obtained experimentally. This is because in practice the molecules are attached to the surface whereas in theory the molecules are assumed to be freely diffusing. However this means that compared to a typical freely diffusing molecule such as ferrocenedimethanol that has a diffusion coefficient of $6.3 \times 10^{-10} \text{ m}^2/\text{s}$, the diffusivity of the attached PEG_{10k} chains is 4 orders of magnitude lower. This can be considered as a drawback when comparing attached RC systems to free diffusion based RC systems. However, by decreasing the inter electrode spacing this diffusivity can be increased, as the molecules do not need to stretch as much to reach the other electrode.

8.3.3 Control 1: blocked linker

The first control experiment was performed using the same experimental conditions as the previous experiment, only this time the NHS linker was blocked by ethanolamine. The results of this experiment are shown in figure 8.6. The aim of this experiment is to provide a control for the attached molecules experiment. Because the linker is blocked the molecules should not attach to the electrode and be flushed out, ideally resulting in flat baseline CVs.

However, for the cycling experiment a steady state current of approximately 60 pA was obtained with a halfwave potential of 0.19 V. The single electrode voltammogram showed a peak separation of 54 mV and a formal potential of 0.21 V versus Ag/AgCl.

The peaks in the single electrode voltammogram show a charge transfer of $17 \times 10^{-12} \text{ C}$, which means the total number of molecules present is 1.06×10^8 . The total number of molecules available for redox cycling is 7.1×10^7 . Given a steady state current of 60 pA this yields a value for the diffusion coefficient of $2.6 \times 10^{-14} \text{ m}^2/\text{s}$. This is approximately half the value of the diffusion coefficient obtained in the attached molecules experiment.

8.3.4 Control 2: short molecule

The second control experiment was performed using NHS-PEG₃₄₀₀-fc instead of NHS-PEG_{10k}-fc. These chains are much shorter than in the original experiment

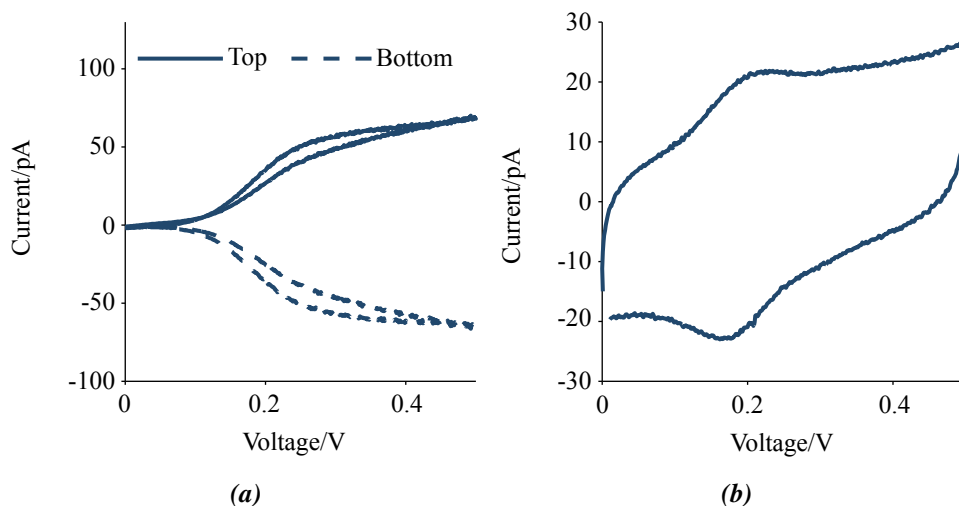


Figure 8.6: Results from the experiment where the NHS linker was blocked and the molecules should not have been able to attach to the surface. (a) Amplified CV recorded at 1 mV/s, showing a steady state of approximately 60 pA. (b) Single electrode CV recorded at the top electrode at 50 mV/s showing the typical peaks resulting from surface attached molecules. Potentials referenced versus Ag/AgCl electrode.

(27 versus 79 nm) and as a result, should not be able to cross the gap between the electrodes. Even half the spacing between the electrodes is already larger than the molecule length which means electron exchange between molecules at the top and at the bottom should also be ruled out. For this experiment it would mean that the single electrode CV should show attached molecule behavior but the amplified CV should not show any RC.

Results of this experiment are shown in figure 8.7. An RC current of approximately 35 pA is obtained with a half wave potential of 0.16 V. In the single electrode CV the peaks are not as clearly visible as in the previous experiments. As a result, it is not possible to define the peak separation and formal potential.

8.3.5 Discussion

Both control experiments should not have resulted in a RC current, and as a result no definitive conclusions can be drawn regarding the cycling of surface attached molecules. However, the results do show potential and some interesting effects that require discussion. For one it means that it is possible to introduce these large

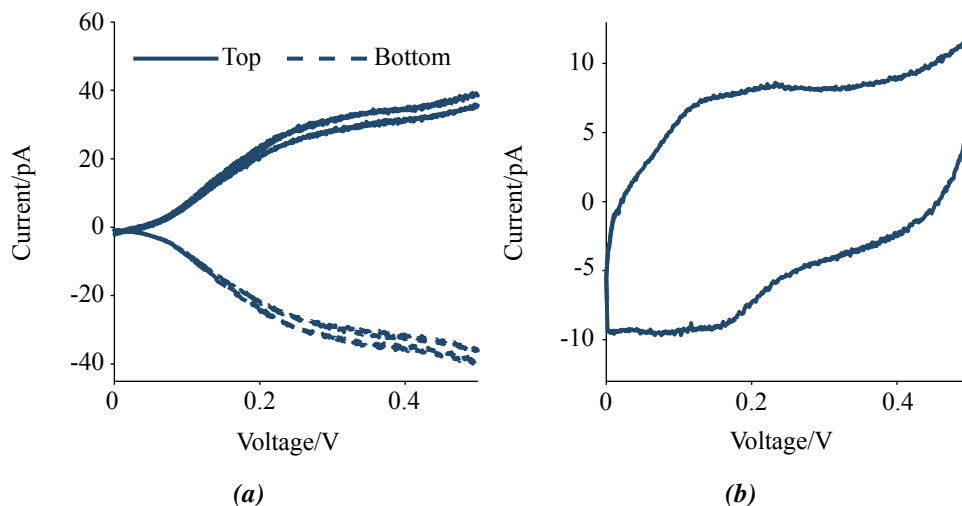


Figure 8.7: Results from the experiment where PEG₃₄₀₀ was used instead of PEG_{10k}. These short PEG chains should not be able to cross the gap between the electrodes. (a) Amplified CV recorded at 1 mV/s, showing a steady state of approximately 35 pA. (b) Single electrode CV recorded at the top electrode 10 mV/s. In this experiments the peaks from surface attached molecules were not as clearly visible compared to the previous experiments. Potentials referenced versus Ag/AgCl electrode.

molecules into a nanochannel. This is a result by itself as it means that the molecules do not aggregate and clog the nanochannel entrance.

The presence of a cycling current and an attached single electrode CV in the blocked linker experiment can be explained by non specific adsorption of molecules at the electrode. Similar behavior was also observed at macroelectrodes in bulk solution. The cystamine layer does not prevent 'sticking' of molecules at the electrodes, which means that molecules will always be present at the surface, whether the NHS group is blocked or not. For this reason an experiment with a shorter chain length was performed.

The cycling current observed in the PEG₃₄₀₀-fc experiment indicates that there are still residual freely diffusing molecules in the nanochannel because the PEG molecules are too short to cross the gap. These free molecules either directly cycle electrons between the top and bottom electrode or they provide an intermediate transport between the molecule layers at the top and bottom electrode. Schematically this is shown in figure 8.8. What percentage of the obtained current is contributed by the attached molecules

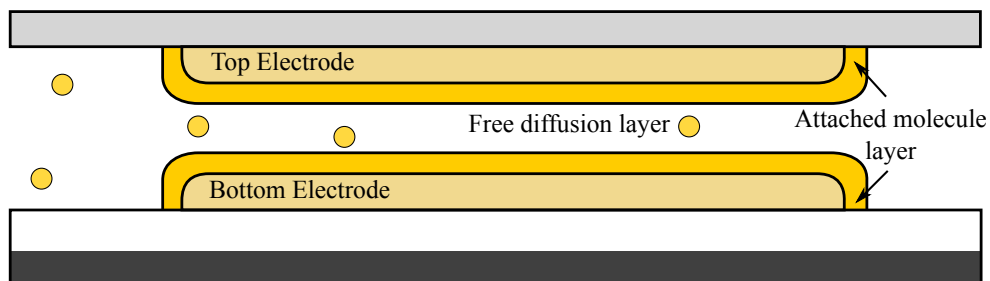


Figure 8.8: From the PEG₃₄₀₀-fc control experiment it seems that diffusive molecules are still contributing to the observed cycling current. At this time it is unknown in what ratio the diffusing and attached molecules are contributing to the electron transport.

cannot be determined. The single electrode CV showed less distinct peaks than the previous experiments. An explanation for this result is a decrease in the effective electrode area which is the result of the molecules from the other electrode no longer being able to contribute to the surface attached CV. The loss of the second electrode decreases the effective area by a factor $2/3$ and as a result the peak height decreases.

Additional experiments are required to determine the contribution of the attached molecules to the obtained cycling current. By decreasing the background concentration, the PEG₃₄₀₀-fc should not show a cycling current. Apparently the current approach of flushing the reservoir above the nanochannel and letting the molecules within the nanochannel diffuse out is not enough. The introduction of flow into the nanochannel would give an additional means of mass transport. However, introducing flow into the nanochannel requires a microfluidic setup with syringes connected via tubing to a PDMS based chip above the nanochannel. All of the additional tubing and PDMS could serve as potential temporary 'sticking' points for the PEG molecules which could potentially be flushed into the nanochannel when the channel is meant to be emptied. Additionally the introduction of a flow into the nanochannel also introduces shear forces onto the attached molecules. Currently it is unknown what the influence of flow is on the attached molecules. If the shear force is too high they could be torn off the electrodes.

8.4 Conclusions

The initial results are positive as both device configurations have shown RC currents. However, these are preliminary results which require further study to determine the reproducibility of the different experiments. For the thin layer cell it remains

challenging to determine the exact cause for the observed RC current, because the control experiments continue to show a cycling current. This is not a problem for the planar devices as these can be put into a fresh measurement solution that is guaranteed to be free of freely diffusing PEG molecules.

The amplified CV experiment shows an initial hint of surface attached species. However, the signal is still quite weak. This is likely due to the unfavorable effective to ineffective surface ratio. Therefore, the most logical approach is to improve the geometry of the planar electrodes. New devices will need to be developed that improve the surface ratio in order to increase the signal to background ratio.

The solution is to create a nanoscale IDE where the fingers as well as the inter-electrode spacing are in the order of tens of nm. To achieve this goal, EBL can be used to define the pattern. Another project within our group has recently shown the fabrication of nanoband electrodes for surface enhanced raman spectroscopy measurements using EBL [21]. These nanoband electrodes have a width in the order of 50 nm with a spacing in the range of 20 nm. Such a geometry would be very beneficial for an improved RC result, while still keeping the benefit of being able to properly clean the electrode surface as it can be in direct contact to be bulk.

Bibliography

- [1] E. G. Hvastkovs and D. A. Buttry. *The Analyst*, **135**(8):1817–1829, 2010. 94
- [2] F. Ricci and K. W. Plaxco. *Microchimica Acta*, **163**:149–155, 2008.
- [3] K. J. Odenthal and J. J. Gooding. *The Analyst*, **132**(7):603–10, 2007.
- [4] F. Lucarelli, S. Tombelli, M. Minunni, G. Marrazza, and M. Mascini. *Analytica Chimica Acta*, **609**(2):139–59, 2008. 94
- [5] R. Thewes, F. Hofmann, A. Frey, B. Holzapfl, M. Schienle, C. Paulus, P. Schindler, G. Eckstein, C. Kassel, M. Stanzel, R. Hintsche, E. Nebling, J. Albers, J. Hassman, J. Schulein, W. Goemann, and W. Gumbrecht. In *2002 IEEE International Solid-State Circuits Conference. Digest of Technical Papers*, volume 1, pages 350–473. IEEE, 2002. 94
- [6] M. Schienle, C. Paulus, A. Frey, F. Hofmann, B. Holzapfl, P. Schindler-Bauer, and R. Thewes. *IEEE Journal of Solid-State Circuits*, **39**(12):2438–2445, 2004.
- [7] B. Elsholz, R. Wörl, L. Blohm, J. Albers, H. Feucht, T. Grunwald, B. Jürgen, T. Schweder, and R. Hintsche. *Analytical Chemistry*, **78**(14):4794–802, 2006.
- [8] E. Nebling, T. Grunwald, J. Albers, P. Schafer, and R. Hintsche. *Analytical Chemistry*, **76**:689–696, 2004.
- [9] X. Zhu, K. Ino, Z. Lin, H. Shiku, G. Chen, and T. Matsue. *Sensors and Actuators B: Chemical*, **160**(1):923–928, 2011. 94
- [10] A. Anne, E. Cambril, A. Chovin, C. Demaille, and C. Goyer. *ACS Nano*, **3**(10):2927–40, 2009. 94
- [11] A. Anne, A. Chovin, C. Demaille, and M. Lafouresse. *Analytical Chemistry*, **83**(20):7924–32, 2011. 94
- [12] A. Anne, E. Cambril, A. Chovin, and C. Demaille. *Analytical Chemistry*, **82**(15):6353–6362, 2010.
- [13] J. Abbou, A. Anne, and C. Demaille. *Journal of the American Chemical Society*, **126**(32):10095–108, 2004. 94, 102
- [14] M. A. G. Zevenbergen, P. S. Singh, E. D. Goluch, B. L. Wolfrum, and S. G. Lemay. *Nano Letters*, pages 2881–2886, 2011. 95
- [15] M. A. G. Zevenbergen, B. L. Wolfrum, E. D. Goluch, P. S. Singh, and S. G. Lemay. *Journal of the American Chemical Society*, **131**(32):11471–11477, 2009.
- [16] B. Wolfrum, M. Zevenbergen, and S. Lemay. *Analytical Chemistry*, **80**(4):972–977, 2008.
- [17] M. A. G. Zevenbergen, D. Krapf, M. R. Zuiddam, and S. G. Lemay. *Nano*

- Letters*, **7**:384–388, 2007. 101
- [18] L. Rassaei, K. Mathwig, E. D. Goluch, and S. G. Lemay. *The Journal of Physical Chemistry C*, **116**(20):10913–10916, 2012.
- [19] K. Mathwig, D. Mampallil, S. Kang, and S. G. Lemay. *Physical Review Letters*, **109**(11):1–5, 2012. 95
- [20] P. E. Rouse. *The Journal of Chemical Physics*, **21**(7):1272, 1953. 102
- [21] L. Le Thi Ngoc, M. Jin, A. van den Berg, and E. Carlen. In *Transducers 2013 & Eurosensors XXVII*. 2013. 106

9

Summary and outlook

This chapter contains a summary of the results obtained during this PhD project followed by an outlook into new experimental designs and a discussion on the expected use of solid state sensors modified with electroactive molecules.

9.1 Summary

Electrochemistry has been performed for over 200 years and the concept of redox cycling (RC) at twin electrode systems is almost 50 years old. RC has since then developed into a technique with applications in various fields of research. However, these developments are far from finished. Chapter 3 contains an overview regarding the various applications of RC. In the area of biosensing, clinically relevant concentrations can already be measured. However, the stability over time of these devices still prevents them from being applied in a clinical setting. If these devices are to transition from proof of concepts to real world applications, additional optimization is needed. Other expected developments are improved nanofabrication designs featuring even smaller inter-electrode separations, an example of this is reported in chapter 7, and the development of new measurement techniques such as the technique of differential cyclic voltammetry (DCV) reported in chapter 4.

In chapter 4 a new analytical technique called DCV is evaluated for a thin layer cell geometry. DCV is the result of a combination of two existing electrochemical techniques, cyclic voltammetry (CV) and RC, in order to obtain *amplified* and *selective* detection of redox active species. Analytical expressions for the DCV voltammogram are derived and an optimal potential offset is calculated. The optimal voltage difference for the trade-off between peak height and width is 0.1 V for redox couples with $n=1$. Experimental voltammograms show good agreement with the analytical expressions. The voltammogram for ferrocenedimethanol has been fitted ($R^2 = 0.9985$) using only the distance between the electrodes as fitting parameter. Therefore, this technique shows promise as a tool for amplified and selective detection of redox active species.

In chapter 5 the modification of electrodes with ferrocene labeled PEG is shown. Although a decay over time is observed, this is less than 40% over a period of 50 minutes, which is suitable for this project. An interesting effect was observed when changing the background electrolyte concentration. The observed formal potential was found to be linearly related to the logarithm of the background electrolyte concentration. This effect could be attributed to an ion pairing effect between the NaClO_4 background electrolyte and the ferrocene label.

During the fabrication of electrodes designed for RC of surface attached molecules, an oxidized layer of titanium was found to block the electrochemical response of freely diffusing ferrocenedimethanol molecules. This was further investigated as a possible

protection layer for gold electrodes, providing an alternative to gold cleaning which typically needs to be performed prior to electrochemical experiments. This is reported in chapter 6. Electrode performance was tested through CV in a ferrocenedimethanol solution. After removal of the titanium dioxide layer, a clear voltammogram is obtained with a peak separation of 67 mV, indicating a clean surface. This means that the removal of a sacrificial layer is a good alternative to conventional electrochemical cleaning methods, while also protecting the electrodes during wafer handling.

In order to cycle PEG_{10k}-Fc molecules between two electrodes, a spacing of less than 79 nm is required. The fabrication of an electrode pair with these dimensions is reported in chapter 7. Using edge lithography as described in this chapter, electrodes with spacings down to 50 nm can be successfully fabricated without e-beam lithography (EBL) or focused ion beam (FIB) etching. The electrodes fabricated in this way show electrochemical behavior that matches with theory. The electrochemical experiments show that these devices can be used for RC of a freely diffusing redox mediator. The obtained amplification is maximally a factor 1.8 for freely diffusing species. The yield of the fabricated devices is high (96%), indicating the lower limit of the fabrication technique has not been reached. It should be possible to scale the gap size down to values below 30 nm. At these size ranges the fabricated devices are suitable for the investigation of electron transport in molecular systems.

These electrodes were subsequently modified with PEG-fc molecules and this is reported in chapter 8. Two electrode configurations were used. One, the planar nanogap device reported in chapter 7 and two, a nanofluidic thin layer cell fabricated in the group of Lemay. The initial results are positive as both device configurations have shown RC currents. However, these are preliminary results which require further study to determine the reproducibility of the different experiments. For the thin layer cell it remains challenging to determine the exact cause of the observed RC current, because the negative control experiments continue to show a cycling current. This is not a problem for the planar devices as these can be put into a fresh measurement solution that is guaranteed to be free of freely diffusing PEG molecules. The amplified CV experiment shows an initial hint of surface attached species. However, the signal is still quite weak. This is likely due to the unfavorable effective to ineffective surface ratio. New devices will need to be developed that improve the surface ratio in order to increase the signal to background ratio.

9.2 Outlook

9.2.1 E-beam fabricated interdigitated electrodes

One solution is to create a nanoscale interdigitated electrode (IDE) where both the finger-width and the inter-electrode spacing are in the order of tens of nm. To achieve this goal, EBL can be used to define the pattern. Another project within our group has recently shown the fabrication of nanoband electrodes for surface enhanced raman spectroscopy measurements using e-beam lithography. These nanoband electrodes have a width in the order of 50 nm with a spacing in the range of 20 nm [1]. Such a geometry would be very beneficial for an improved RC result while still keeping the benefit of being able to properly clean the electrode surface as the electrode is in direct contact to be bulk.

9.2.2 Reducing gap spacing by electrodeposition

Preliminary work that has not been included in this thesis has focused on using electrodeposition as an alternative to conventional cleanroom processing, for the creation of nanospaced electrodes. By putting gold electrodes into a gold sulphite bath and applying current pulses, gold is electrodeposited onto the existing structure. An interdigitated structure with a 2.7 μm gap between its fingers was subject to electrodeposition until a gap of 0.44 μm was obtained, after which local defects caused a short circuit in the connections. These local defects were the result of the lift off process used to fabricate the electrodes. Fabricating electrodes with other techniques such as wet etching should remove these defects and gap widths of 100 nm or less should be attainable.

9.2.3 Influence of PEG chain length on mass transport

Besides its use in RC systems, the PEG molecules of various chain lengths can also be of use for the determination of electron transfer and mass transport mechanisms at a single electrode. At low scanrates, all chains show the characteristics of an adsorbed electroactive layer. However, upon increasing the scanrate, the longer chains such as PEG_{10k} should start to show diffusive properties as well, e.g., an increase in peak separation. Investigations into the specific mass transport mechanisms for PEG_x-Fc layers at various chain lengths have not been reported in literature.

9.2.4 The future of dual-electrode surface-attached-molecule systems

To define which geometry or experimental setup is most functional, it is important to look at the desired application. If the aim is to fabricate a bio-sensor that is to be integrated into a commercial system, then dual electrode systems with surface attached molecules are not the best approach. Single electrode e-DNA systems are already commercially available [2], and it remains questionable whether dual electrode systems would be able to outperform its single electrode competitors. The RC effect is able to provide electrochemical amplification which is missing in single electrode systems. However, this is compensated in part by the lower diffusion coefficients of the large molecules that are required for shuttling between two electrodes. A promising compromise is the combination of surface attached molecules with freely diffusing redox-active molecules. In this concept the surface attached molecules provide the biosensing element while the freely diffusing molecules are able to undergo rapid RC. This is described in chapter 3, section 3.2.1.2 of this thesis [3–7].

If the aim is to perform fundamental studies on the properties of surface attached electroactive layers then dual electrode chip based systems are very suitable. Currently these types of studies are performed at electrochemical AFM systems where an AFM tip can be approached to the surface. A solid state system would be able to provide additional benefits that these systems are lacking. Due to their geometry, solid state based sensors are less fragile than AFM tips and it is relatively easy to multiplex the sensor readout which would allow simultaneous experiments at multiple electrode pairs. Moreover, the inter-electrode separation is constant which should provide an improved reproducibility of experiments. On the other hand, the ability to modify the distance between tip and substrate can also be considered an advantage of AFM systems, as this will allow the investigation of cycling behavior at various electrode spacings within a single experiment. As both systems have their own advantages, it is to be expected that these systems will exist in parallel for the investigation of surface attached electroactive layers.

Bibliography

- [1] L. Le Thi Ngoc, M. Jin, A. van den Berg, and E. Carlen. In *Transducers 2013 & Eurosensors XXVII*. 2013. 112
- [2] F. Lucarelli, S. Tombelli, M. Minunni, G. Marrazza, and M. Mascini. *Analytica Chimica Acta*, **609**(2):139–59, 2008. 113
- [3] R. Thewes, F. Hofmann, A. Frey, B. Holzapfl, M. Schienle, C. Paulus, P. Schindler, G. Eckstein, C. Kassel, M. Stanzel, R. Hintsche, E. Nebling, J. Albers, J. Hassman, J. Schulein, W. Goemann, and W. Gumbrecht. In *2002 IEEE International Solid-State Circuits Conference. Digest of Technical Papers*, volume 1, pages 350–473. IEEE, 2002. 113
- [4] M. Schienle, C. Paulus, A. Frey, F. Hofmann, B. Holzapfl, P. Schindler-Bauer, and R. Thewes. *IEEE Journal of Solid-State Circuits*, **39**(12):2438–2445, 2004.
- [5] B. Elsholz, R. Wörl, L. Blohm, J. Albers, H. Feucht, T. Grunwald, B. Jürgen, T. Schweder, and R. Hintsche. *Analytical Chemistry*, **78**(14):4794–802, 2006.
- [6] E. Nebling, T. Grunwald, J. Albers, P. Schafer, and R. Hintsche. *Analytical Chemistry*, **76**:689–696, 2004.
- [7] X. Zhu, K. Ino, Z. Lin, H. Shiku, G. Chen, and T. Matsue. *Sensors and Actuators B: Chemical*, **160**(1):923–928, 2011. 113

A

Electrode cleaning protocol

This appendix contains the protocol for the cleaning of gold disk electrodes.

A.1 Polishing

1. Start by polishing the electrodes for 5 minutes on a polishing cloth containing a slurry of 50 nm aluminum oxide particles. Polish in a figure eight pattern as shown in figure A.1.

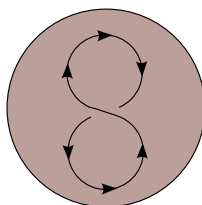


Figure A.1: Polishing in a figure eight pattern results in an even polish of the entire electrode surface.

2. After polishing is finished, rinse the electrodes using Milli-Q water followed by ethanol to remove most of the particles.
3. Place the electrode in a beaker filled with ethanol. Make sure the electrode is not touching the bottom.
4. Put the beaker in a ultrasonic bath for 5 minutes.
5. Rinse the electrode with Milli-Q water and put the electrode in a beaker filled with Milli-Q water.
6. Put the beaker in an ultrasonic bath for 5 minutes.
7. Store in Milli-Q water until electrochemical cleaning is started.

A.2 Electrochemical cleaning

1. Prepare an electrochemical cell containing a solution of 0.5 M H_2SO_4 , a mercurous/mercurousulphate reference electrode (MSRE), and a Pt counter electrode.
2. Bubble the solution with nitrogen for > 10 minutes to remove oxygen from solution.
3. Overlay the solution during measurements with a stream of nitrogen to prevent oxygen from diffusing back into the solution.
4. To clean the electrode, perform cyclic voltammetry at a scanrate of 100 mV/s between 0.65 and 1.1 V versus MSRE for a total of 30 cycles. The electrode is considered to be clean when a stable voltammogram is obtained, which is typically within 30 cycles.
5. To confirm that the voltammogram is stabilized and the typical properties of a clean voltammogram are obtained, record another 5 CVs using the same settings. An example of a clean gold voltammogram is shown in figure A.2. The voltammogram should be flat except for three individual gold oxidation peaks and a single gold reduction peak.

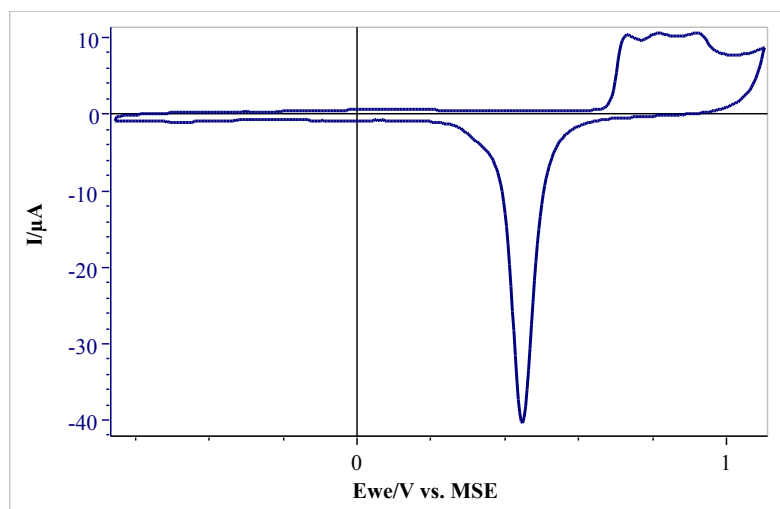


Figure A.2: Example of a typical CV for a clean gold disk electrode

B

Protocol for PEG-Fc synthesis

In order to synthesize the NHS-PEG_x-Fc molecule that is used during surface attached measurements, the following protocol was used. PEG_{10k}-(NHS)₂ was purchased from Nanocs, all others chemicals were purchased from Sigma-Aldrich.

B.1 2-Ferroceneethylamine

2-Ferrocenethylamine was synthesized by reduction of ferrocenylacetonitrile by LiAlH₄ as described in literature [1], with some modifications. 0.25 g (6.5 mmol) LiAlH₄ and 0.6 g (4.5 mmol) AlCl₃ were carefully added to 10 mL dry THF while stirring in an ice bath. 0.5 g (2.25 mmol) ferrocene acetonitrile was dissolved in 5 mL dry THF and subsequently added to the cooled mixture and refluxed overnight under an argon atmosphere. After cooling, water was added drop wise to decompose the excess LiAlH₄. 0.25 mL of concentrated NaOH was added to destroy the formed AlCl₃/2-ferroceneethylamine complex. The aqueous phase was thrice extracted with diethylether. The combined organic phases were dried with MgSO₄ and filtered and the solvent was removed with rotary evaporation. The product was purified by column chromatography with dichloromethane as eluent. After drying in vacuo a brown solid was obtained (0.13 g; 26%). ¹H NMR (300 MHz, CDCl₃): δ(ppm) = 4.2 (m, 9H, Fc), 2.82 (t, 2H, CH₂-Fc), 2.48 (t, 2H, CH₂-N).

B.2 PEG₂₅₀-(NHS)₂

The activated ester of the PEG₂₅₀ diacid was prepared according to the procedure described in [2]. 0.44 g (3.8 mmol) N-hydroxysuccinimide (NHS) and 0.78 g (3.8 mmol) dicyclohexylcarbodiimide (DCC) were added to a stirred solution of 0.4 g (1.6 mmol) poly(ethylene glycol) bis(carboxymethyl) ether in 30 mL 1,4-dioxane. After stirring over night at room temperature under an argon atmosphere, the mixture was filtered to remove the 1,3-dicyclohexylurea precipitate. The solvent was removed

with rotary evaporation and the residue was further dried under vacuum. ^1H NMR (300 MHz, CDCl_3): $\delta(\text{ppm}) = 4.56$ (s, 4H, $\text{CH}_2\text{C}=\text{O}$), 3.66 (s, 12H, $\text{C}_2\text{H}_4\text{-O}$), 2.81 (s, 8H, NHS).

B.3 NHS-PEG₂₅₀-Fc

0.04 g (0.17 mmol) 2-Ferrocene-ethylamine and 0.06 g (0.13 mmol) $\text{PEG}_{250}\text{-(NHS)}_2$ were dissolved in 3 mL chloroform and 30 μL triethylamine and stirred over night at room temperature under an argon atmosphere. The solvents were removed with rotary evaporation and the product was purified by column chromatography with dichloromethane as eluent. After the first fraction was removed, the eluent was changed to DCM/EtOH (95:5).

B.4 NHS-PEG_{10k}-Fc

6.9 mg (0.03 mmol) 2-Ferrocene-ethylamine and 0.25 g (0.024 mmol) $\text{PEG}_{10k}\text{-(NHS)}_2$ were dissolved in 1 mL chloroform and 2 μL triethylamine and stirred over night at room temperature under an argon atmosphere. The solvents were removed with rotary evaporation and the product was purified by size exclusion chromatography (Biobeads SX-1) with DCM as eluent.

Bibliography

- [1] B. Seiwert and U. Karst. *Analytical and Bioanalytical Chemistry*, **388**(8):1633–42, 2007. 117
- [2] A. Anne and J. Moiroux. *Macromolecules*, **32**(18):5829–5835, 1999. 117

Frequently used abbreviations

AFM	Atomic Force Microscopy
ACV	Amplified Cyclic Voltammetry
CV	Cyclic Voltammetry
DCV	Differential Cyclic Voltammetry
EBL	Electron Beam Lithography
FIB	Focused Ion Beam
IDE	Interdigitated Electrode
PEG	Polyethyleneglycol
RC	Redox Cycling
RIBE	Reactive Ion Beam Etching
RIE	Reactive Ion Etching
SECM	Scanning Electrochemical Microscopy
STM	Scanning Tunneling Microscopy
TLC	Thin Layer Cell

Curriculum vitae

Maarten van Megen was born the 29th of June 1984 in Arnhem. He received his MSc degree in electrical engineering in 2009 at the University of Twente, Enschede. Since then he started his Phd Project on redox cycling and surface attached molecules at the BIOS Lab on a Chip group of the MESA+ Institute of Nanotechnology. His scientific interests are nanofabrication, electrochemistry, sensors and signal processing.

Samenvatting

‘redox cycling’ aan electrodes op nanometer afstand

in de richting van elektrochemisch versterkte biomoleculaire detectie

Molecuul synthese is gemakkelijker uit te voeren op klein formaat terwijl elektrode fabricage makkelijker is op groot formaat. In dit project is gezocht naar een compromis tussen deze twee aspecten om een ontwerp met twee elektroden te realiseren, waarbij redox actieve moleculen vast zitten aan het elektrode oppervlak. Deze moleculen ondergaan ‘redox cycling’ tussen deze twee elektroden. Het onderzoek is gericht op nieuwe toepassingen van dit ‘redox cycling’ effect, fabricage van elektroden met een onderlinge afstand in de nanometers, en het elektrochemische gedrag van aan een oppervlak vastgezet polyethyleenglycol (PEG) molecuul met ferrocene als redoxactief label. De opgedane kennis over deze verschillende onderwerpen is gecombineerd in experimenten waar de PEG moleculen ‘redox cycling’ ondergaan tussen twee elektroden met een afstand kleiner dan 100 nanometer. Deze opstelling kan worden gebruikt als een transducerend element van een elektrochemische sensor indien de vastzittende moleculen zodanig worden gemodificeerd dat ze kunnen reageren op andere chemicaliën.

Output

Publications

M.J.J. van Megen, J.G. Bomer, W. Olthuis, A. van den Berg, Solid state nanogaps for electrochemical detection fabricated using edge lithography, *Microelectronic Engineering*, 2012 (*submitted*)

M.J.J. van Megen, M. Odijk, J. Wiedemair, W. Olthuis and A. van den Berg, Differential Cyclic Voltammetry for selective and amplified detection, *Journal of Electroanalytical Chemistry*, 681:6-10, 2012.

M. Odijk, J. Wiedemair, M.J.J. van Megen, W. Olthuis, A. van den Berg, Differential Cyclic Voltammetry - a Novel Technique for Selective and Simultaneous Detection using Redox Cycling Based Sensors, *Proceedings IEEE Sensors Conference 2010*; IEEE, 2010; pp. 918-922.

Presentations

M.J.J. van Megen, Towards the electrochemical detection of macromolecules at nanometer spaced electrodes, *SRO meeting enabling technologies*, Enschede, Netherlands, 2011

Posters

M.J.J. van Megen, N. Middelhuis, W. Olthuis, A. van den Berg, Reducing electrode gap spacing by gold electrodeposition, *IC-MAST2013*, Prague, Czech Republic, 2013

M.J.J. van Megen, W. Olthuis, A. van den Berg, Differential Cyclic Voltammetry for selective and amplified detection, *COAST/analytical chemistry meeting*, Lunteren, Netherlands, 2012

M.J.J. van Megen, W. Olthuis, A. van den Berg, SECM for nanogap sensors, *CUSO SECM Workshop*, Lausanne, Zwitserland, 2011

Acknowledgements

Congratulations you have reached the end of this thesis, or welcome, for those who started at the end. Four years have passed by rather quickly, and just weeks before the date of my defense I write these last words in my thesis. Now that the end of my PhD is near it is time to reflect on these past years, and give credit where credit is due. Because without a doubt you would not be reading this if it weren't for the support of a large number of friends and colleagues.

Wouter, you should be the first to be thanked because of your supervision of my project. Your rapid and thorough feedback on the thesis chapters that I handed in is much appreciated. I also have great respect for the way in which you are able to construct sentences. Your creative way of combining several concepts into a single nuanced sentence is a continued inspiration for my own short and to the point writing style.

Albert, thanks for giving me the opportunity to work within your group. Progress meetings with you were always a great source of new ideas, thanks to your creativity and knowledge on a wide variety of subjects. Besides this scientific aspect, you also strongly encouraged social and sportive interaction between colleagues with activities like the mountain-biking tour and BBQ. Thanks for this as well.

On a technical level I also had great support from Johan and Hans. Thank you Johan, for discussing new fabrication strategies and providing me with your excellent knowledge on all kinds of cleanroom processes. Your work in the cleanroom for the device fabrication is also much appreciated. I will remember you as someone who does not talk too much, but when you do it's either a very smart or funny comment. Hans I have you to thank for realizing the very convenient chipholders that I used during my electrochemical measurements and of course for your excellent jokes ;)

My fellow linux-nerd in the most positive sense of the word: Mathieu. Thank you for assisting me as a paranymph. Besides this, you were always available for a discussion on all things related to electrochemistry or computer configurations. Thanks as well for letting me reuse your thesis template. This has definitely saved me a lot of time.

Loes, my second paranymph, always ready with a positive remark to cheer people up. I will certainly miss our cycling trips. Thank you for going through my thesis to find

the last inconsistencies and spelling errors. I wish you all the best with your little boy or girl.

My travel buddy in Hawaii and electrochemical expert Justyna. Your previous experience with SECM experiments was very helpful. Keep up the good work on arranging those Friday afternoon drinks!

Thanks as well to people from the Molecular Nanofabrication group and the Nanionics group. Tom, although your project started a few years later than mine, we still had a good cooperation. Serge, thanks for letting me participate in your book club discussions. Shuo, your help with the device measurements is greatly appreciated.

One of the great experiences during my PhD was the workweek to the USA, and I have three excellent committee members to thank for organizing this great trip together with me: Paul, Lingling, and Evelien. Even though it was stressful at times we did not lose anyone and most things went smoothly. It was a pleasure working with you guys.

Daniel, Jelmer and Niels it was great to have you as my students. I hope you guys learned as much from me as I did from you.

Work is of course not only performed in the lab but also for a large part in the office. Over the years I have seen quite a few offices and roommates. Each and everyone of them provided a pleasant working environment. Thanks for being great roommates: Severine, Lingling, Arpita, Iris, Fleur, Evelien, Justyna, Songyue, Lonneke, Rerngchai, Yanbo, and Laura.

I had a great time working together with the other teachers for the course IEEE. It was a pleasure to work together with JanE, Cora, Ferdi, Erik, Mathieu, Fleur, Henriette, Eddy, Loes, Adithya, Yawar and Floris.

And then there are all the other people at BIOS (past & present) that I haven't mentioned yet. You all contributed to a great working environment. Thanks Floor, Ad, JanvN, Hermine, Rogier, Verena, Lennart, Bjorn, Susan, WouterS, Egbert, Mingliang, Masood, Edwin, Sourav, Jean-Philippe, Zhenxia, Alexander, Liza, Sertan, Wesley, Allison, Burcu, Natalia, Loan, Trieu, Georgette, Ganesh, and Iris.

A PhD project can be stressful at times, but luckily distraction was available in the form of friends. Thanks, Hefney, Pjotter, Roland, Roos, Anita, Bettina, Brenda, Wouter, Jasper, Maurice, Ivo, and Antal. I hope the future brings us many excellent parties.

And last but definitely not least, those people closer to home. Mom and dad, thanks for your support through the years. Who knew we would end up here after my MAVO advice. Sanne, these last few months I had to blur the line between work and private life. Thanks for being very understanding and supporting of this. Finally, my daughter Vera, even though you might not have been aware of it yourself. Thanks for being the most relaxed and cheerful baby I could have wished for, and for letting me finish my thesis on time.

Thanks everyone!

Maarten